Skolkovo Institute of Science and Technology

Curtin University

DYNAMIC MODELLING AND EXPERIMENTAL EVALUATION OF NANOPARTICLES APPLICATION IN SURFACTANT ENHANCED OIL RECOVERY

Doctoral Thesis

by

Ivanova Anastasia

DOCTORAL PROGRAM IN PETROLEUM ENGINEERING JOINTLY WITH SKOLKOVO INSTITUTE OF SCIENCE AND TECHNOLOGY AND CURTIN UNIVERSITY

Supervisors

Associate Professor of Practice Alexey Cheremisin

Professor Ahmed Barifcani

Moscow 2020

I hereby declare that the work presented in this thesis was carried out by myself at Skolkovo Institute of Science and Technology, Moscow and Curtin University, Perth, except where due acknowledgment is made and has not been submitted for any other degree.

Candidate (Anastasia Ivanova)

Supervisor (Prof. of Practice Alexey Cheremisin)

Abstract

Effective production of oil from carbonate reservoirs often requires the application of improved oil recovery technologies such as waterflooding. However, conventional waterflooding in carbonates usually results in low hydrocarbon recovery as most of these formations exhibit a complex pore throats structure and are mostly oil-wet. Therefore, surfactant augmented water injection is applied in order to either alter wettability towards more water-wet or to lower the brine/oil interfacial tension (IFT). The application of surfactant flooding aids in additional oil recovery up to 25%. The effectiveness of surfactant flooding depends on many factors, including fluid distribution and fluid-rock interactions. The characterization of fluid-rock interactions is, however, challenging with existing laboratory methods, which are typically based on macroscale (mm) observations. Therefore, in this study, the wettability of carbonate rocks has been studied using advanced imaging techniques that allowed to comprehensively analyze the variation of wetting properties on the micro-level and find the reason of the mixed wettability of carbonates. These findings can be used for further planning of wettability modification using chemical formulations. As such in this work, different surfactant and nanoparticles augmented surfactant formulations have been studied in order to enhance surfactant properties for brine/oil IFT reduction and wettability alteration towards more water-wet. The obtained results show that depending on reservoir conditions (high temperature and/or salinity content) nanoparticles – surfactant compositions should be optimized and selected to effectively control the interfacial tension, wettability alteration, and to avoid negative synergism. Molecular-level investigation on nanoparticles and surfactant molecules interactions have been performed using molecular dynamic (MD) simulations. The results illustrate that the models established can be used for screening different surfactants at various temperatures and salinities. Furthermore, the models of SiO_2 nanoparticles have been established for MD simulations, showing a good agreement with the experimental data. The findings of this work show that nanoparticles augmented surfactant formulations are promising solutions for enhanced oil recovery from carbonate reservoirs through the wettability alteration.

Publications

International peer-reviewed journals

Publications forming part of the thesis

1. Ivanova, A., Mitiurev, N., Cheremisin, A., Orekhov, A., Kamyshinsky, R., Vasiliev, A. Characterization of Organic Layer in Oil Carbonate Reservoir Rocks and its Effect on Microscale Wetting Properties. Scientific Report Nature 9, 10667 (2019). https://doi.org/10.1038/s41598-019-47139-y
2. Ivanova, A.A., Phan, C., Barifcani, A., Iglauer, S., Cheremisin, A.N. Effect of Nanoparticles on Viscosity and Interfacial Tension of Aqueous Surfactant Solutions at High Salinity and High Temperature. Journal of Surfactants and Detergents 23, 327-338 (2020). doi: https://doi.org/10.1002/jsde.12371
3. Ivanova, A.A., Cheremisin, A.N., Barifcani, A., Iglauer, S., Phan, C. Molecular insights in the temperature effect on adsorption of cationic surfactants at liquid/liquid interfaces. Journal of Molecular Liquids 299, 112104 (2020). doi: https://doi.org/10.1016/j.molliq.2019.112104
4. Ivanova, A.A., Mitiurev, N.A., Shilobreeva, S.N., Cheremisin, A.N. Experimental Methods for Studying the Wetting Properties of Oil Reservoirs: A Review. Izvestiya, Physics of the Solid Earth, 55, 496-508 (2019). doi:https://doi.org/10.1134/S1069351319030042
5. Ivanova, A.A., Cheremisin, A.N., Barifcani, A., Iglauer, S., Phan, C. Molecular Dynamics Study of the Salinity Effect on the Interfacial Behavior of Cationic Surfactants at Oil/Water Interfaces. Submitted to the Journal Chemical Physics.

Publications relevant to thesis but not forming part of it

1. Ivanova A. Current technological trends in development and production of oil and gas: a public analytical report - M,: BTB, 2017.- p. 216. (book chapter)

Conferences/Conference proceedings

1. Ivanova, A.A., Cheremisin, A.N., Spasennykh, M.Y. Application of Nanoparticles in Chemical EOR. IOR 2017-19th European Symposium on Improved Oil Recovery (2017). doi:https://doi.org/10.3997/2214-4609.201700247
2. Ivanova A.A., Miturev M.A., Cheremisin A.N. and Spasennykh M.Y. Effects of high salinity and high temperature on nano-surfactant formulations properties. Abstracts of IOR 2018 Norway conference.
3. Ivanova, A., Mitiurev, N., Cheremisin, A., Orekhov, A., Vasilev, A., Hairullin, M., Afanasiev I. Direct Wettability Characterization of the Carbonate Reservoirs Using Different Microscopic Techniques. 80th EAGE Conference and Exhibition 2018 (2018). doi:https://doi.org/10.3997/2214-4609.201801599
4. Ivanova, A., Orlov, D., Mitiurev, N., Cheremisin, A., Khayrullin, M., Zhirov, A., Afanasiev, I., Sansiev G. Microstructural Imaging and Characterization of Organic Matter Presented in Carbonate Oil Reservoirs, SPE Europec featured at 81st EAGE Conference and Exhibition (2019). doi:https://doi.org/10.2118/195456-MS
5. Ivanova A., A. Barifcani, C. Phan. Molecular dynamic simulations of temperature effect on adsorption of cationic surfactants at liquid/liquid interface. Abstracts of Chemeca Conference Sydney (2019).

Acknowledgments

I would like to express my sincere gratitude to my supervisor Associate Professor of Practice Alexey Cheremisin, who continuously supported me throughout my Ph.D. study and research. Thanks for his leadership, help, patience, inspiration and invaluable input into my research plan and study.

I also would like to express my deepest and sincere appreciation to my co-supervisors Professor Ahmed Barifcani, Professor Stefan Iglauer and Senior Lecturer Chi Phan for their continuous and prompt support, for their motivation, and unwavering contribution to my research. I am very grateful to them for all knowledge and skills I have learned from them during this work.

Special thanks go to my lab colleagues and faculty members at Skolkovo Institute of Science and Technology and at the Department of Petroleum Engineering of Curtin University for being friendly and wonderful. My sincere thanks also go to the colleagues at Kurchatov Institute for the great research we did together.

Moreover, my sincere gratitude goes to Leading Researcher Svetlana Shilobreeva from the Vernadsky Institute of Geochemistry and Analytical Chemistry of the Russian Academy of Sciences for her endless support and fruitful technical discussions.

Last but not least, I am grateful to my family for always believing in me and supporting me during my Ph.D. journey.

Table of Contents

List of Symbols, Abbreviations

IFT – interfacial tension

EOR – enhanced oil recovery

SiO_2 – silicon dioxide

SOS – sodium olefin sulfonate

EHAC – erycyl bis-(hydroxyethyl)-methylammonium chloride

CTAB – cetyl trimethyl ammonium bromide

CTAC – cetyl trimethyl ammonium chloride

ESEM – enviromental scanning electron microscope

Cryo – FIB - cryo-focused ion bean

EELS – electron energy loss spectroscopy

MD – molecular dynamics

OOIP – original oil in place

WOR - water-oil ratio

Fe_2O_3/SiO_2 – iron (III) dioxide/silicon dioxide

PIT - phase-inversion temperature

Al_2O_3 – aluminum dioxide

ZnO – Zinc dioxide

TiO_2 – titanium dioxide

ZrO_2 – Zirconium dioxide

NiO_2 – nickel dioxide

SE - secondary electrons

BSE - back-scattered electrons

WDS - wavelength-dispersive X-ray spectroscopy

EDX or EDXS - energy-dispersive X-ray spectroscopy

HAADF - high angle annular dark field detector

DLVO - Derjaguin-Landau-Verwey-Overbeek

Chapter 1. Introduction

1.1 Carbonate oil reservoirs

Carbonate oil reservoirs, such as limestone and dolomite, represent approximately half of all hydrocarbon reserves in the world[1]. The study and development of such reservoirs have started in the 1950s. Since then, the interest in carbonate reservoirs has been rapidly growing both in industry and academia, especially at times of oil resources nationalization and oil "revolutions" in the Middle East and South Africa, where carbonate reserves are the biggest (Figure 1)[2]. For instance, it was discovered that almost 70% of proved conventional oil reserves belong to carbonate rocks in Middle East[2].

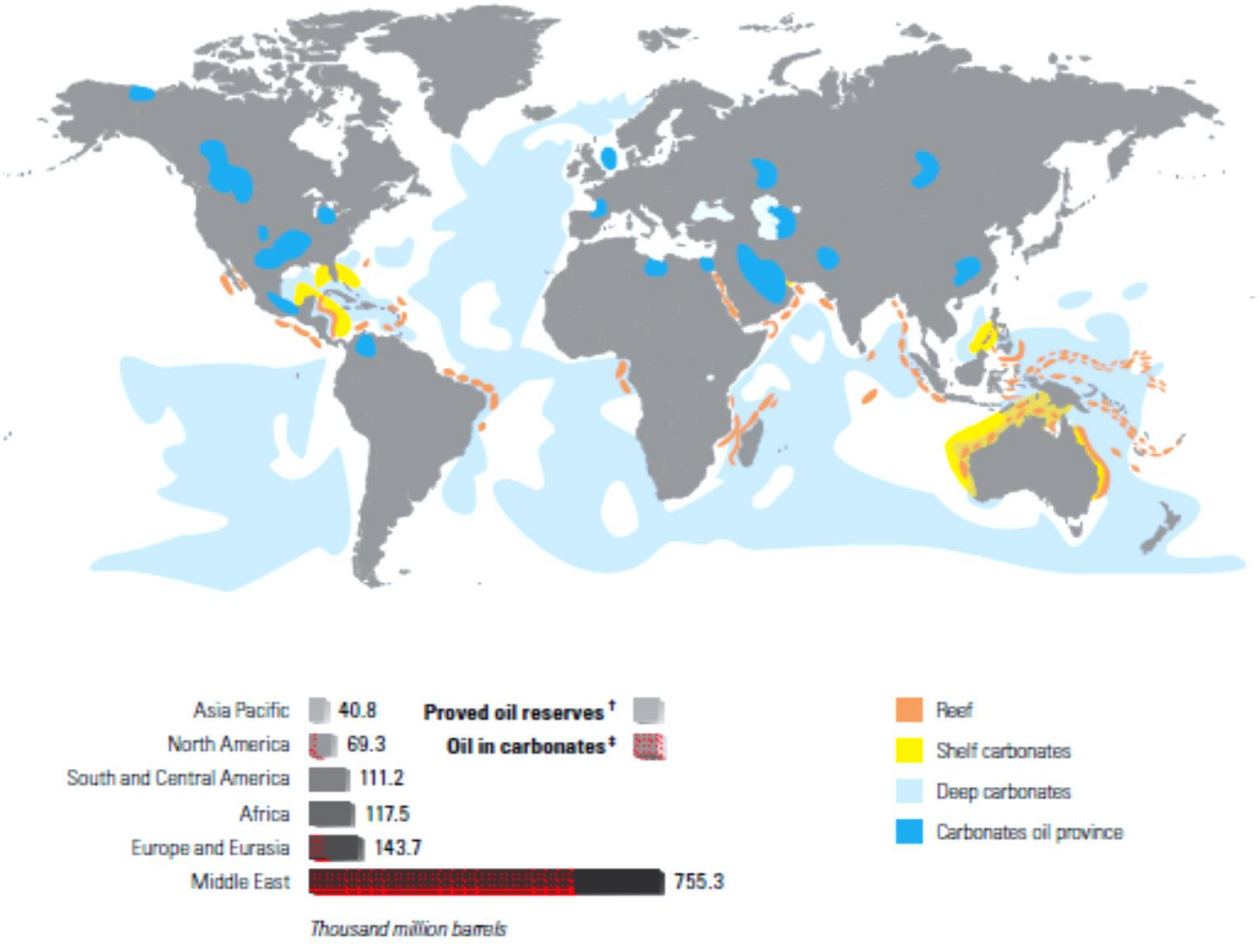

Figure 1. Geographic map of carbonate reservoirs distribution in the world[2].

Due to the diagenetic effects and depositional history of carbonate reservoir rocks, they exhibit unique heterogenic properties varying from nano to macro scales. Previous studies of carbonate

rocks illustrate that in comparison with siliciclastic reservoirs, these heterogenic issues pose a challenge to the exploration, development, and commerciality of such reservoirs. The most common aspects to deal with include uneven pore-size distribution, various ranges of permeability (several orders of magnitude) for a given porosity, and physical-chemical properties of the reservoir environment that control fluids flow[3].

Unfortunately, all these complexities are still challenging and remain unresolved, and thus, are considered as the most important for carbonate reservoir characterization and management. For instance, in 2009, at the Industry Technology Facilitation meeting, the main concerns related to carbonate reservoirs have been classified into five areas: 1) Rock typing; 2) Permeability prediction; 3) Understanding of fluids flow and microporosity; 4) Fracturing and 5) Impact of dolomitization[3]. Hence, carbonate reservoir rocks require complex approaches for developing and generating high recovery factors, which hardly reach 30%[4]. For example, the oil recovery factor from one of the biggest Omani fractured carbonate Ghaba North field has shown only 2% throughout 20 years of production[5].

It should be noted that reservoir fluids flow, and thus, the oil recovery factor is mainly controlled by the wettability of the rocks, which ranges from mixed to oil-wet state for carbonate reservoir rocks[6]. The fact that carbonates exhibit hydrophobic wetting properties makes conventional water flooding less effective due to the capillary pressure effects in oil-wet reservoirs, which prevent water from penetrating through pores with oil. As a result, trapped in pore throats oil would reside unrecovered. Hence, changing the wetting state of rocks or interfacial tension between oil and brine would modify capillary pressure and fluids distribution through the pore networks that in turn would generate the highest oil displacement efficiency from carbonate rocks[7, 8].

1.2 Wettability of carbonates

In terms of oil recovery, wettability is a crucial parameter to control injected and produced fluids arrangement in the porous media, which in turn influences the properties of multiphase flow of water, gas, and oil. The wetting state of reservoir rocks is a result of chemical equilibrium between brine/oil/rock reached over millions of years. The wetting states and their classification are presented in Figure 2. Traditionally, wetting preferences of surfaces are divided into three types – water-wet (hydrophilic), mixed-wet, and oil-wet (hydrophobic). In the water-wet state (Figure

2a, d)[9, 10], oil forms droplet with the minimum contact area at the surface, showing contact angle θ~0˚. If oil drop spreads (Figure 2c, f)[9, 10], the surface is referred to as oil-wet or hydrophobic, and the contact angle θ is approaching close to 180°. If a surface has intermediate wettability, the shape of the drop and the contact angle would be determined by the balance of the surface tension forces between the contacting phases (Figure 2b).

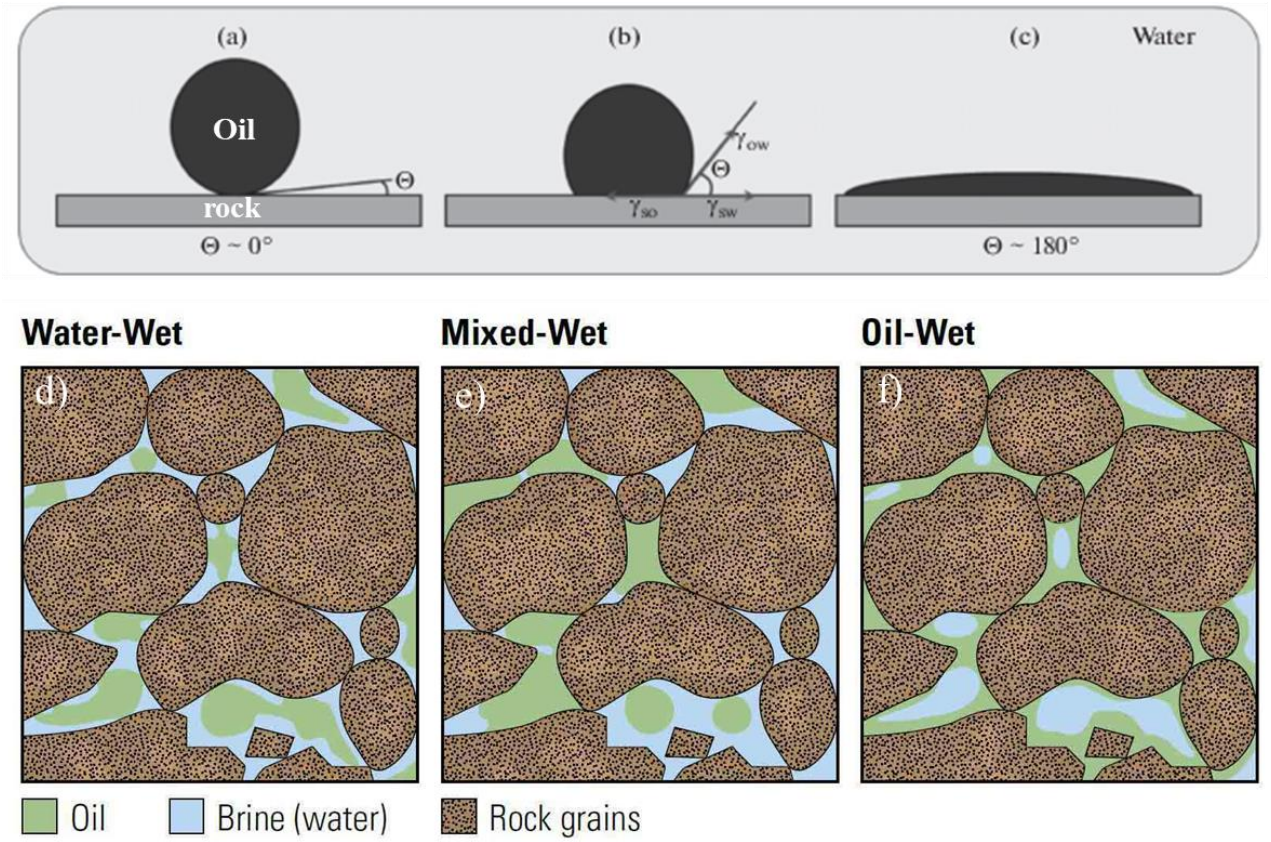

Figure 2. Wetting states of rocks – a), d) water-wet; b), e) intermediate, mixed wet and c), f) oil-wet [9, 10].

In the case when a rock surface shows no strong preference to water-wet or oil-wet (Figure 2b), the contact angle (θ) formed on the interfacial surface can be calculated from Young's equation[11]:

$$\gamma_{so} = \gamma_{sw} + \gamma_{ow} \cos\theta,$$

where $\gamma_{so}, \gamma_{ow}, \gamma_{sw}$ are surface energies at the interfaces of the oil-surface, oil-water, and surface-water phases, respectively.

Notably, that rock surface can also have mixed wettability (Figure 2e)[9]. This phenomenon appears when some surface areas demonstrate a hydrophobic state while others - hydrophilic.

The wetting character of rock surface (water-wet, oil-wet, or mixed type) determines the migration and distribution of reservoir fluids throughout the pore throats. Indeed, due to capillary forces, the wetting fluid has lower free surface energy. Since smaller pores have a larger specific surface area than large pores, wetting and non-wetting fluids will be redistributed in the pore channels in such a way that the wetting fluid occupies small pores, whereas the non-wetting fluid occupies large pores. In practice, this means that when the rock surface is hydrophobic, water as a non-wetting fluid will predominantly move through the pores with a larger diameter[12]. This fact explains the inefficiency of waterflooding in hydrophobic carbonate reservoirs, as the majority of oil would be left trapped in small pores, where water cannot access due to the capillary pressure effect.

It should be noted that the initial wettability of carbonate reservoir rocks can be altered towards more oil-wet when interactions between minerals and oil components occur. Several possible mechanisms of chemical interactions depending on reservoir properties and oil composition have been proposed in the literature:

1) Adsorption of polar organic components from oil, such as asphaltene and resin fractions[13];
2) Adsorption of carboxylic acids, including benzoic, palmitic, oleic, and octanoic acids[14, 15];
3) Ion binding that is led by the surface charge of carbonates[4].

It should be pointed out that the wetting properties of carbonates can be described by means of the zeta potential of the mineral surface. The zeta potential influences the electrostatic forces, which act between the polar organic groups in the oil and the surface, in accordance with the Derjaguin-Landau-Verwey-Overbeek (DLVO) theory. Indeed, the zeta potential of carbonate surface depends on the adsorption of ions, such as Ca^{2+}, CO_3^{2-} and Mg^{2+} in the Stern layer. In typical formation brines, the concentration of Ca^{2+} and Mg^{2+} is high, resulting in the positive zeta potential of the carbonate surface. Reduction of Ca^{2+} and Mg^{2+} concentration, for instance, by bulk dilution, leads to negative zeta potential. Therefore, in the initial state, the zeta potential of carbonate surface is positive, resulting in the facilitation of adsorption of carboxylic acids or polar

organic components from oil. As a result, the initial wettability of carbonate reservoir rocks is generally oil-wet or mixed-wet.

1.3 Wettability measuring techniques

Traditionally, wettability studies are conducted with core-scale measurements using Amott – Harvey[16] (Figure 3a)[9], USBM[17, 18] (Figure 3b)[9,] and contact angle methods[19]. The popularity of these methods stems from their simplicity and cost-effectiveness.

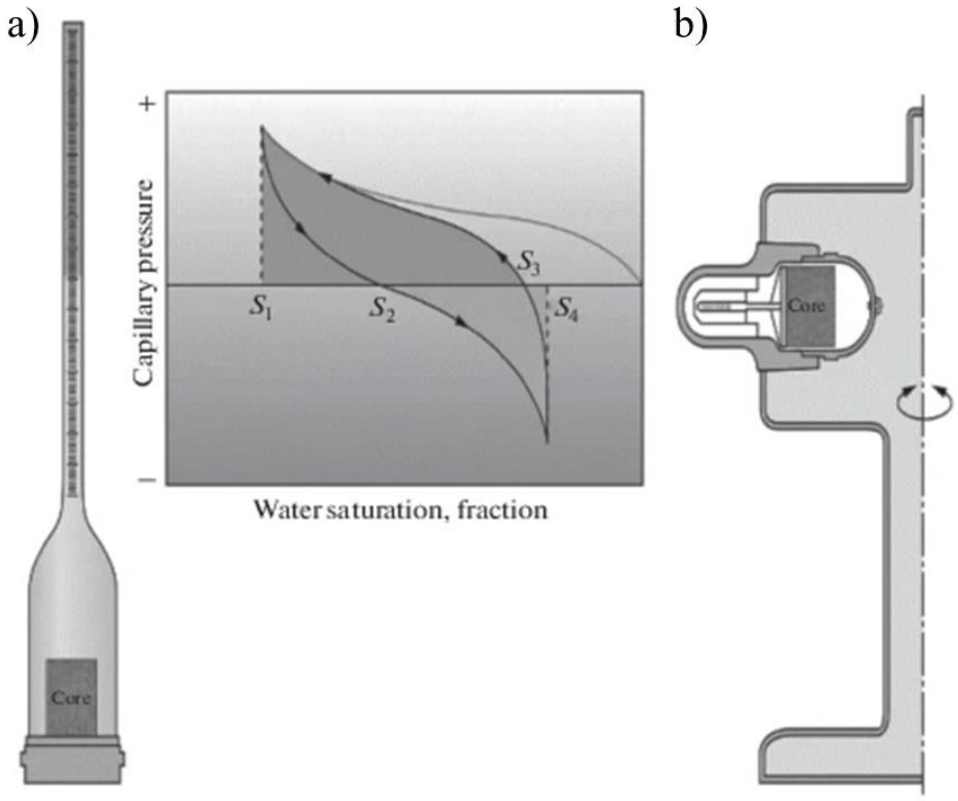

Figure 3. Examples of wettability measurement using a) Amott–Harvey method and b) USBM[9].

For instance, the Amott–Harvey technique is based on the spontaneous imbibition of the wetting fluid (water or kerosene) and the displacement of the non-wetting fluid. As a result of this test, water (I_w) and oil (I_o) imbibition indexes can be calculated using the following equations:

$$I_w = \frac{V_w}{V_{wt}};$$

$$I_o = \frac{V_o}{V_{ot}},$$

where V_w (mL) and V_o (mL) are volumes of water and oil displaced by oil and water under spontaneous imbibition, respectively; V_{wt} (mL) and V_{ot} (mL) are total volume of water and oil displaced under oil and water imbibition and centrifuging, respectively.

In this method, wettability is estimated in terms of the Amott–Harvey parameter J, which is the difference between the water (I_w) and oil (I_o) imbibition indexes:

$$J = I_w - I_o.$$

As such, it is assumed[20] that when $0.1 < J < 1$, the sample's wettability is water-wet; at $-0.1 < J < 0.1$, the sample has intermediate wettability, and if $-1 < J < -0.1$, the sample is oil-wet.

Although this method is widely used in laboratories, it provides information about the average wettability of the sample (the same as USBM). Moreover, the determination of rock wettability by this method is limited, because as it was shown in work[21] samples with permeability below 10 mD are unsuitable for the study. Another disadvantage of this method is that this method cannot determine mixed wettability (when the sample has several different types of wettability), as it is challenging to estimate the number of hydrophobic or hydrophilic surface areas[22].

The wettability of rock samples can also be measured by determining the contact angle between fluids and the surface. This method is based on water or oil drop shape analysis when it is in contact with the surface. Traditionally, wettability is assumed to be water-wet if oil forms an angle $0° < \theta < 70°$ with the surface, intermediate wet - $70° < \theta < 110°$ and oil-wet - $110 < \theta < 180°$. The reverse trend should be considered if using water drops. This method provides information about the wetting preferences of a particular sample surface, which makes it different from the USBM and Amott - Harvey methods that give average wettability indexes.

However, direct investigation of the rock-fluid interactions by these methods is limited, as they yield the average wettability indexes on macroscale (mm) and cannot account for rock surface roughness, pore structure, or chemical rock composition, which strongly affect fluids flow properties[23].

Recently it has been proposed that advanced microscopic techniques, including high resolution scanning electron microspore (SEM), can be used for the analysis of fluids distribution throughout porous media[24]. The authors showed the distribution of different fluids (oil and brine) throughout the pore network by collecting the elemental maps obtained by coupling SEM imaging with the X-ray analysis of the elements. Moreover, with the recent advances in microscopy, it has become possible to utilize the cryogenic techniques and Environmental Scanning Electron Microscopy (ESEM) in order to study surface wettability on microscale[25, 26]. For instance, the authors[150] carried out the micro-wettability (μm) measurements using ESEM with the middle Bakken samples and inferred that these results could be used for more accurate estimation of multi-phase flow parameters (e.g. relative permeability, capillary pressure), which in turn would improve primary and secondary oil recovery processes. The application of these techniques is particularly important in the carbonate reservoir as it can reveal the nature of mixed-wet or oil-wet wetting properties of such reservoirs.

The average wettability has been measured for many sandstone and carbonate rocks[27-31], whereas there is a serious lack of information about microscale wettability characterization of pores that describes the fluid-rock interactions. Hence, studying the rock/brine/oil chemical interactions would give an insight of how to optimally modify wettability towards mixed or water – wet, which in turn would increase oil recovery factor from carbonate reservoirs.

1.4 Enhanced oil recovery (EOR) in carbonate reservoirs

Various methods are being developed and applied to improve the recovery of trapped oil in carbonate rocks. In general, all oil recovery methods for hydrocarbon recovery are divided into three groups - primary, secondary, and tertiary, depending on their purposes. Primary recovery happens due to the natural energy that moves oil from formation to the producing wells by the pressure differential between high pressure in rock formation and low pressure in the wellbore. Usually, this method is limited when the pressure drops and helps in recovery up to 20% of original oil in place (OOIP)[4]. In secondary recovery or improved oil recovery water or gas are injected for pressure maintenance. Waterflooding is the widely used method for decreasing residual oil saturation by oil displacement, which has been proven to be more effective in applying in water-wet rather than mixed or oil-wet reservoirs[32,33]. In mixed or oil-wet reservoirs, such as carbonates, approximately 50% of original oil in place is still left trapped in the reservoir due to high capillary

forces after waterflooding[34]. Therefore, in order to increase the oil recovery factor from carbonate reservoirs, advanced methods should be applied. Indeed, tertiary recovery or enhanced oil recovery (EOR) methods include, but are not limited to, chemical (e.g. surfactant and/or polymer and/or alkaline) flooding, gas methods (e.g. CO_2 injection), thermal recovery (e.g. air injection). For instance, around 67% of all CO_2 floods in the US (WAG or continuous mode) are being used in carbonate reservoirs, whereas the number of air injection projects in carbonates has been declining for several decades[35]. However, despite several successful projects, air and CO_2 injections are considered highly challenging and risky due to environmental impacts[36].

In comparison with CO_2 flooding, the application of chemical EOR is more dependent on the cost of chemicals used, and its application is limited by the low oil price. Despite this fact, many research activities are still focused on improving the existed solutions in terms of reducing the cost of chemicals per barrel of recovering oil[37, 38]. As a result, chemical EOR has demonstrated great potential to increase total recovery factors and sustain the economic feasibility of carbonate reservoirs.

Among other chemical EOR methods, surfactant injection in carbonate reservoirs has been shown to be more effective, and its widely accepted as a promising stimulating technology mostly for depleted, matured and waterflooded reservoirs.

1.5 Surfactant flooding in carbonate reservoirs

Historically, surfactant flooding as an EOR method was developed for sandstone oil reservoirs[39]. However, many studies have shown that surfactant injection into oil-wet carbonate reservoirs could be a beneficial way of enhancing oil recovery[40]. The main goal of using surfactants in flooding carbonates is to alter rocks' wettability towards more water-wet and to reduce brine/oil interfacial tension (IFT). For these purposes, different types of surfactants have been tested, including ionic (anionic[41, 42], cationic[41, 42, 44] and zwitterionic[43, 44]) and non-ionic [42, 45] (Figure 4).

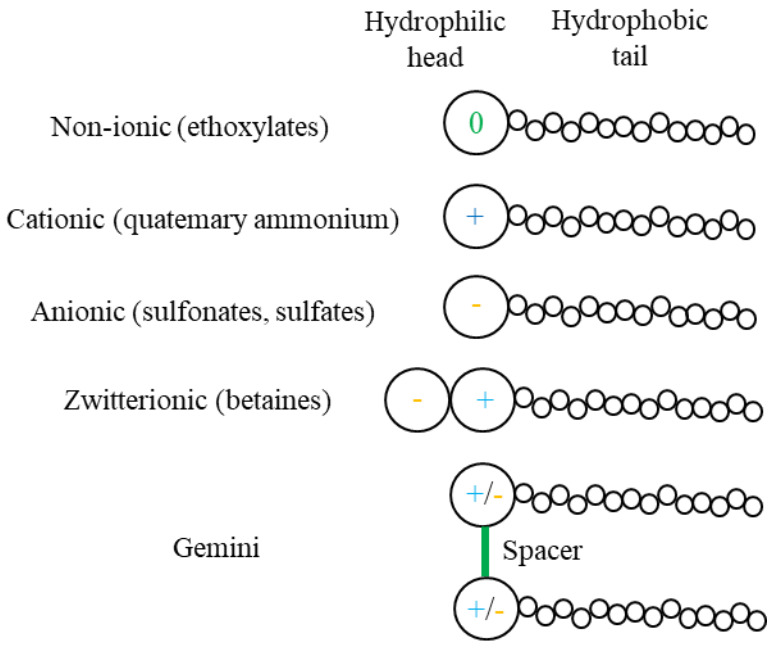

Figure 4. Classification of surfactants.

For instance, anionic surfactants such as sulfates and alkyl aryl sulfonates have shown significant IFT reduction to values less than 10^{-2} mN/m at brine/crude oil interface[46]. Cationic (cetyl trimethyl ammonium bromide (CTAB) and dodecyl trimethyl ammonium bromide (DTAB)) and non-ionic (polyoxyethylene alcohol (POE) and octyl phenol ethoxylate (Triton-100)) surfactants have been also widely tested for wettability alteration and IFT reduction in carbonate reservoirs, showing promising results[47].

Despite many studies, there are not many field projects reported in carbonates utilizing surfactant flooding as an EOR method. As such, only two projects were performed in the USA – Cottonwood Creek[48, 49] and Yates field[50, 51], and one project in Semoga field Indonesia[52]. As it can be seen in Figure 5, the number of surfactant projects conducted worldwide in sandstone reservoirs surpasses the number in carbonates[53]. Data collected from the 1990s to the 2000s.

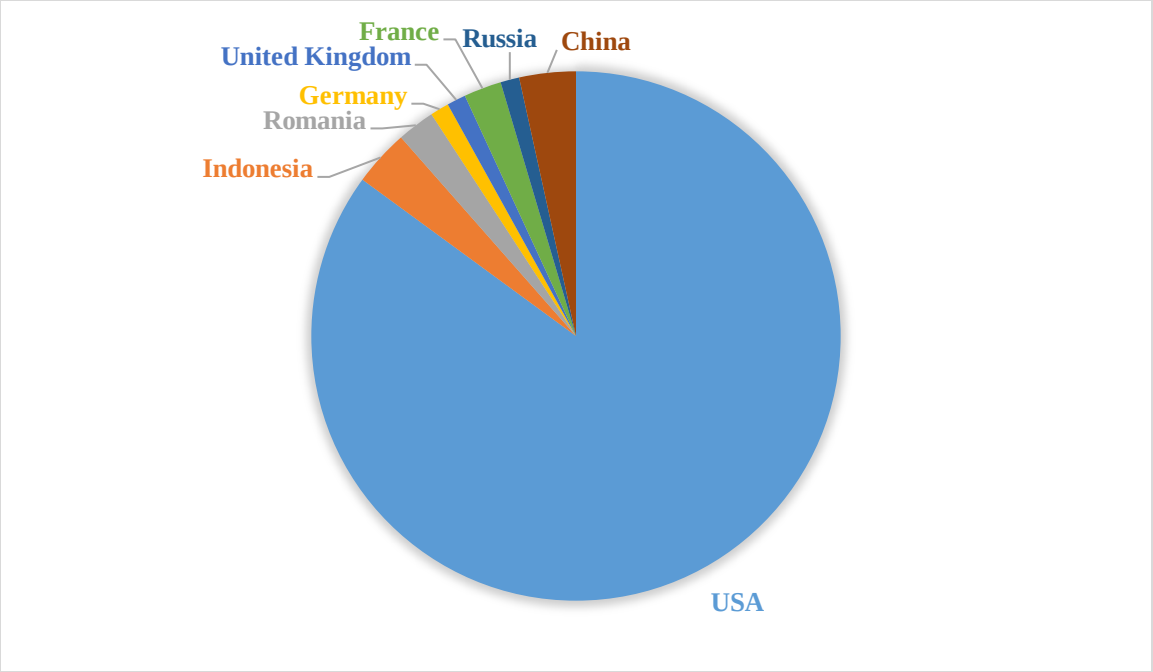

Figure 5. Surfactant flooding projects that were conducted worldwide from the 1990s to 2000s[53].

However, it is interesting to point out that pilot tests of surfactant injection in carbonate reservoirs gave promising results. For instance, the Yates field pilot test showed a two-fold increase in oil recovery factor by using commercial surfactant Shell 91-8[50, 54]. Therefore, surfactant flooding has been regarded as a promising alternative to CO_2 injection in carbonates[35].

1.6 Impact on oil/brine interfacial tension

Conventionally, carbonate reservoirs show low additional oil recovery during waterflooding because more than half of OOIP is still left trapped in the complex pore matrix due to the low capillary number of water[55, 56]. The capillary number is defined as the ratio between viscous and capillary forces (Equation 1) and controls the residual oil saturation[57].

$$N_c = \frac{v * \mu}{\gamma * cos\theta}, \qquad \text{(Eq.1)}$$

where v – is Darcy's velocity, μ – is the brine viscosity, γ – is oil/water interfacial tension, θ – is contact angle.

The relation between the capillary number and residual saturation is known as the capillary desaturation curve.

It is well known[58] that to reduce residual oil saturation (i.e. enhance oil recovery), the capillary number should be increased drastically to 10^{-3} or higher from the typical number of waterflooding – 10^{-7}. Technically capillary number can be increased by several orders of magnitude by lowering the IFT from 20-50 mN/m to 10^{-3}-10^{-2} mN/m between displacing fluid and oil. In other words, adding a surfactant to injection fluid decreases capillary forces of water, as a result, capillary trapping of oil also reduces.

1.7 Factors affecting IFT

The ability of surfactant to lower IFT to values $\sim 10^{-3}$-10^{-2} mN/m is highly dependent on many factors, including surfactant concentration, oil composition, the concentration of monovalent and divalent ions in brine (salinity), water-oil ratio (WOR), and reservoir temperature and pressure. Reservoir temperature and salinity have been found to have a more critical influence on brine/oil IFT in the presence of surfactant[59, 60].

1.7.1 Temperature effect

In general, the effectiveness of surfactant to reduce IFT between immiscible fluids (brine and oil) is governed by the adsorption of surfactant molecules at the liquid/liquid interface, quantified by the Gibbs adsorption equation[61]. Temperature is one of the main factors that can cause significant changes in the surfactant adsorption at the interface, and thus IFT[62, 63]. According to Gibbs's theory, an increase in temperature results in an increase in the area per molecule, with a consequent decrease in the surface excess concentration of the surfactant[64]. Thus, IFT is expected to decrease with increasing temperature. However, there are a considerable number of experimental studies showing that IFT can also increase at high temperatures[65-68]. For instance, Ye et al.[65] published that oil-water-surfactant IFT decreased with increasing temperature up to 70 °C, and above this temperature increased ("V" pattern) when studying gemini surfactants. The authors considered this temperature as a phase-inversion temperature (PIT) of oil-water-gemini surfactant systems when the emulsion type inverted from oil-in-water (below 70 °C) to water-in-oil (above 70 °C). The same "V" patterns of IFT dependence on temperature were reported by Aoudia et al.[66] and Mosayebi et al.[67] for oil/water systems in the presents of anionic and non-ionic surfactants, respectively. In the work of Aoudia et al.[66], the authors explained the well-defined minimum IFT

with the complex composition of the used oil, which consisted of aromatic, paraffinic, and naphthenic components. This explanation was supported by El-Batanoney et al.[69], who tested the influence of different asphaltene and paraffin wax contents on interfacial behavior between aqueous surfactants solutions and oils. Authors[69] reported that IFT values between surfactant and oil with high asphaltene percentage were lower than corresponding IFT values of oil with high wax content.

Whereas the increase of IFT between crude oil and aqueous surfactant solutions with temperature increasing may be explained by the impact of various oil components[70], the IFT between water and hydrocarbons (n-decane, n-heptane and n-dodecane) was also found to increase at high temperatures[71]. According to the author[71], the water/hydrocarbon IFT increased because hydrogen bonds (H-bonds) broke down between water molecules at the interfacial zone. The reduction of hydrogen bond number in the water at high temperatures was also experimentally demonstrated by using X-ray adsorption spectroscopy (a 10% reduction)[72] and neutron diffraction (a 9% reduction)[73, 74]. Moreover, several experimental and simulation studies[75-77] of water/oil interfacial properties showed that at the interface water molecules oriented themselves in order to create more hydrogen bonds with surrounding water molecules. Notwithstanding, experimental investigations of temperature effect on liquid/liquid interfacial properties at microscale are challenging due to complexities associated with experimental procedures and limitations of experimental equipment to capture the structural properties of molecules at the interface.

1.7.2 Salinity effect

The effectiveness of surfactant solutions in IFT reduction, and consequently, oil recovery efficiency, also strongly depends on the concentration and type of ions present in the formation brine[46]. In general, the presence of salt in natural brines causes a decrease in the solubility of surfactants in the aqueous phase due to the salting-out effect[78, 79]. Thus, more surfactant molecules are forced to approach the interface closely, which leads to the brine/oil IFT decrease. In addition, salts can also enhance the packing of surfactant molecules at the interface due to the counter-ion screening effect between similarly charged surfactant heads, resulting in further brine/oil IFT reduction[80]. Indeed, an increase in NaCl concentration from 10 000 ppm to 100 000 ppm in aqueous cationic surfactant solutions gradually reduced the aqueous phase/oil IFT[79]. This behavior was attributed to the neutralization of surface charges on the surfactant heads with oppositely

charged counter-ions[79]. As a result, the accumulation of surfactant molecules at the interface increased, leading to IFT reduction. A decrease in surfactant/paraffin IFT values was also reported with increasing $MgCl_2$, NaCl, NH_4Cl, and LiCl concentrations measured up to 0.2 M in the aqueous phase[81]. The same decreasing trend was also shown for anionic surfactant systems when NaCl concentration was increased from 0.1 M to 0.5 M[82]. Moreover, the IFT between petroleum sulfonate and heavy oil (and also the oil's polar components, i.e. resins and asphaltenes) was found to decrease rapidly (from 8.5 to 1 mN/m) when NaCl concentration was below 0.2 M and more slowly (from 1 to 0.01 mN/m) at higher NaCl contents[83]. It was suggested that the presence of salt promoted and accelerated the diffusion of petroleum sulfonate molecules to the oil/water interface, resulting in interfacial activity increase, with a consequent IFT decrease[83].

Interestingly, in contrast, Liu et al.[82] illustrated a minimum in IFT when NaCl concentration was increased in the fatty alcohol polyoxyethylene carboxylate surfactant solutions, clearly exhibiting a "V" shaped curve. This observation is supported by the results of Kumar and Mandal[80], who reported that passes through a minimum with increasing NaCl content in anionic and cationic surfactant solutions. Notably, such a "V" shape of IFT as NaCl concentration function was also observed for nonionic surfactants[60]. Bera et al. associated the decrease in IFT with in situ formation of surface-active agents when NaCl salt was added[60].

Despite a considerable number of experimental studies, the existence of two different IFT-salinity patterns cannot be satisfactorily explained. Therefore, while the descending IFT trend can be attributed to the surfactant molecules packing tightly at the interface (due to the reduction of electrostatic repulsive forces between charged molecules), the ascending IFT trend is not well understood. Bera et al.[60] suggested that IFT starts to increase at the point where an accumulation of surface active-agents terminates. Another promising explanation is the partitioning of surfactant molecules into the oil phase as salinity increases, with a consequent formation of micelles in the oil phase[84].

However, due to complexities associated with the experimental procedures and limitations of experimental equipment, it is challenging to investigate the effect of ions at the atomic scale in such systems and capture their precise molecular arrangements at the interface, especially in the presence of surfactants[85].

1.8 Impact on the wettability of carbonate reservoir rocks

The wettability alteration from oil-wet towards more water-wet promotes the spontaneous water imbibition into a porous network and thus enhances the oil recovery during the injection. In this regard, many different surfactants have been tested as surface-active agents for wettability alteration in carbonates[41].

Table 1 represents some literature data of water advancing contact angle changes by using different surfactants in carbonates. As it can be seen in Table 1, the contact angle between water and carbonate surface changes toward a more hydrophilic state upon the addition of surfactants.

Interestingly that the process of wettability alteration of rocks depends on the ionic nature and structure of surfactants. For instance, some anionic surfactants with proxy and ethoxy groups in the presence of Na_2CO_3 have been found to change carbonates' wettability to water-wet[86]. Contrary to this, Standnes and Austad[41] proposed that cationic surfactants are more effective in terms of wettability alteration in carbonates than anionic ones. The authors suggested the formation of ion pairs between positively charged surfactant heads and negatively charged acidic components adsorbed onto carbonate surfaces. As a result, this phenomenon facilitated the desorption of oil from the carbonate surfaces and thus, enhanced the oil recovery factor. It was also observed that the wettability alteration process caused by the electrostatic interactions predominates over the process caused by hydrophobic interactions. This suggestion has also been supported by Jarrahian et al., who studied wettability alteration of carbonate cores using the cationic (CTAB), anionic (SDS), and non-ionic (TritonX-100) surfactants[42]. The authors concluded that CTAB was more effective than TritonX-100 and SDS in changing the wetting state of the surface. The mechanism of wettability alteration has been proposed to stem from the irreversible desorption of stearic acid from carbonate surfaces by CTAB. The non-ionic surfactant changed wettability to a weak water-wet state by adsorbing onto the surface by ion exchange and polarization of π - electrons. Whereas ionic surfactant adsorbed onto a surface by hydrophobic interactions between surfactant tail and adsorbed acid and resulted in a neutral wetting state of surfaces[42].

Table 1. Summary of contact angles changes caused by surfactants treatment.

Surfactant	Type	Contact angle, °		Ref.
		Before treatment	After treatment	
C12TAB	cationic	70	12	41
C16TAB	cationic		27	
C8TAB	cationic		57	
C10TAB	cationic		31	
Hyamine	cationic		21	
Cropol	anionic		55	
ADMBACl	cationic		26	
B 1317	anionic		40	
APES	anionic		44	
Gafac	anionic		75	
SDS	anionic		39	
S-74	anionic		49	
Akypo	anionic		48	
S-150	anionic		63	
C16TAB	cationic	150	86	87
TritonX-100	non-ionic		97	
CTAB	cationic	86	10	80
SDS	anionic	86	3	
Tween-80	non-ionic	86	8	

The anionic surfactant adsorption onto carbonates by hydrophobic interactions has also been observed using molecular dynamic simulations[88]. The authors illustrated a decrease in 20-30° of contact angle and weakening interactions between polar/non-polar oil components by using an anionic surfactant.

It is interesting to point out that some surfactants can be less effective in wettability alteration but, on the other hand, very effective in IFT reduction[80].

1.9 Surfactant adsorption onto carbonate reservoir rocks

Surfactant adsorption during the injection process in an oil reservoir is one of the critical parameters to consider while planning surfactant flooding. The loss of surfactant decreases its effectiveness to lower brine/oil IFT and thus affects project technical and economic feasibility.

Furthermore, despite anionic surfactants have shown a great potential for IFT reduction, the adsorption rate of such surfactants onto carbonate rocks was found to be very high in comparison with sandstone reservoirs. For instance, it was reported that the adsorption amount of anionic surfactant on limestone and sandstone equaled to 0.21 mg/g rock and 0.03 mg/g rock, respectively. In contrast, the adsorption amount of cationic surfactant onto carbonate rocks was found to be 0.12 mg/g rock[89]. The high adsorption rate of anionic surfactants onto carbonates can be explained in terms of electrostatic interactions between the charged part of surfactant and rock surfaces. Generally, brine pH is approximately 7-8 at typical carbonate oil reservoirs with high Ca^{2+} content[90]. At these conditions, the surface charge of carbonate rocks is positive, which makes anionic surfactant with a negative charge attractive to it, resulting in high adsorption. Moreover, in high salinity brines with 5% $CaCl_2$, $MgCl_2$, or NaCl, the adsorption of anionic surfactant has been found to be higher due to the increased positive zeta-potential of the carbonate surfaces[91].

Several promising ways have been reported in the literature to overcome the challenge with high surfactant loss in carbonates. Traditionally, “sacrificial” agents, such as sodium bicarbonate, sodium carbonate, or polyacrylate, have been used in a mixture with injected surfactant fluids in order to decrease the adsorption[92]. The principal scheme of anionic surfactant adsorption onto carbonates and its reduction with agents is presented in Figure 6[92].

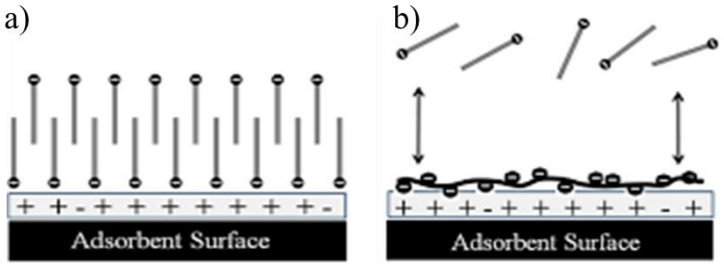

Figure 6. The scheme of anionic surfactant adsorption onto carbonate rock (a) and reduced adsorption due to the use of a “sacrificial” agent (b)[92].

In general, the inclusion of alkali causes pH increase (>7-8), resulting in an alteration of surface charge towards negative, which in turn leads to a decrease in electrostatic interactions of

anionic surfactant and surface. However, some carbonates consist of anhydrite ($CaSO_4$) that can affect the effectiveness of alkali due to $CaCO_3$ precipitation caused by the reaction[93]:

$$CaSO_4 + Na_2CO_4 \rightarrow Na_2SO_4 + CaCO_3 \downarrow$$

It is important to point out that using cationic or non-ionic surfactants results in less adsorption in carbonates compared to anionic surfactant[41]. However, these types of surfactants have been reported to be less effective for brine/oil IFT reduction due to their chemical structure[91]. Therefore, more studies are required in this field in order to discover the optimal chemical composition based on surfactants and "sacrificial" agents that, on the one hand, reduce IFT and, on the other has low adsorption value onto carbonates.

Recently, the use of novel nanoparticle suspensions has also been proposed to be effective and alternative to alkali way for decreasing adsorption of surfactant onto carbonates[94].

1.10 Surfactant flooding modification with nanoparticles

A new class of additives, such as nanoparticles, have been recently proposed to enhance surfactant injection [87, 95-97]. Since then, the interest in using nanoparticles in surfactant EOR has been rapidly growing, with many studies carried out. Nanofluids or nano-assisted chemical EOR is defined as an injection fluid consisted of 1-100 nm nanoparticles in colloidal suspension.

Generally, nanoparticles are classified into three groups – metal oxides (Al_2O_3, ZnO, TiO_2, ZrO_2, SiO_2, etc.), magnetic (Fe_3O_4, etc.), and metallic (Au, Ag, Cu, Pt, etc.)[98-100]. In terms of oil recovery, the most commonly tested nanoparticles are metal oxide owing to their unique physical and chemical properties, among others[101]. Importantly, these nanoparticles have shown high thermal stability and tolerance in the presence of mono – and divalent ions (brine)[102]. In this regard, many studies have been performed to evaluate experimentally the effectiveness of metal oxide nanoparticles aqueous suspension or combination thereof with surfactants as EOR agents.

The main EOR mechanisms of nanoparticles addition to injection fluids (e.g. water, brine, or surfactant) include IFT reduction, wettability alteration, pore channels plugging, disjoining pressure effect, viscosity increase of injected fluids, and blocking asphaltene precipitation. The scheme of mechanisms of nano-assisted EOR is summarized in Figure 7[103].

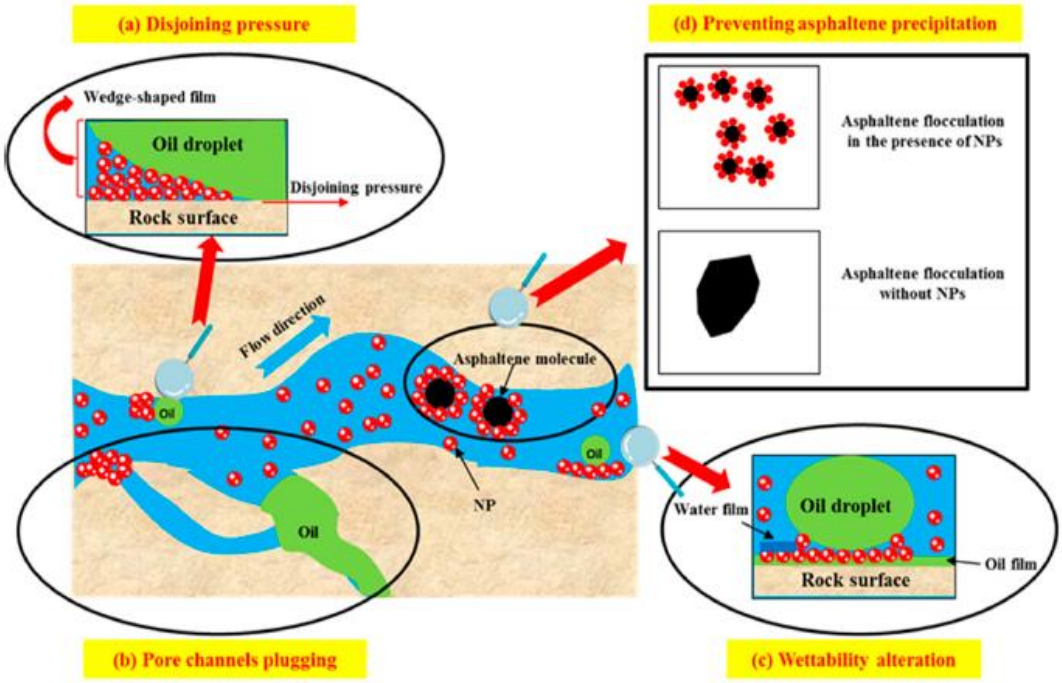

Figure 7. The scheme of mechanisms of nano-assisted EOR[103].

1.11 Nanoparticles influence on oil/surfactant interfacial tension

One of the main purposes of surfactant flooding is decreasing capillary forces of water by reducing the water/oil IFT. Technically, water/oil IFT should be reduced to very low values (10^{-3}-10^{-1} mN/m) in order to increase the capillary number and decrease residual oil saturation[58]. However, such a significant IFT lowering effect has been observed only for the limited class of surfactants, the use of which is unfavorable economically as compared to other EOR methods at the field scale. Moreover, the thermal stability of surfactants and their salinity tolerance remain challenging to achieve at common reservoir conditions.

The addition of nanoparticles has been regarded as a promising way for enhancing surfactant properties by aiding in brine/oil IFT reduction and in increasing the stability of surfactant suspensions[103]. Furthermore, studies also suggest the nanoparticles could reduce the volume of surfactant needed for productivity improvement and thus could improve the project economy.

By now, several studies have been published on the influence of different nanoparticles (ZnO_2, Al_2O_3, SiO_2) on water/oil interfacial and water/air surface tensions in the presence of surfactants[96, 104, 105]. However, in these studies, limited ranges of nanoparticle concentrations (less than <500

ppm or higher than >5000 ppm) have been tested. Furthermore, there are limited data available regarding the influence of salts and temperature on IFT of nanoparticles–surfactant formulations as almost all measurements were conducted in distilled water under atmospheric conditions or only under specific reservoir conditions[106]. Moreover, the impact of nanoparticles on the interfacial layer remains unclear, with some contradicting trends reported in the literature. For instance, Ravera et al.[107] reported that both interfacial and surface tensions of SiO_2 nanoparticles augmented cationic surfactant solutions increased.

On the contrary, Al-Anssari et al.[108] and Lan et al.[109] demonstrated that the addition of SiO_2 nanoparticles to both cationic and anionic solutions led to an IFT decrease. These results are supported by a study[110], in which IFT reduction was observed in the presence of anionic surfactant and relatively high (10 wt.%) amounts of negatively charged nanoparticles. Furthermore, according to the results of Zargartalebi et al.[111], the IFT between the anionic surfactant solutions with small inclusions of either hydrophobic or hydrophilic nanoparticles (1000 ppm SiO_2) and oil significantly decreased when the surfactant concentration was below the critical micelle concentration (CMC). Contrary to this, Esmaeilzadeh et al.[105] observed a slight IFT reduction between diluted surfactant solutions with 0.5 wt.% ZnO_2 and oil. A further increase of surfactant concentration in solutions showed constant IFT for all nanoparticle concentrations tested[105]. In addition, SiO_2 nanoparticles in a mixture with non-ionic surfactant Tween 20 showed a 77% reduction of IFT from 44 to 10 mN/m[112]. The same IFT decrease from 39 to 17.5 mN/m has been observed upon testing the Fe_2O_3/SiO_2 nanocomposites for EOR application that resulted in 31% OOIP improving[113].

Despite having a significant number of publications in this area, researchers worldwide remain inconclusive over the interfacial behavior of nanoparticles augmented surfactant injection fluids. Therefore, further research in this area is required to unveil and explain the mechanism of nanoparticles effects on IFT.

1.12 Nanoparticles influence on mobility ratio of injected fluids

An important parameter for an indication of a displacement process is the mobility ratio between displacing fluid and displaced fluid (oil). The mobility ratio is defined as a ratio of injected fluid mobility to oil mobility[39]:

$$M = \frac{\lambda_{inj}}{\lambda_o} = \frac{k_{rinj}/\mu_{inj}}{k_{ro}/\mu_o} = \frac{k_{rinj}\mu_o}{k_{ro}\mu_{inj}}, \quad \text{(Eq.2)}$$

where λ_{inj} and λ_o are mobilities of injected fluid and oil, respectively; k_{rinj} and k_{ro} – injected fluid and oil relative permeabilities, respectively; μ_o, μ_{inj} - viscosities of oil and injected fluid, respectively.

It is known that high mobility ratio results in viscous fingering of injected fluids showing poor volumetric sweep efficiency and low oil recovery[39, 40]. As can be seen in Equation 2, the mobility ratio can be decreased when either the viscosity of injected fluids is increased, or the viscosity of an oil is decreased. One of the promising ways to increase the viscosity of injected fluids is to add nanoparticles. Indeed, the inclusion of nanoparticles to surfactant and CO_2 based injection fluids showed a viscosity increase by several orders of magnitude compared to the neat fluids[114]. Indeed, Helgeson et al.[115] proposed structural modification of cationic surfactant molecules into cylindrical micelles by the addition of cationically modified SiO_2 nanoparticles (30 nm diameter). A monotonic increase in viscosity was also observed by Nettesheim et al.[116] for cationic solutions in the presence of sodium nitrate and positively charged nanoparticles (30 nm). On the other hand, Bandyopadhyay and Sood[117] observed that nanofluid viscosity first increased and then started to decrease with the increase of nanoparticle content in cationic surfactant cetyltrimethylammonium tosylate solutions. Therefore, more studies in this field are required in order to explain controversial trends in the literature.

It is interesting to note that not only the concentration of nanoparticles affects the viscosity of surfactant solutions, but also the type of nanoparticles. For instance, the addition of SiO_2 nanoparticles resulted in a higher viscosity increase in comparison with Al_2O_3[118].

1.13 Nanoparticles influence on wetting properties of carbonates

Since the development of oil-wet carbonate reservoirs is emerging, different types and combinations of nanoparticles have been tested as additives to surfactant solutions in order to alter wettability towards more water-wet and thus enhance oil recovery[87, 119].

For instance, Omidi et al.[120] tested the effect of Fe_3O_4/eggshell nanocomposites on wetting properties of carbonates separately and in mixture with commonly used surfactants CTAB

(cationic) and TR-880 (zwitterionic). It was observed that Fe_3O_4/eggshell nanocomposites decreased contact angle from 134.2° to 70.28° upon increasing the concentration of Fe_3O_4/eggshell from 100 to 1000 ppm. Moreover, the contact angle has been found to decrease in the presence of TR-880 surfactant and Fe_3O_4/eggshell mixture from 111.9° to 80.8° when only 500 ppm of nanocomposites was added. Notably, that the authors showed that the use of surfactant solutions in the absence of nanocomposites did not change the contact angle significantly. The minimum was achieved at 100°, which represented the oil-wet state of carbonate rocks.

These results were supported by the finding of work[119]. The authors observed that the addition of SiO_2 to SDS surfactant solutions resulted in further contact angle reduction in carbonates. Moreover, the effect was more significant when the surfactant's concentration equaled to CMC. As such, it was found that the water advancing contact angle changed from ∼140° to 72° when only 0.2 wt.% of SiO_2 was added to the SDS solution. In comparison, the treatment in the surfactant only solution resulted in contact angle reduction from ∼150° to 110°, showing hydrophobic wetting properties of carbonates. Therefore, the authors proposed that a mixture of SiO_2 nanoparticles with surfactant solutions could be an effective injection fluid for EOR application in carbonates, where the oil recovery process depends on wettability alteration.

The effect of wettability alteration of carbonate surfaces has also been observed in other studies upon the addition of nanoparticles and/or nanocomposites to surfactant solutions. The results of these studies are presented in Table 2.

As it can be seen from Table 2, the addition of nanoparticles and/or nanocomposites aids a surfactant solution to alter the wettability of carbonates towards more water-wet. As a result, the oil recovery factor also increases. These results have been obtained in different studies with different types of nanoparticles tested, and thus, nanoparticles have been widely regarded as a promising EOR agent in terms of wettability alteration.

The mechanism of nanoparticles' effect on the surface's wetting properties has been found to stem from the structural disjoining pressure. The explanation of this phenomenon was first addressed in the work of Nikolov et al. [130]. According to the authors, the effect of structural disjoining pressure was observed when there was a wedge between fluid (oil) and rock (e.g. intermediate state), whereas no effect occurred when the water contact angle was more than 90° (e.g. hydrophobic state)[131]. Moreover, the structural disjoining pressure was found to be prevalent at the scales larger than the nanoparticles diameter[130].

Table 2. The summary of studies on nanoparticles and/or nanocomposites effect on contact angle, and thus, wettability of carbonates.

Type of chemicals	Chemicals	Contact angle, °		% OOIP	Ref.
		Before treatment	After treatment		
Nanoparticles	SiO_2 + DIW	54.8	57.7	2.9	121
	SiO_2 + Brine	12	40	28	122
	SiO_2 + Ethanol	55	78	23	123
	SiO_2 + Xanthan	86	20	7.81	124
Nanocomposites	Fe_2O_3/SiO_2	138	52	31	125
	Fe_3O_4/chitosan	127	92	10.8	126
	TiO_2/SiO_2/ xanthan	135	45	19.3	127
	NiO/SiO_2	174	32	-	128
Surfactant + Nanoparticles	L-Arg + SiO_2	141	57	13.1	129
	SDS + SiO_2	132	61	-	119
	L-Cys+SiO_2	141	48	12.7	129
	CTAB + NiO	150	60	-	87
	Triton + NiO	150	75	-	
	CTAB + ZrO_2	150	48	-	
	Triton + ZrO_2	150	78	-	

Indeed, when the surface substrate is immersed in a solution containing nanoparticles, nanoparticles tend to order inside the confined geometry of the wedge between oil droplet and surface (Figure 8). This phenomenon stems from the fact that such ordering increases the entropy of the dispersion due to permitting more freedom to nanoparticles in the bulk[131]. As a result, ordered layers of nanoparticles exhibit excess pressure, namely structural disjoining pressure, that tends to separate surfaces confining the nanoparticles. As such, the spreading of nanoparticle films on surfaces is driven by the structural disjoining pressure gradient directed towards the wedge from

the bulk solution and results in a change in the wetting state of the surface by desorbing the oil droplet.

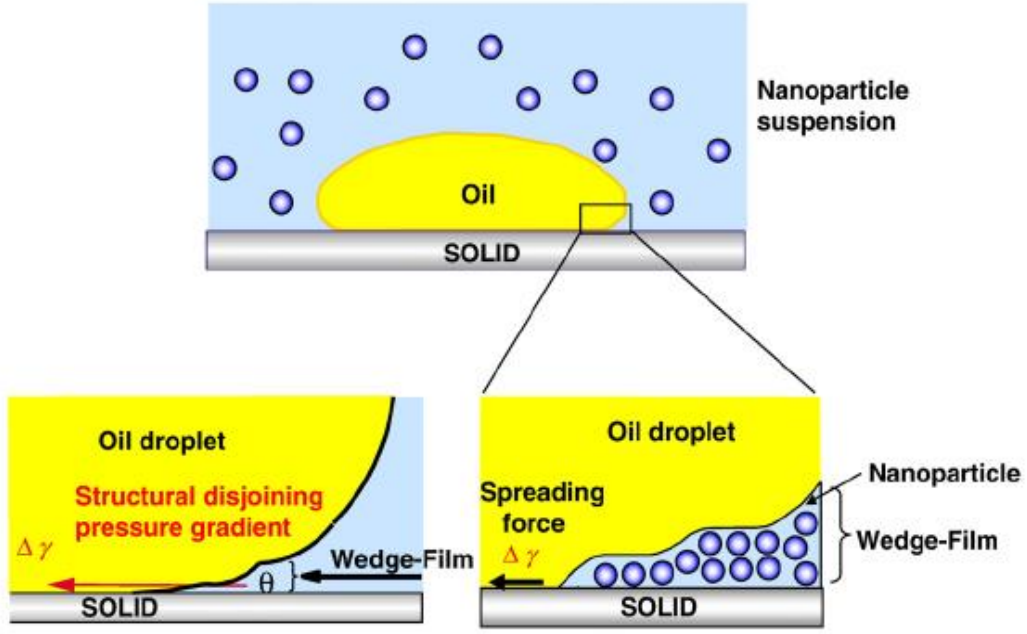

Figure 8. Structuring and ordering of nanoparticles in the wedge between oil and surface resulting in structural disjoining pressure gradient and desorption of oil from surface[131].

1.14 The principles of molecular dynamic simulations

It was shown that an effective approach for detailed studying of effects associated with molecular interactions, arrangements, and orientations at microscale either at air/liquid[85, 132, 133], liquid/liquid[134, 135] or liquid/solid[88] interfaces is molecular dynamic (MD) tool. The MD simulations have been regarded as a complement to traditional experiments, allowing to study the phenomena that cannot be captured in conventional ways. Apart from the MD technique, there is another well-known approach – Monte-Carlo (MC) simulations. However, the main advantage of MD over MC is that it provides information about the dynamic properties of the system, including phase diagrams, transport coefficients, time-dependent responses, etc.

Overall, simulations serve as a bridge between experiments and theory (Figure 9). As such, a theory can be tested by performing simulations with the same model, while the model can be compared with experimental data. Another advantage of simulations is that it allows studying

system properties at conditions that are dangerous or impossible to achieve, e.g. high pressure or temperature.

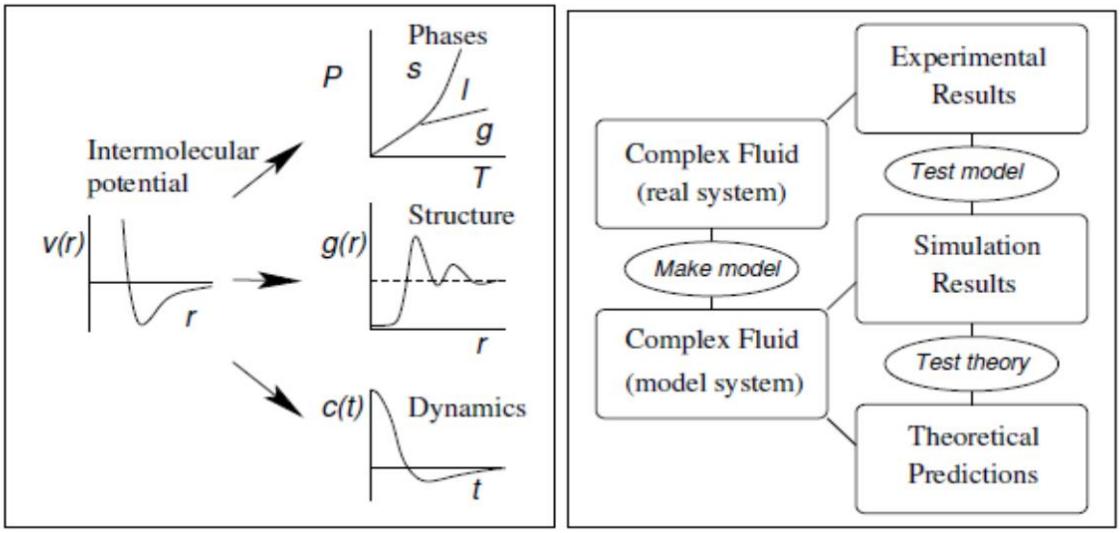

Figure 9. The schematic representation of simulations that serve as a bridge between microscopic and macroscopic properties of the system (left) and experiment with theory (right)[136].

The principle of MD simulations stems from numerical, step by step solution of Newton's equation of motion, which for an atomic system with i components can be written[136]:

$$m_i \ddot{r}_i = f_i;$$
$$f_i = -\frac{d}{dr_i} U,$$

where f_i – forces acting between the atoms, $\ddot{r}_i$ – acceleration, U – potential energy that is a function of $r^N = (r_1, \ldots r_N)$ – a set of atomic coordinates.

In order to calculate forces acting on atoms, the potential energy should be specified and calculated. In general, all information about potential energy in simulations is located in force fields. Force field is a set of functions that describe the interactions between atoms within one

molecule and between different molecules, intramolecular bonding interactions, and non-bonded interactions. As such, total potential energy can be represented by the sum of potential energy derived from non-bonded interactions and bonding potentials[136]:

$$U = \sum_{bonds} \frac{1}{2} k_{ij}(r_{ij} - r_o)^2 + \sum_{angles} \frac{1}{2} k_{ijk}(\theta_{ijk} - \theta_o)^2 + \\ + \sum_{\substack{torsion \\ angles}} \sum_m \frac{1}{2} k_{ijkl}(1 + \cos(m\varphi_{ijkl} - \gamma_m)) + \\ + \sum_{Coloumb} \frac{q_i q_j}{4\pi\varepsilon_0 r_{ij}} + \sum_{vdW} \left\{ 4\varepsilon_{ij} \left[\left(\frac{\sigma_{ij}}{r_{ij}} \right)^{12} - \left(\frac{\sigma_{ij}}{r_{ij}} \right)^{6} \right] \right\},$$

where U_{bond} – oscillations about the equilibrium bond length; U_{angle} – oscillations of 3 atoms about an equilibrium bond angle; $U_{torsion}$ – torsional rotation of 4 atoms about the central bond; $U_{non-bonded}$ – Lennard-Jones and Coulomb potential.

Conventionally, bonding potentials include U_{bond}, U_{angle} and $U_{torsion}$. The U_{bond} is given as a sum of the contributions of all bonds in the system. This can be taken as a chromonical oscillator, where our atoms are presented as balls, connected to a string. Angle bonding term (U_{angle}) involves three coordinates of atoms and is usually taken to be quadratic in the angular displacement from θ_o. The torsion potential $U_{torsion}$ is defined as is a rotation between two groups, i.e. rotation between one bond, and involves four coordinate of atoms. The non-bonded interactions are represented by Coulomb potential and Lennard-Jones potential that calculates the Van der Waals interactions between atoms (Figure 10). The accurate handling of long-range forces is especially important while studying the systems of polyelectrolytes[136].

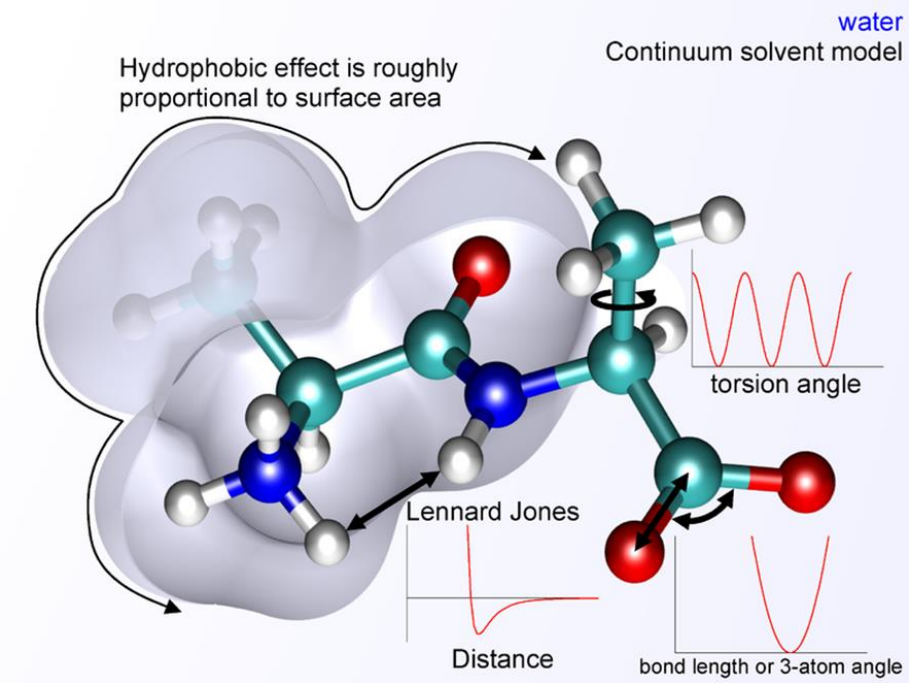

Figure 10. Schematic representation of bonded and non-bonded interactions[138].

1.15 MD applications for studying surfactant and nanoparticles properties

In the past decades, a considerable number of MD simulation studies have been published in the context of surfactant molecules adsorption at the liquid/liquid interfaces[110, 134, 135, 138, 139]. Some results of interfacial tension and configuration of surfactant molecules at water/oil interface calculated and predicted in simulation studies are in good agreement with experimental observations and theoretical models[140, 141]. For instance, Goodarzi and Zendehboudi[142] performed the MD simulations of interfacial behavior of brine/oil in the presence of the non-ionic surfactant at various salt and different temperatures. It was shown that upon salt (NaCl and $CaCl_2$) addition and increasing temperature up to 345 K, brine/surfactant/oil IFT started to decrease. The same descending IFT trends in the presence of anionic sodium dodecyl sulfate (SDS)[143] and cationic cetyltrimethylammonium bromide (CTA)[108] surfactants have been experimentally obtained in the literature. Moreover, MD has appeared to be an effective tool to study the conditions of micelles formation in solution, including size and molecular packing, and the counterions diffusion near the water/oil interface[144]. Chowdhuri and Chandra[145] were the first to apply the MD tool to calculate the hydrogen bonds correlation functions of water molecules in aqueous NaCl and KCl solutions. Further, Bruce et al.[144] showed that counterions diffusion in the water phase was

governed by the shell of surrounding water molecules that ions carried and the formation of contact-ion pairs between ions and the headgroup of SDS surfactant. However, despite this recent progress in understanding the surfactant and counterions interactions and arrangements, there is still a lack of studies regarding fundamental questions of surfactant properties under conditions representing reservoir ones, e.g. high salinity and temperature.

Moreover, there is a limited number of MD studies about nanoparticles' influence at the liquid/liquid interface. By now, the simulations of 3 nm SiO_2 nanoparticles at the n-decane-water interface have been performed in the work[146]i. Authors showed that nanoparticles have a small impact on IFT between n-decane and water and tend to desorb from the interface further inside the aqueous phase, given their hydrophilic nature.

Importantly, there are no MD simulation studies developing nanoparticles and surfactant molecules interaction models at the interfaces so far. The lack of this information can stem from the absence of well-tested hydrocarbon–water force fields and complexities associated with nanoparticles parametrization. Indeed, in practical applications nanoparticles diameter can be up to 80-90 nm, which requires high computational resources[146]. Therefore, in our work, we aimed to cover this knowledge gap by developing the models for nanoparticles and surfactant interactions with regard to make the screening process for nano EOR easier and convenient.

1.16 Research goal

The main goal of this research is to improve the performance of surfactant injection into carbonate oil reservoirs using low-cost additives (such as nanoparticles) and investigate the mechanism of recovery through the scrutiny of the nanoparticles – surfactant and nanoparticles – rock interactions.

As shown in Chapter 1, it is important to study the rock/brine/oil chemical interactions as it gives insight into how to optimally modify wettability towards mixed or water – wet using surfactant-based solutions, which in turn would increase the oil recovery factor from carbonate reservoirs. However, due to complexities associated with existing laboratory methods, which are typically based on macroscale (mm) observations, there is a serious lack of information about microscale wettability characterization of pores that describes the fluid-rock interactions.

Furthermore, although many studies have been published regarding the nanoparticles' influence on surfactant properties, there is still a lack of understanding of their interactions' mechanisms. A systematic and comparative study of interactions between nanoparticles and surfactant molecules under different temperatures and various salinity conditions is also missing in this field.

Moreover, due to complexities associated with the experimental procedures and limitations of experimental equipment, it is challenging to investigate the effect of ions at the atomic scale in surfactant systems and to capture their precise molecular arrangements at the interface.

Importantly, there are no MD simulation studies developing nanoparticles and surfactant molecules interaction models at the interfaces so far. The lack of this information can stem from the absence of well-tested hydrocarbon–water force fields and complexities associated with nanoparticles parametrization.

Therefore, in this research work, we covered the above-mentioned research gaps by resolving the following:

- Investigation of the micro-scale wettability of carbonate reservoir and the reason of hydrophobicity of the rocks;
- Screening, formulation, and optimization of nano-surfactant injection solutions with respect to the wettability results obtained in the previous stage, including determination of

interfacial behavior and measurements of the viscosity of nano-surfactant solutions under varying salt concentrations at different temperatures.

- Investigation of the interfacial behavioral phenomena of different surfactants by molecular dynamics (MD) simulations at various salinities and temperatures. Formulation of principles and predictions of surfactants behavior at the interface for a wide class of ionic surfactants under varying salt concentrations at different temperatures. Explanation of non-Gibbs interfacial behavior of some surfactants at elevated temperatures and salt effects at the interface.
- Establishing and validating the model of silicon nanoparticles to be used in MD simulations. To investigate the molecular nano – surfactant interactions and nanoparticles effect on IFT of the injection solutions through MD simulations.

Chapter 2. Characterization of Organic Layer in Oil Carbonate Reservoir Rocks and its Effect on Microscale Wetting Properties

2.1 Motivation

Effective production of oil from carbonate reservoirs often requires the application of improved oil recovery technologies such as waterflooding. However, conventional waterflooding in carbonates usually results in low hydrocarbon recovery as most of these formations exhibit a complex pore throats structure and are mostly oil-wet. Therefore, improved insight into the causes of the hydrophobic wetting behavior of such reservoirs is important for understanding the fluid distribution, displacement and further enhancing recovery processes. The characterization of fluid-rock interactions is, however, challenging with existing laboratory methods, which are typically based on macroscale (mm) observations. Therefore, in this work, the methodology for the comprehensive investigation of microscale (μm) wettability variations in carbonate rocks covered with organic layers has been developed. As such, the key element of this chapter is to investigate the nature of the layers adsorbed onto real carbonate surfaces that make wettability of carbonates oil-wet.

Moreover, the chemical bond of this layer and carbonate rock surfaces should be discovered in order to formulate the optimal injection fluid with surfactant for future EOR.

2.2 Materials and methods

2.2.1 Core samples

Carbonate rocks were sampled from the oil-saturated zone of an oil carbonate reservoir (Figure 11). All of the cores consisted of 99.8% of calcite with small impurities of magnetite and quartz. Samples were subsequently cut and prepared for microscopic measurements.

2.2.2 Core preparation

Original core samples were broken into several clumps. Then, clumps were flooded with kerosene and toluene consistently to remove initial crude oil from the cores until effluents became transparent. Once the extraction was finished, clumps were dried to a constant weight and then placed in vials under the exhaust hood for 48 hours to complete solvent evaporation. Experiments were conducted with original core samples and the cores after kerosene and toluene extractions.

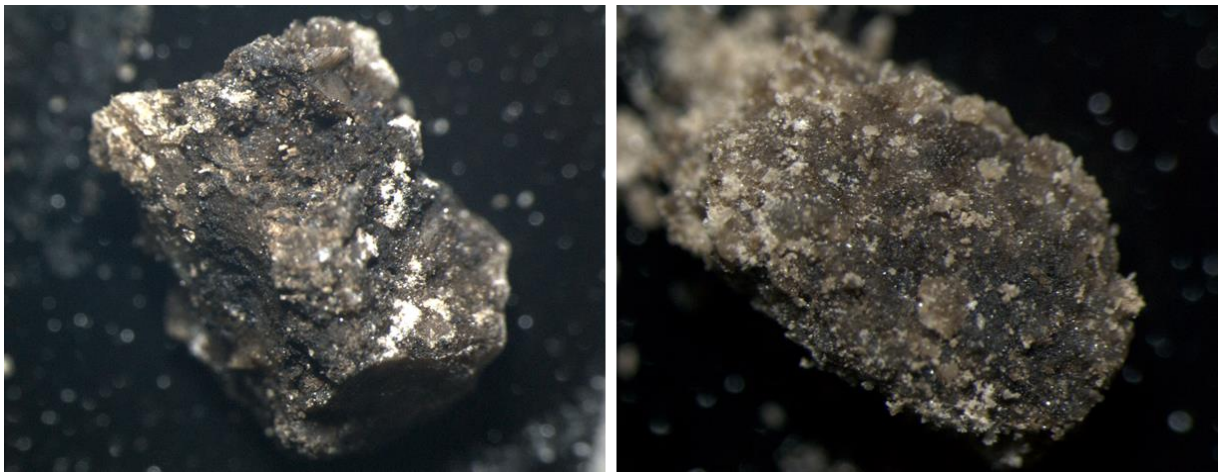

Figure 11. Optical image of studied carbonate rocks samples before treatment with kerosene and toluene

2.2.3 SEM and ESEM tests

In general, the principle of scanning electron microscope lies in detecting the interactions between the atoms in the analyzed object and the electron beam directed on the object at different depths. The interaction between electrons of the beam and the sample material results in the generation of various types of signals, including secondary electrons (SE), back-scattered electrons (BSE), characteristic X-rays and transmitted electrons. This data provides information about the topography of the sample and its elemental composition. Usually, detectors of secondary electrons are equipped in all SEMs, whereas not all SEMs have detectors of all other signals.

Secondary electrons are detected from the first few nanometers (in-depth) of the sample surface as they have low energies $\sim$ 50 eV that limits their travel through the sample. However, the signal from SE provides images of a sample surface with a high-resolution $\sim$ 1 nm. In contrast, back-scattered electrons are a result of reflection from the sample by elastic scattering effect and have higher energies than SE. Therefore, BSE are emitted from deeper areas of the sample, and thus, the image has less resolution than the SE image. However, the intensity of BSE signals is correlated with a particular atomic number of the sample, and thus, is usually coupled with characteristic X-ray analysis. Characteristic X-rays are produced when the beam electron interacts with an atom from the sample and removes an inner shell electron from it, resulting in energy release. The wavelength or energy of such characteristic X-rays can be detected by Wavelength-dispersive X-ray spectroscopy (WDS) or Energy-dispersive X-ray spectroscopy (EDX or EDXS), respectively.

This analysis provides information about the quantitative data of elemental composition in the sample and their distribution throughout the sample (map distribution).

Conventionally, the work with a scanning electron microscope can be divided into two parts: the work in high vacuum mode (below 10^{-5} Pa) and the work in low vacuum mode (up to 4000 Pa). The main advantage of the high vacuum mode is that it has the best spatial resolution, whereas the advantage of the low vacuum is the possibility to examine the samples in their initial state. However, the advantages of both modes can be combined by using cryogenic microscopy (Cryo-SEM) under a high vacuum. By freezing the object, one can preserve its structure (the object is "alive") and obtain an image with high spatial resolution due to the high vacuum. Importantly that it was shown that freezing a sample by liquid nitrogen would not affect the relative location of the fluids in the porous network[147].

Interestingly the wetting properties of surfaces can be studied by using advanced SEM coupled with a special Peltier table, namely Environmental Scanning Electron Microscopy (ESEM). The idea of this method is to achieve the condition to condense the moisture from the microscope chamber onto the sample surface. ESEM experiment suggests that the sample is placed into the vacuum chamber of the SEM on a Peltier stage, which allows maintaining the sample temperature in a range between −25 °C and +25 °C. For water condensation on the samples' surface, the temperature should be held near 0 °C, and the chamber pressure should be varied in a wide range between 600 Pa and 900 Pa in order to achieve the dew point of water.

Therefore, in this chapter, the wetting properties of carbonate surfaces with hydrocarbon layers were analyzed using SEM/FIB Versa 3D DualBeam (FEI, USA), equipped with a Schottky field emission gun and EDXS system (EDAX, USA). The study was conducted in high vacuum and ESEM modes. The images were obtained in the secondary electron (SE) mode using the gaseous secondary electron detector (GSED).

At the beginning of the wettability study, it was important to achieve the conditions when water droplets start to condense from the chamber environment to the sample surface. Therefore, by varying the pressure and temperature in the chamber, it was experimentally observed that for sessile droplets, formation pressure should be kept around 850 Pa and a temperature of 0 °C. This is illustrated in Figure 12, which provides the sequence of droplets growing on an initial carbonate sample under conditions near the triple point of water: 0.1 °C, 850.1 Pa.

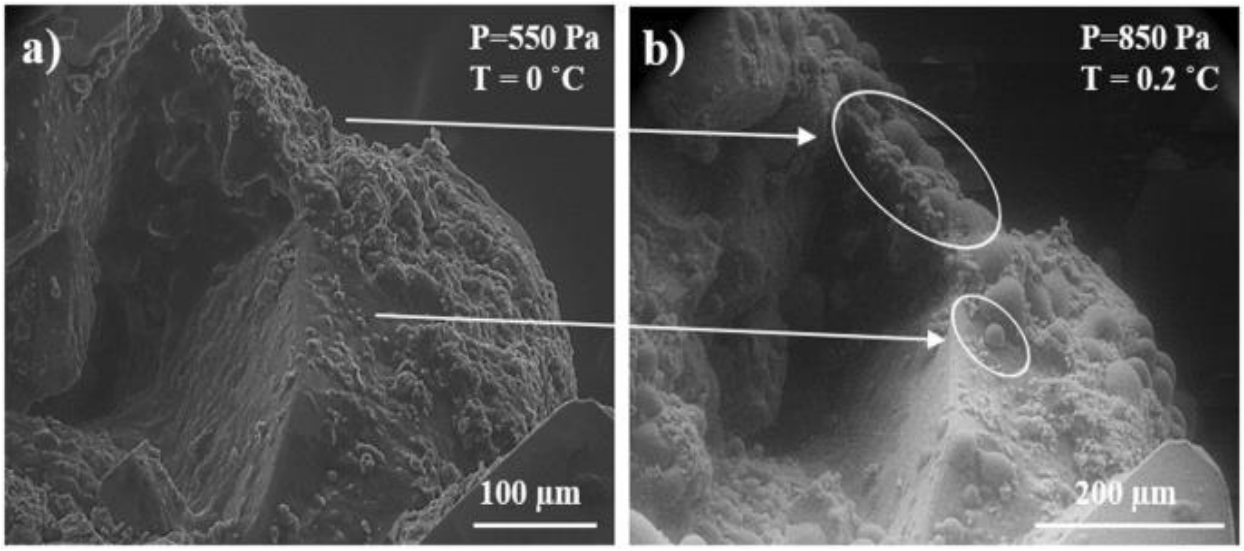

Figure 12. (a) ESEM image of the initial carbonate rock sample. The sample temperature was 0 °C and chamber pressure was 550 Pa. (b) ESEM image of the same sample with formed water droplets. Micro-droplets of distilled water are marked by the white circles. The sample temperature was 0.2 °C and the chamber pressure was 850 Pa.

2.2.4 Cryo-FIB

In this chapter, we also aimed to study the physical-chemical properties of layer adsorbed onto carbonate rocks, including its elemental composition and thickness, and bonds within the layer and with the surface.

Therefore, in order to study the properties of such layers, the cryogenic focused ion beam (Cryo-FIB) approach has been utilized. The main advantage of the Cryo-FIB technique is that it provides a unique opportunity to prevent structural damage of the sample during the preparation of thin cross-sections of heat-sensitive materials. The cross-section area of the sample was prepared by Ga+ FIB and the sample was protected with 2 µm Pt layer deposited by e− beam on the top of the area of interest before the FIB procedure.

The experiments were carried out using Versa 3D FIB/SEM and Quorum PP3010T Cryo-FIB/SEM Preparation System (Quorum Technologies Ltd, UK) at a temperature below −140 °C. Samples were placed into the vacuum chamber of the microscope on Cryo-stage. Cooling of the latter was ensured by the continuous circulation of liquid nitrogen. Sequential thinning of the sample with decreasing of accelerating voltages from 30 kV to 2 kV of Ga+ was used to minimize amorphization.

2.2.5 S/TEM

The cross-section of the sample was studied in a Titan 80–300 S/TEM (FEI, USA), equipped with a Schottky field emission gun, spherical aberration corrector (Cs probe corrector), energy-dispersive X-ray spectroscopy (EDXS) system (EDAX, USA) and Gatan Image Filter (GIF) (Gatan, USA). The research was carried out at an accelerating voltage of 300 kV in bright field and dark field modes. A high angle annular dark field (HAADF) detector (Fischione, USA) was used for obtaining Z-contrast images in the S/TEM mode.

2.2.6 EELS

The electron loss spectroscopy (EELS) has been utilized in order to study the chemical bonding within the layer and with the carbonate surface. The idea of this method lies in detecting the amount of energy loss by beam electron when it undergoes inelastic scattering (plasmon excitations, inner shell ionizations, inter-and intra-band transitions, phonon excitations and Cherenkov radiation) that in turn can be interpreted in terms of what resulted in energy loss.

In this chapter EELS spectra were obtained in STEM mode from thin layers of the specimen. Qualitative analyses were carried out by comparing the actual shape of the ionization energy loss for the measured points from sample areas containing calcite and amorphous carbon[148].

2.2.7 Contact angle evaluation

Once the appropriate conditions for droplets formation were found, droplet dimensions were determined using Fiji platform[149]. Contact angles (θ) were calculated using the height (h) and the radius (r) of extracted droplet profiles (Figure 13). Assuming that the droplet size is small, its profile can be approximated in the form of a circle. The following procedure was used to evaluate the contact angle on the microscale (μm):

1. For the contact angles calculations, the images of droplets sitting on the sample surface tilted respectively their normal were obtained.
2. After recording the images, the droplet profiles were cut from the SEM images using open-source image processing software ImageJ coupled with Fiji platform[149].
3. After droplet profiles had been cut, they were rotated to a horizontal position in the image coordinates (pixels), where the shape of the droplet was quite clear.
4. Distance in pixels was then converted into the length dimension (μm) using ImageJ software.

5. Once optimal orientation and length conversion had been obtained, the height and radius of droplets were determined by measuring the length of corresponded edges of droplets using ImageJ software.
6. Once geometric parameters (h, r) had been detected, contact angles were calculated using the following equations:

$$\theta = \tan^{-1}\frac{h}{r};$$
$$\theta = 2\theta_1.$$

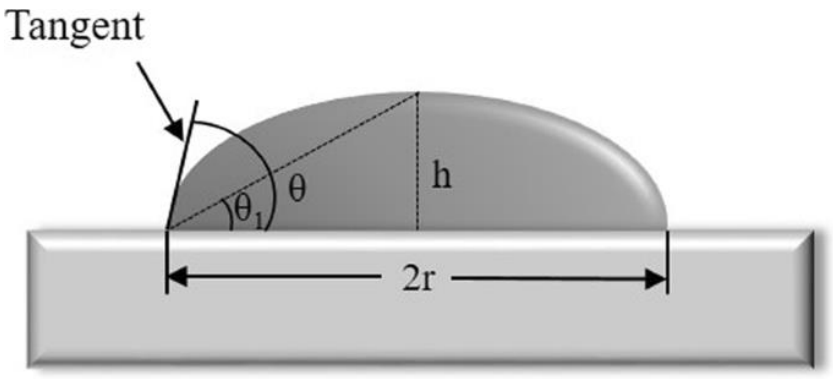

Figure 13. Drop shape analysis for contact angle evaluation.

Wetting properties were defined by the contact angle value. The surface was considered to be hydrophobic if $\theta > 90°$ and hydrophilic if $\theta < 90°$. Surfaces had mixed wetting properties if they consisted of both hydrophobic and hydrophilic zones.

2.3 Results

2.3.1 Micro-wettability investigation of the initial carbonate sample

Before studying the physical-chemical properties of the adsorbed layer and the wetting properties of core samples after kerosene and toluene extractions, we established the methodology for obtaining reliable data of droplets growing at the surfaces. Owing to the fact that water droplets formation is an uncontrollable process in such conditions, and droplets condense randomly at the

surface, it was important to establish the measuring procedure for all samples to get accurate contact angle results.

Indeed, as can be observed from Figure 14a, water droplets started appearing on the surface at 1:32 minutes and then continue to grow until almost all of them coalesce into one large droplet (Figure 14d). Such coacervating changes the contact line between phases and impedes contact angle calculation. An example for the initial carbonate sample is shown in Figure 14, which illustrates that after a while droplets start to merge into each other, forming a large droplet that covers all surfaces.

Thus, for the appropriate contact angles evaluation, we selected a water condensation time of around 1:30 minutes for this sample. Notable that this time is slightly different for different samples owing to the sample size, structure, and cooling rate.

Therefore, we performed the time-lapse analysis of droplets formation with all samples prior to contact angle calculation in order to select the moment when droplets have just appeared. The same procedure has been suggested in the literature that describes ESEM method[150, 151].

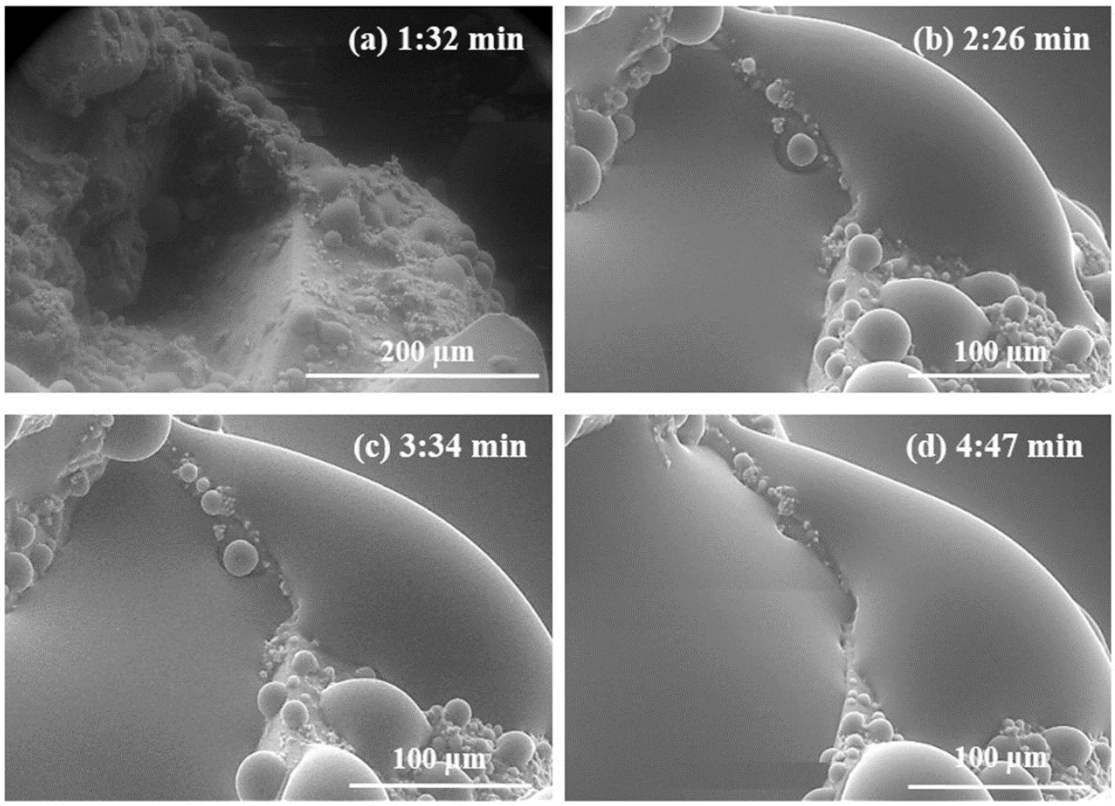

Figure 14. Water droplets formation on the initial carbonate surface in dependence of time from 1:32 minutes (a) to 4:47 minutes (d). The sample temperature and chamber pressure were kept around 0 °C and 850 Pa, respectively for every experiment.

Once thermobaric conditions and time for droplets growth have been experimentally found, the droplets were cut from the imaged region (Figure 15) and analyzed using image processing software ImageJ[149] (see contact angle evaluation procedure) to calculate contact angle values (Figure 15b).

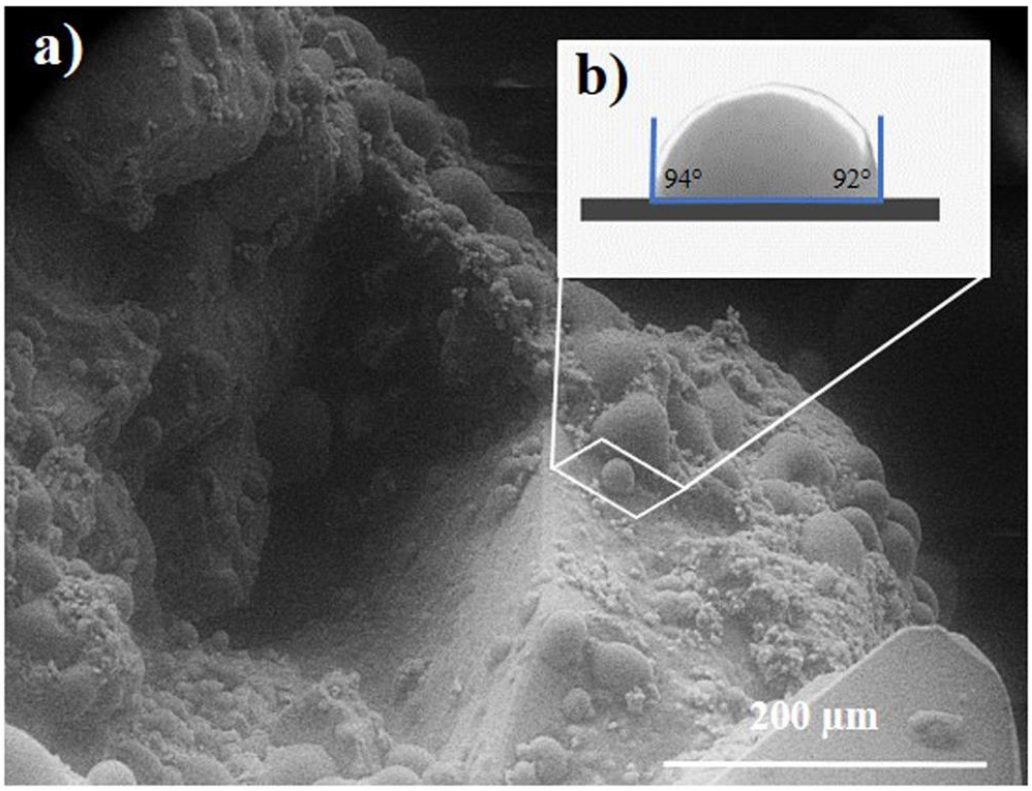

Figure 15. (a) ESEM image of initial carbonate rock with formed water droplets. (b) Extracted from (a) droplet with measured dimensions – the height of 0.24 µm and radii of 0.22 µm (left) and 0.23 µm (right). The average contact angle is 93 ± 1°.

The measured micro-droplet height was 0.24 µm, and radii from the right side and the left side equaled to 0.23 µm and 0.22 µm, respectively. Then, the average contact angle was calculated to be 93 ± 1°. This value corresponded to the hydrophobic wetting behavior of the surface.

The same procedure has been implemented for all other original samples (at least two droplets were cut and analyzed). The results are presented in Table 3.

Table 3. The contact angles that were calculated for all original samples.

№ sample	Time of droplets formation, min	Contact angle	Wetting preference
1	1:28	1. 94˚± 2˚ 2. 96˚ ± 4˚	Oil-wet
2	1:33	1. 98˚± 4˚ 2. 102˚ ± 4˚	Oil-wet
3	1:35	1. 101˚± 1˚ 2. 97˚ ± 6˚	Oil-wet
4	1:30	1. 93˚± 1˚ 2. 95˚± 3˚	Oil-wet
5	1:31	1. 118˚± 7˚ 2. 109˚ ± 3˚	Oil-wet
6	1:27	1. 106 ˚± 5˚ 2. 98 ˚± 3˚	Oil-wet
7	1:32	1. 97˚± 3˚ 2. 95˚ ± 3˚	Oil-wet
8	1:28	1. 93˚± 5˚ 2. 91˚ ± 3˚	Oil-wet
9	1:27	1. 93˚± 2˚ 2. 96˚± 3˚	Oil-wet
10	1:24	1. 99˚± 3˚ 2. 103˚± 4˚	Oil-wet
11	1:30	1. 102˚± 6˚ 2. 105˚± 2˚	Oil-wet
12	1:25	1. 100 ˚± 7˚ 2. 108˚ ± 2˚	Oil-wet

As can be seen from Table 3, all original samples before kerosene and toluene extractions showed oil-wet preference on micro-level with contact angles more than 90˚. This can be due to the impact of oil that is presented on the carbonate surface.

2.3.2 Micro-wettability investigation of the sample after kerosene extraction

As it was found in the previous section, the wettability of the original rock is hydrophobic, which is caused by the abundance of oil in the samples. Kerosene solvent extraction has been

regarded as a mild extraction that removes the majority of oil from the sample, and thus, affects wettability. However, the effect of kerosene on wetting properties of the surface is still remained unrevealed due to complexities associated with capturing fluid-rock interactions. Therefore, in this part, we aimed to analyze the contact angle calculated on samples after kerosene extraction at the micro-level.

Following the procedure (see the previous section) of water droplets growing at the surface, we first determine the time of their appearance for all samples studied. The data is presented in Table 4.

As can be seen in Figure 16, kerosene removed all oil from the samples. However, a detailed study revealed that there are still some areas on surfaces that exhibit oil wetness (Figure 16b). The existence of areas with different wetting preferences suggests that microscale wettability is mixed wet.

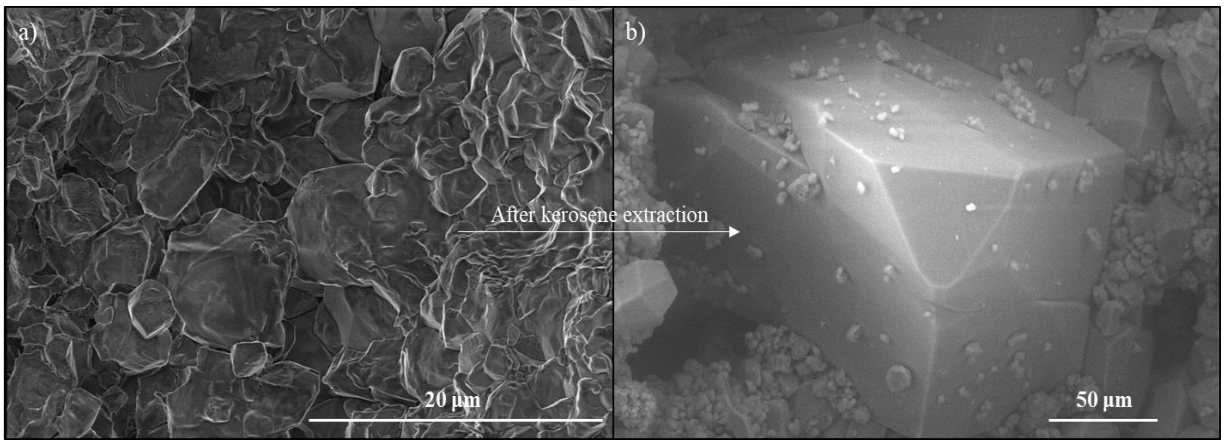

Figure 16. SEM images of carbonate rock surfaces before (a) and after (b) kerosene extraction.

As such, some surface areas have shown strongly hydrophilic wetting preferences, while others – hydrophobic (Figure 17). This can be explained by considering the fact that kerosene is a mild solvent, i.e. it removes free or weakly bonded oil and cannot remove chemically adsorbed components from oil onto the interface.

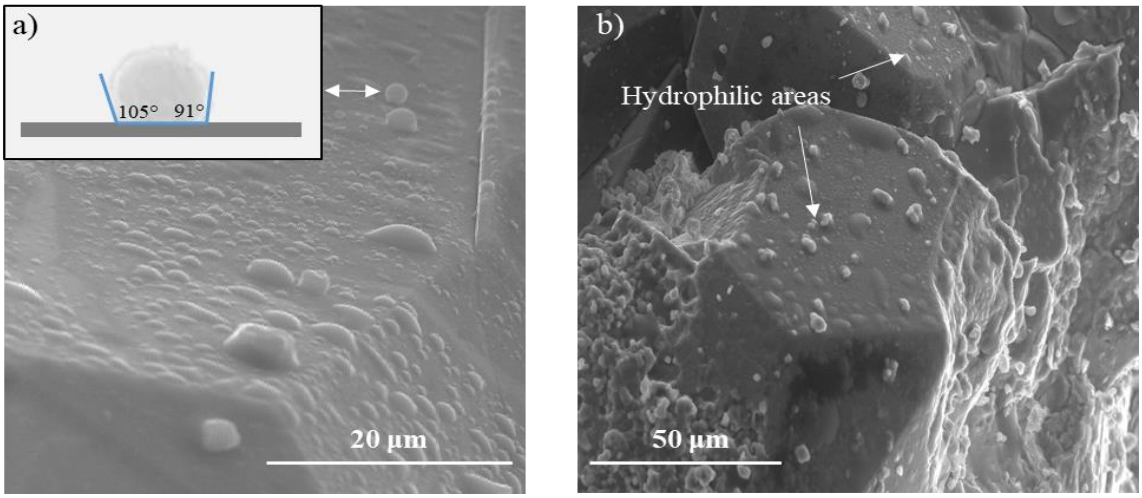

Figure 17. ESEM images with formed water droplets on carbonate surface after kerosene extraction – (a) represents hydrophilic and hydrophobic areas, while (b) hydrophilic.

The same results have been obtained for all samples after kerosene extraction (Table 4). The contact angles were calculated in two points in a way that one point represents the hydrophobic surface (where the droplet is approaching the shape of a sphere) and another one – hydrophilic (where the droplet is wetting the surface). However, in some samples, e.g. №4, 6, 8, 9, 10, and 11 it was challenging to cut the area with a droplet as it has completely spread on the surface, showing the contact angle close to 0°.

Interestingly that in comparison with data for original samples, contact angles have decreased after kerosene extraction. Although contact angles have been reduced up to ∼ 2-14% (Table 4), the wetting state of the surface shows more hydrophobic behavior than hydrophilic. This fact can be explained in terms of forces that act between molecules within the adsorbate and between adsorbate and surface. As it was shown, kerosene removed the oil that was free or physically bonded with the surface or another layer of oil at a surface. As a result, oil components that have been chemically adsorbed onto the surface remained unmoved by kerosene. However, cleaning oil resulted in a decrease of forces acting within the adsorbate, making the attractive force acting between adsorbate and surface higher than them, and thus, the contact angle changed towards slightly hydrophobic.

Table 4. The contact angles that were calculated for all samples after kerosene extraction.

№ sample	Time of droplets formation, min	Contact angle	Wetting preference
1	1:30	1) 92˚± 7˚ 2) 16˚ ± 3˚	Mixed-wet
2	1:28	1) 88˚± 3˚ 2) 18˚ ± 4˚	Mixed-wet
3	1:25	1) 93˚± 2˚ 2) 21˚ ± 5˚	Mixed-wet
4	1:31	1) 98˚± 8˚ 2) ∼0 ˚	Mixed-wet
5	1:27	1) 101˚± 8˚ 2) 43˚ ± 3˚	Mixed-wet
6	1:34	1) 96˚± 4˚ 2) ∼0 ˚	Mixed-wet
7	1:31	1) 86˚± 3˚ 2) 27˚ ± 5˚	Mixed-wet
8	1:25	1) 87˚± 5˚ 2) ∼0 ˚	Mixed-wet
9	1:30	1) 85˚± 2˚ 2) ∼0 ˚	Mixed-wet
10	1:32	1) 89˚± 3˚ 2) ∼0 ˚	Mixed-wet
11	1:28	1) 94˚± 2˚ 2) ∼0 ˚	Mixed-wet
12	1:22	1) 86˚± 6˚ 2) 25˚ ± 2˚	Mixed-wet

2.3.3 Micro-wettability investigation of the sample after toluene extraction

In order to ensure that no free oil is left in the samples, rock samples have been further cleaned with toluene, which is regarded as a strong solvent. The oil-free samples were needed in order to study the properties of remained strongly adsorbed layers that are the first layers to adsorb onto carbonates, and thus, the reason of wettability alteration towards oil-wet.

Therefore, using the same procedure, experiments were conducted with the samples after toluene extraction. As it can be seen in Figure 18 (Sample 4) four water droplets were highlighted and analyzed – two were very similar with an average contact angle of $160 \pm 3°$ (Figure 18c,d), one had dimensions of 0.19 µm (height) and 0.51 µm (diameter) with the average contact angle of $73 \pm 1°$ (Figure 18e), and the last droplet had dimensions of 0.07 µm (height) and 0.74 µm (diameter) with the average contact angle of $22 \pm 2°$ (Figure 18f). The presence of several distinct contact angles, which represent hydrophobic and hydrophilic zones of surface, suggests that the sample's micro-wettability is mixed. The same results have been obtained with samples after kerosene extraction.

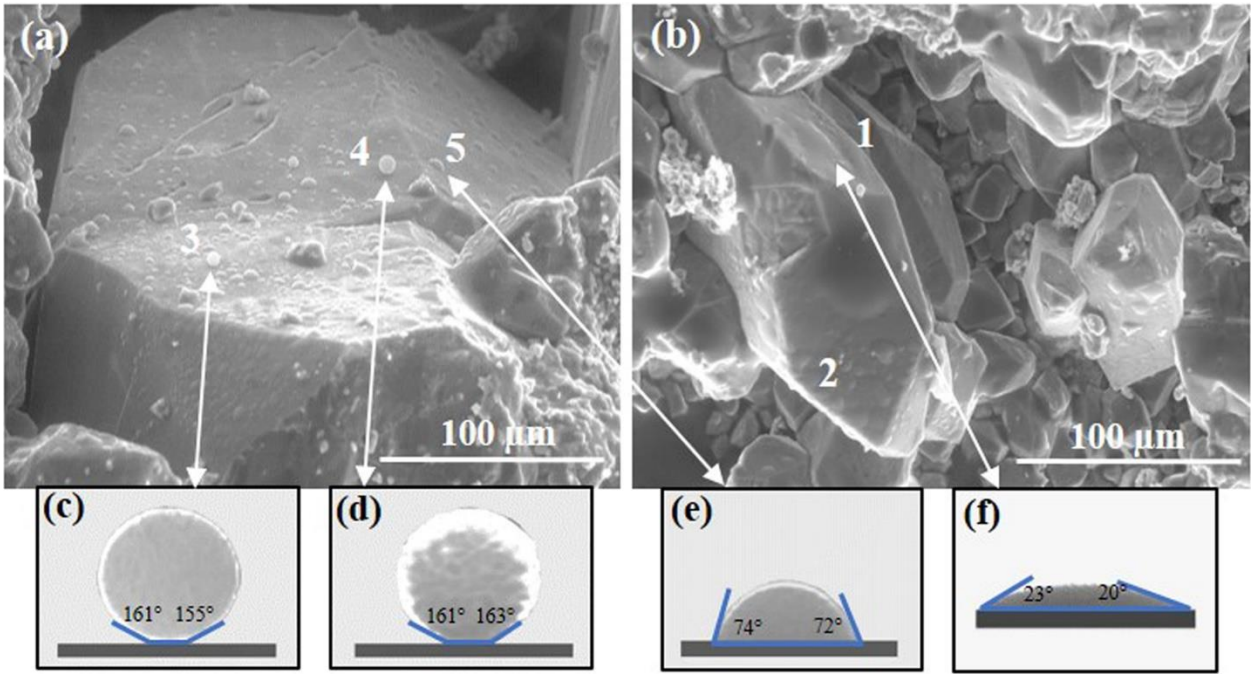

Figure 18. (a,b) ESEM images with formed water droplets on carbonate surface after solvent extraction; (c–f) Extracted droplet profiles from the picture (a,b) respectively with calculated contact angles; (c–e) droplet images represent mixed wetting properties of carbonate surface with two different types of contact angle – $160 \pm 3°$ and $73 \pm 1°$; (f) image refers to hydrophilic wetting properties with the average contact angle of $22 \pm 2°$. X-ray analyses were performed in points 3, 4, 5 in (a) and 1, 2 in (b) ESEM images. The sample temperature and chamber pressure were kept around 0 °C and 850 Pa, respectively.

Results for all samples are presented in Table 5. As it can be seen in Table 5, the wetting preferences of carbonate surfaces have been changed towards more water-wet after toluene extraction. This is due to the fact that toluene is stronger as a solvent than kerosene. As such, almost all samples, except №3 and 4 showed complete water spreading on a surface with a contact angle close to 0˚. Interestingly that the hydrophobic areas have been still observed in all samples except for one sample, that showed completely water-wet wetting behavior. This finding can be explained by assuming that the analyzed area of this sample was not big enough to find hydrophobic zones.

Furthermore, to analyze the type of surface to which water droplets have adhered, the EDX approach has been used. Elemental composition was determined for sample №7 in different points highlighted in Figure 18. Analysis of the surface which showed the non-oil-wet nature (Figure 18b points 1 and 2), showed the pure calcite ($CaCO_3$) with less than 1% impurities, while elemental estimation of oil-wet surfaces (Figure 18a points 3 and 4) demonstrated strong carbon signal (Figure 19).

Calcite ($CaCO_3$) was determined at points 1 and 2 (Figure 19) using a simple proportion between concertation of elements:

$$Ca: C: O = 20: 17: 63 \sim 1: 1: 3$$

However, at points 3 and 4 no molecular formula was determined using this ratio due to the high amount of carbon, which exceeded the necessary amount for the calcite. As such, elemental composition, captured at points 3 and 4, confirmed the presence of the additional carbon, which represented the adsorbed organic layer on calcite.

Table 5. The contact angles that were calculated for all samples after toluene extraction.

№ sample	Time of droplets formation, min	Contact angle	Wetting preference
1	1:26	1) 85˚± 3˚ 2) ∼0˚	Mixed-wet
2	1:22	1) 91˚± 4˚ 2) ∼0˚	Mixed-wet
3	1:23	1) 95˚± 5˚ 2) 18˚ ± 6˚	Mixed-wet
4	1:28	1) 162˚± 1˚ 2) 158 ± 3˚ 3) 73˚± 1˚	Mixed-wet
5	1:24	1) 104˚± 4˚ 2) ∼0˚	Mixed-wet
6	1:30	1) 88˚± 2˚ 2) ∼0˚	Mixed-wet
7	1:26	1) ∼0˚ 2) ∼0˚	Hydrophilic
8	1:21	1) 85˚± 4˚ 2) ∼0˚	Mixed-wet
9	1:30	1) 82˚± 3˚ 2) ∼0˚	Mixed-wet
10	1:25	1) 81˚± 1˚ 2) ∼0˚	Mixed-wet
11	1:22	1) 88˚± 3˚ 2) ∼0˚	Mixed-wet
12	1:26	1) 82˚± 3˚ 2) ∼0˚	Mixed-wet

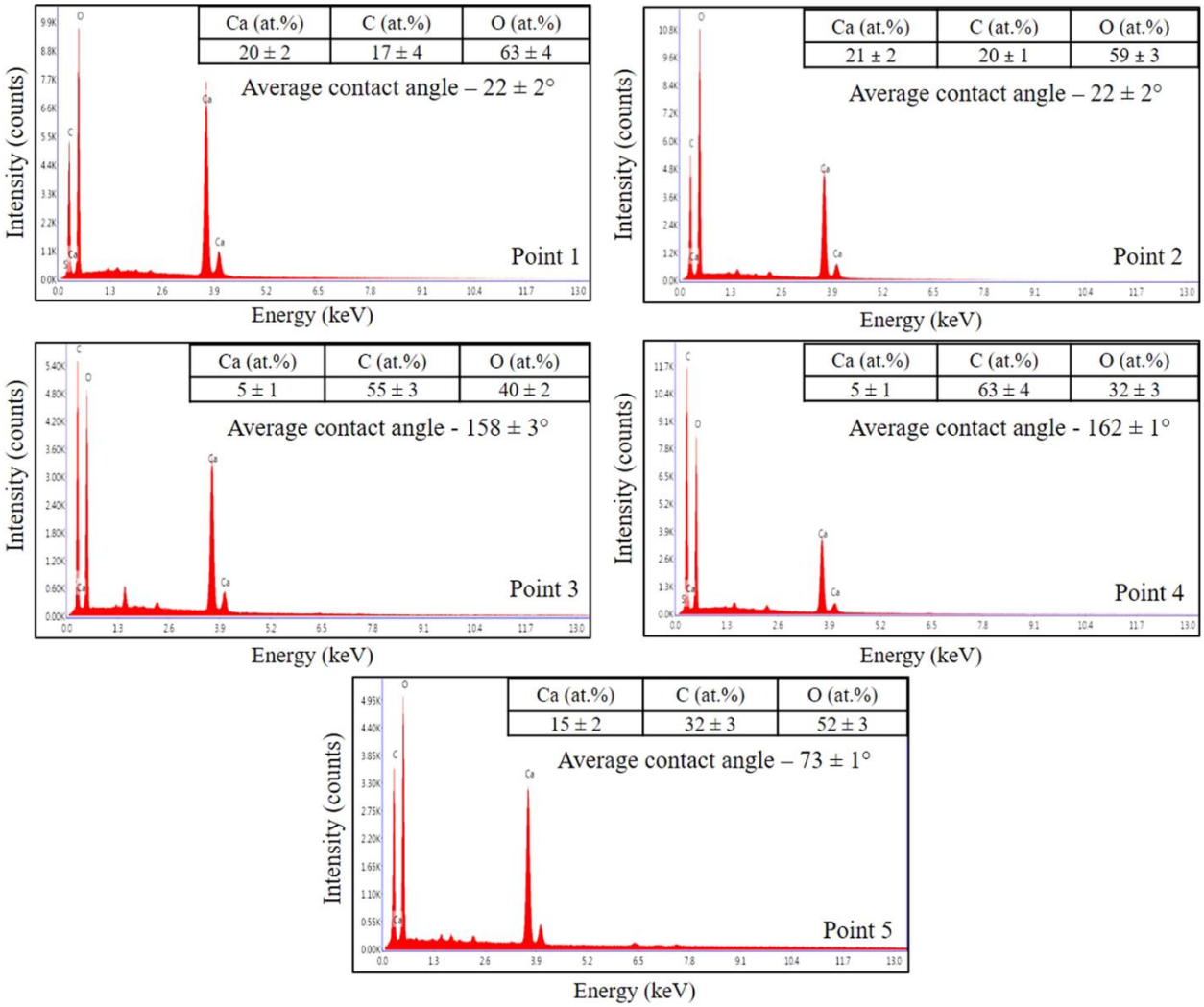

Figure 19. EDX spectra of different points on the surface, showing element concentrations. Points 1 and 2 represent surfaces with the average contact angle of 22 ± 2°; points 3 and 4– 158 ± 3° and 162 ± 1° respectively; point 5–73 ± 1°. At points 3 and 4 a large amount of carbon − 55 ± 3 at.% and 63 ± 4 at.% was obtained, respectively.

2.3.4 Characterization of the thin organic layer

To demonstrate the presence of the organic layer on the carbonate surface and study its physical-chemical properties, we used a carbonate sample after toluene treatment. Analysis of the sample after toluene extraction allowed the remaining organic layer to be determined without the influence of oil. The location of the organic layer on the sample was identified using the results for the micro-wettability study and supported by EDXS experiments with the cross-section specimen. The sample surface, which had hydrophobic wetting properties (Figure 18a), was cut

by the Cryo-FIB technique. Then, S/TEM, EDXS, and EELS analyses were carried out to characterize the microstructure of the sample, elemental composition, and thickness of the organic layer, respectively. This part of the study illustrates the most innovative and complicated procedures in micro-and nanoscales experiments presented in this chapter.

Owing to the crisp contrast between phases (Figure 20d), the thickness of the organic layer was estimated by measuring the length of the dark layer between platinum and calcite. Using this criterion, the estimated thickness of the organic layer was 180 ± 12 nm.

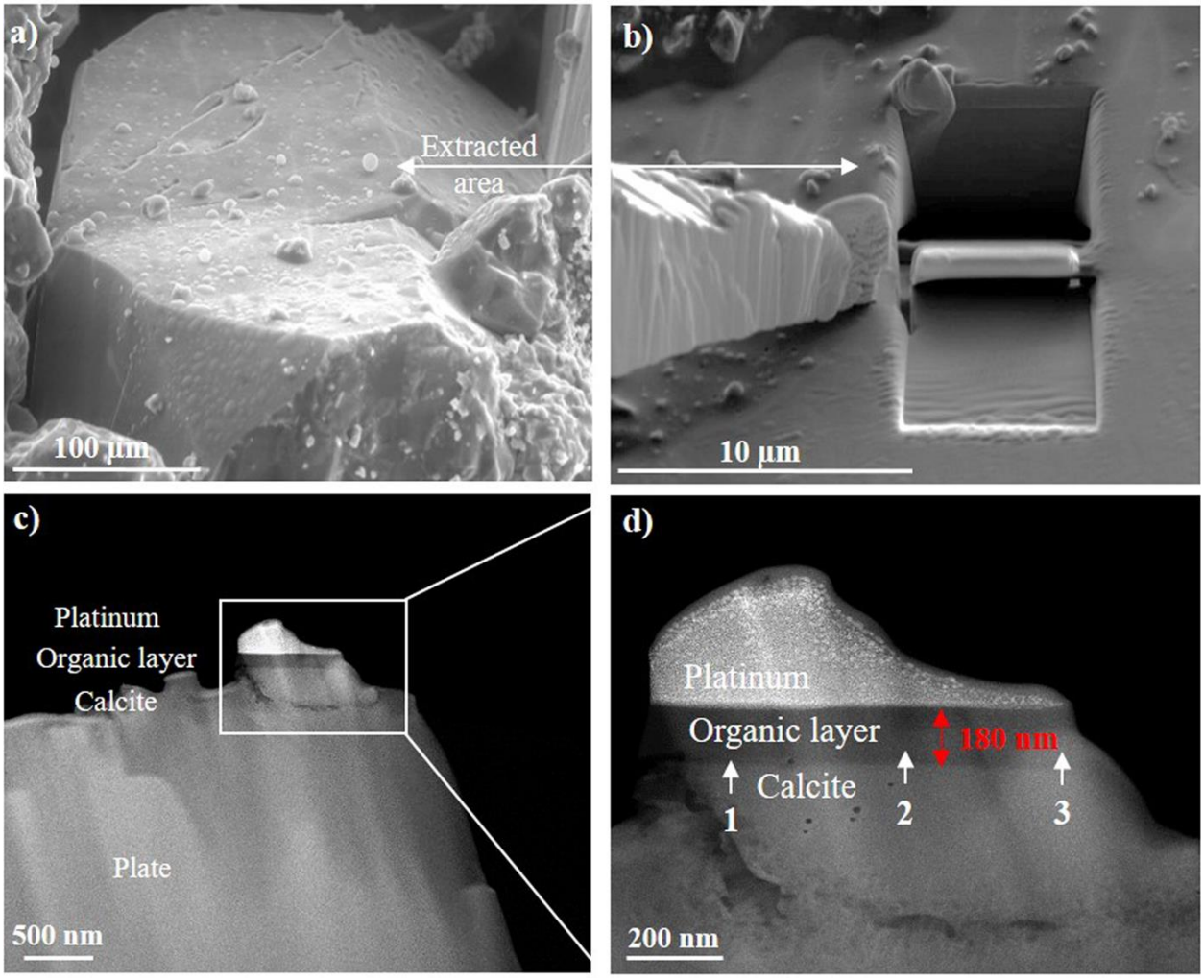

Figure 20. (a) ESEM image of the sample surface after toluene cleaning with formed water droplets. (b) The sample area from (a) after performing FIB milling procedure. (c) HAADF-STEM image of an extracted cross-section of the sample with a platinum layer on the top for

sample protection. (d) Zoom-in of the sample in (c) illustrating that calcite was covered by an organic layer.

To determine the chemical bond between the organic layer and calcite, we compared the EELS spectra from calcite, an organic layer, and the interface between calcite and organic layer (Figure 21). In the EELS spectrum from calcite, the carbon K edge (C-K) indicates two narrow peaks at 290 eV and 299 eV, which are well-defined as C=O ($1s \rightarrow \pi^*$) and C-O ($1s \rightarrow \sigma^*$) bonds of carbonate ion respectively[148, 152, 153]. The Ca L2,3, and O-K edges located at 351 eV and 548 eV were also identified.

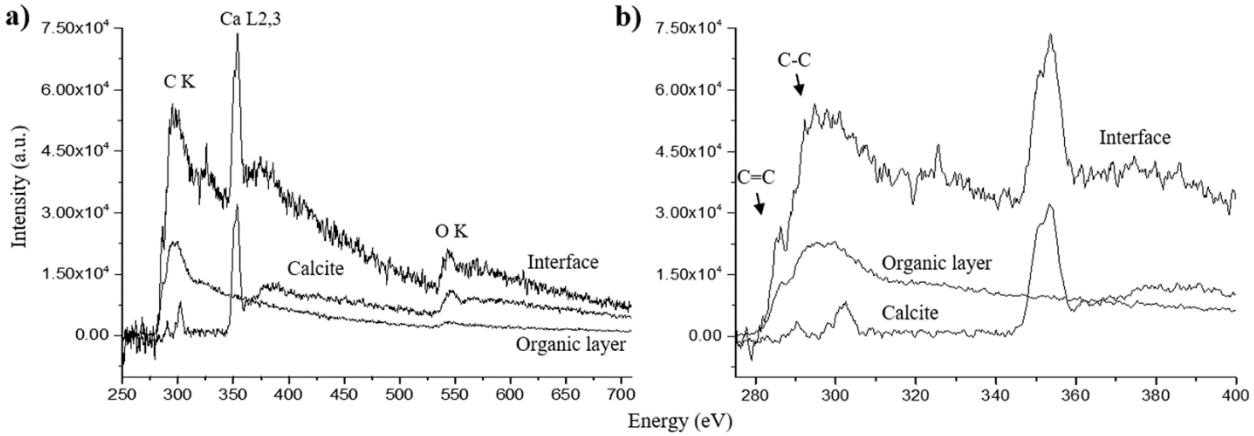

Figure 21. (a) The EELS spectra from calcite, an organic layer, and the interface between them. (b) The zoom-in of the EELS spectrum from the picture (a) representing the energy interval from 275 eV to 400 eV.

Focusing on the EELS spectrum from the organic layer, two peaks can be identified – one small sharp peak at 285 eV and a broader peak at 291.5–292 eV, which correspond to amorphous carbon[152]. A small O-K edge located at 547 eV was observed, indicating that oxygen was presented in the organic layer. In comparison with EELS spectra from calcite and from the interface between the organic layer and calcite, Ca L2,3 edge did not appear.

The EELS spectrum from the interface between the organic layer and calcite represents one tiny shoulder at 285 eV and one broad peak at 292 eV, which are well-known as organic carbon C=C ($1s \rightarrow \pi^*$) and C-C ($1s \rightarrow \sigma^*$) bonds[152]. The sharp peaks of Ca L2,3 edge at 351 eV and O-K edge at 548 eV were also detected, indicating the presence of calcium and oxygen at the interface.

However, no carbonate group was observed, implying that the bond between the organic layer and calcite was not caused by carbonate bonding. The observations confirm that the organic layer is bound to calcite by the ionic bond between calcium (Ca^{2+}) and oxygen (O^{-}), which forms a constituent part of the carboxyl group (COO^{-}) of oil acids or asphaltenes.

Elemental analysis of the organic layer was then captured in three points (Figure 20 points 1, 2, 3) in order to study the homogeneity of the layer composition along its length. We observed that the elemental composition of the organic layer remained the same throughout its length and the average concentration of elements was 96 ± 3 at.%, 2 ± 0.2 at.%, 1 ± 0.1 at.%, 1 ± 0.1 at.% for C, O, Si and S, respectively. However, the registration of hydrogen by EDXS is impossible. Nevertheless, such a large amount of carbon means that observed organic layers consisted most likely of hydrocarbons from oil, which were chemically adsorbed on the calcite by an ionic bond between Ca^{2+} and COO^{-}.

2.4 Summary

In this chapter, water condensation experiments were accomplished by controlling the chamber pressure and temperature. With the temperature being kept near 0 °C, it was observed that water droplets started to form on carbonate surfaces at the pressure of 850 Pa. In this kind of experiment, one of the possible errors of contact angle estimation can occur when water droplets merge with each other and form one large drop (Figure 14). In this case, contact angles and surface wettability can be determined incorrectly due to an increase of the contact line between water and the surface. This problem can be resolved by performing the time-lapse experiments before measuring contact angles. To avoid further possible errors in the contact angle calculation caused by non-optimally oriented water droplets, we applied the procedure to extract the droplet from the image. Then, the geometrical dimensions of each droplet can be calculated more accurately (see the contact angle evaluation section).

In the current work, the advanced microscopic technologies were first applied to identify the organic layers on carbonate surfaces. It was observed that the surface covered by hydrocarbon layers had hydrophobic wetting properties, while pure calcite exhibited hydrophilic. This result was also confirmed by EDXS analysis in the corresponding points of the surface. Additionally, the EDXS spectra were acquired from a number of points in order to obtain reliable quantitative data. One of the disadvantages of EDXS is the inability to detect hydrogen atoms. Thus, results obtained

for the elemental composition of the organic layer (Figure 20) are relative, and the presence of hydrogen should be considered in further studies.

The Cryo-FIB approach with a combination of S/TEM experiments outlined in this work provides a significant contribution to the characterization of the organic layers on carbonate surfaces. Herein, the presence of a thin hydrocarbon layer was proved by using a combination of microscopic techniques. The number of authors[154, 155] suggested that fatty acids and asphaltenes from oil had strong adsorption tendency to calcite and proposed that they could alter initial water-wet wettability of minerals towards more oil-wet, which in turn would impact on oil or water displacement processes. However, by now, there was a lack of information about properties of the adsorbed layers because typically wettability was measured by standard methods on a macro-scale, which are limited and cannot account for the influence of the organic layers on micro-scale wetting properties. While the average wettability of a core sample was not addressed in this work, the calculated thickness of the hydrophobic organic layer (180 ± 12 nm) can be used in fluids displacement models in order to evaluate in a more accurate way the key parameters of fluids multi-phase flow through pore throats, such as capillary pressure curves. Moreover, the results obtained from methods developed herein can be used in understanding the causes of wettability alteration in carbonates. Herein, we suggest that asphaltenes react with calcium ions by the ionic bond between calcium (Ca^{2+}) and oxygen (O^{-}) from the carboxyl group (COO^{-}). Then, on the surface of this organic layer other hydrocarbons from oil start to adsorb. As a result, wettability changes towards more oil-wet and water-injection ceases to be effective. Furthermore, we expect that other carbonate reservoirs with the high asphaltenes content in oil will have a similar cause of the surface wettability modification.

Chapter 3. Effect of nanoparticles on viscosity and interfacial tension of aqueous surfactant solutions at high salinity and high temperature

3.1 Motivation

As it was observed in the previous chapter oil components that consist of carboxylate groups (COO^-) form the first adsorption layer onto carbonate surfaces. These adsorbed molecules further promote other components from oil to adsorb on them due to dipole-dipole or hydrophobic interactions. As a result, organic layers will be formed on carbonate surfaces, making carbonates wettability mixed or oil-wet. In such conditions, due to negative capillary pressure waterflooding will be ineffective unless surface modifying chemicals are added to injection fluid. It was shown that surfactants, as surface-active agents, can desorb organic layers from carbonate surfaces, resulting in wettability alteration towards more water-wet[41]. The driving force of organic layer desorption from a surface depends on a surfactant charge[41]. For instance, anionic surfactant with a negative charge will tend to react through hydrophobic interactions with adsorbed oil components. On the contrary, cationic surfactant with a positive charge will tend to form an ion-pair interaction with negatively charged absorbed oil components, i.g. (COO^-).

Importantly the IFT between injection fluid and oil should also be lowered in order to avoid oil trapping and increase its production. Recently, it has been shown that nanoparticles can enhance surfactant properties, and thus, increase oil recovery. Although many studies have been published, the impact of nanoparticles on the interfacial layer remains unclear, with some contradicting trends reported in the literature[104, 108, 111]. Moreover, there is a lack of information regarding the influence of temperature and salinity on nanofluids' effectiveness that limits their application in real oil fields.

Therefore, in this chapter, we systematically studied the influence of nanoparticles on cationic and anionic surfactant properties under different temperatures and salinities. For this study, surfactants have been chosen based on their promising properties to desorb organic layers and increase oil recovery. The range of studied temperatures and salt concentrations corresponds to typical reservoir conditions.

3.2 Materials and Methods

Therefore, two ionic surfactants were chosen based on a literature survey - one anionic (sodium olefin sulfonate, SOS, > 97 mol.% from Stepan Company, Northfield, IL, USA), and one cationic (erucyl bis-(hydroxyethyl)-methylammonium chloride, EHAC, > 99% mass fraction from Akzo Nobel) (Figure 22). The hydrophilic-lipophilic balance (HLB) of SOS surfactant is 40, which corresponds to a solubilizing agent for oil-in-water emulsions. Owing to the lack of information available for cationic hydrophilic groups, it is challenging to calculate the HLB value for EHAC surfactant. However, for typical cationic surfactant CTAB, the HLB value is 21.8, which also represents the solubilizing agent for oil-in-water emulsions.

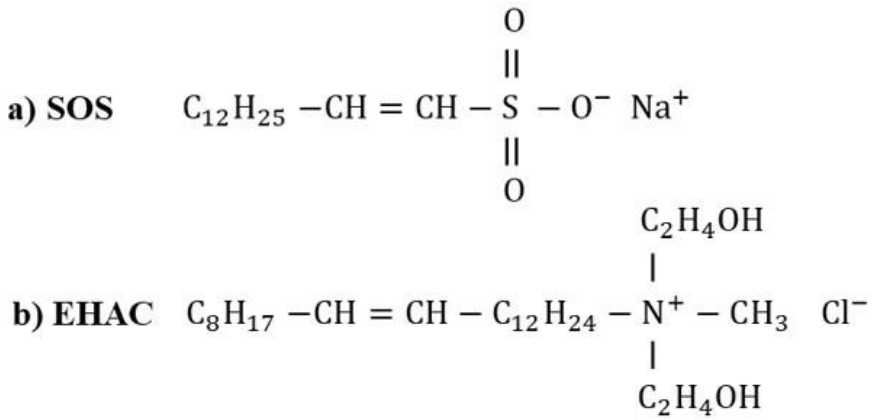

Figure 22. Surfactants used in this study a) sodium olefin sulfonate, b) erucylbis-(hydroxyethyl) methylammonium chloride.

N-decane (> 99 mol.% purity from Sigma-Aldrich, St. Louis, MO, USA) was used as a light phase for IFT measurements. Deionized water was used to prepare different brines with sodium chloride (NaCl, >99.5 mol.% purity from Sigma- Aldrich). Hydrophilic silicon dioxide nanoparticles (trademark AEROSIL® 200, supplied by Evonik, Essen, Germany) were used as received to prepare surfactant nanofluids. The physicochemical properties of nanoparticles are listed in Table 6.

3.2.1 Surfactant Nanofluids Preparation

The brine solution with 6 wt.% concentration of NaCl was prepared using a magnetic stirrer at 300 rpm at 25 °C and later diluted to make 1, 2, and 3 wt.% NaCl brines. Various solutions with

surfactant (0 – 1 wt.%) concentrations were prepared by mixing the appropriate amount of surfactants in the aqueous phase (water or NaCl brine) with a magnetic stirrer for a minimum of 2 h at 25 °C. Subsequently, nanoparticles with varying concentrations (0.05 – 1 wt.%) were mixed with brine or surfactant solutions by sonication for 1 h (with 5 minutes break after every 15 minutes to avoid overheating) in order to obtain homogeneous solutions[108].

The high viscous samples were left to equilibrate and let all the air bubbles out for 1 day at room temperature. The phase separation in solutions was inspected by visual examination before every experiment under experimental conditions, and surfactant nanofluids were stable during testing time.

Table 6. Properties of used nanoparticles.

Properties	Units	Value
SiO2	wt.%	≥99.8
Type	-	Hydrophilic
Molecular mass	g/mol	60.07
Specific surface area (BET)	m^2/g	200 ± 25
Average primary particle size	nm	12
Bulk density	g/L	Approx. 50

3.2.2 Interfacial tension measurements

IFT measurements between n-decane and different aqueous solutions of surfactants and nanoparticles–surfactant mixtures were conducted using the spinning drop method (Kruss Tensiometer) as it is more convenient and accurate for measuring IFT below 20 mN/m[156]. Here, a drop of liquid with less density (n-decane) was placed inside the denser fluid (surfactant or surfactant–nanoparticle solutions) in the horizontal tube. Then, the tube was rotated, and the drop deformed into an elongated shape. Samples were assumed to be equilibrated when measured IFT values remained unchanged (±2%) for 30 min[157]. At the equilibrium point, the balance between surface tension and centrifugal forces defined the shape of the droplet. At a high angular velocity

ω (max. 15,000 rpm), the droplet shape becomes very close to a cylinder. In this case, the IFT values (γ) were calculated using the Vonnegut expression:

$$\gamma = \frac{\Delta\rho\omega^2 R^3}{4},$$

where $\Delta\rho$ - is the density difference between light and heavy phases (n-decane and surfactant–nanoparticles formulations, measured with an Anton Paar DMA 4200 M instrument); ω^2 - angular velocity and R^3 is a shape radius.

To avoid the influence of impurities on the results, before and after each experiment, the tube was cleaned with acetone and water and then dried with air.

3.2.3 Viscosity Measurements

Rheological experiments were carried out on an Anton Paar Physica MCR 302 stress-controlled rheometer in order to measure the viscosity of surfactant solutions with and without nanoparticles. All tests were performed at atmospheric pressure and 25 ± 0.5 °C. After loading, the sample was left for at least 10 min at a certain temperature to reach equilibrium. Experiments with samples in the viscosity range of 1–100 mPa*s were carried out with coaxial cylinders (cup diameter – 10.84 mm and bob diameter and length – 10 and 14.98 mm, respectively). Samples in the viscosity range higher than 100 mPa*s were measured using a cone-plate sensor (diameter – 25 mm and cone angle – 2°). The zero-shear (η_0) viscosity of samples was estimated at the low shear stress regime when viscosity was an independent function of the shear rate.

3.3 Results

3.3.1 Critical micelle concentration and temperature effect on IFT

It is well known that surfactant molecules reduce IFT between two immiscible fluids, such as oil and water, by adsorbing at the liquid-liquid interface. A surfactant concentration at which spherical micelles start to grow is known as CMC and varies for different surfactants[158]. The CMC is the main controlling parameter for surfactant properties and needs to be optimized for every surfactant system for improving oil recovery[47].

The IFT of aqueous anionic and cationic surfactant solutions was measured and plotted as a function of their concentrations at 25 and 65 °C (Figure 23). The minimum equilibrium IFT was achieved for anionic and cationic surfactants at concentrations of 0.1 and 0.001 wt.%, respectively. These concentrations corresponded to the turning points of the curves and represented the CMC. It can be seen in Figure 23 that further addition of surfactants led to a slight IFT increase. Such gentle IFT growth could be caused by spherical micelles' formulation in solutions when fewer free surfactant molecules remained at the phases' interface.

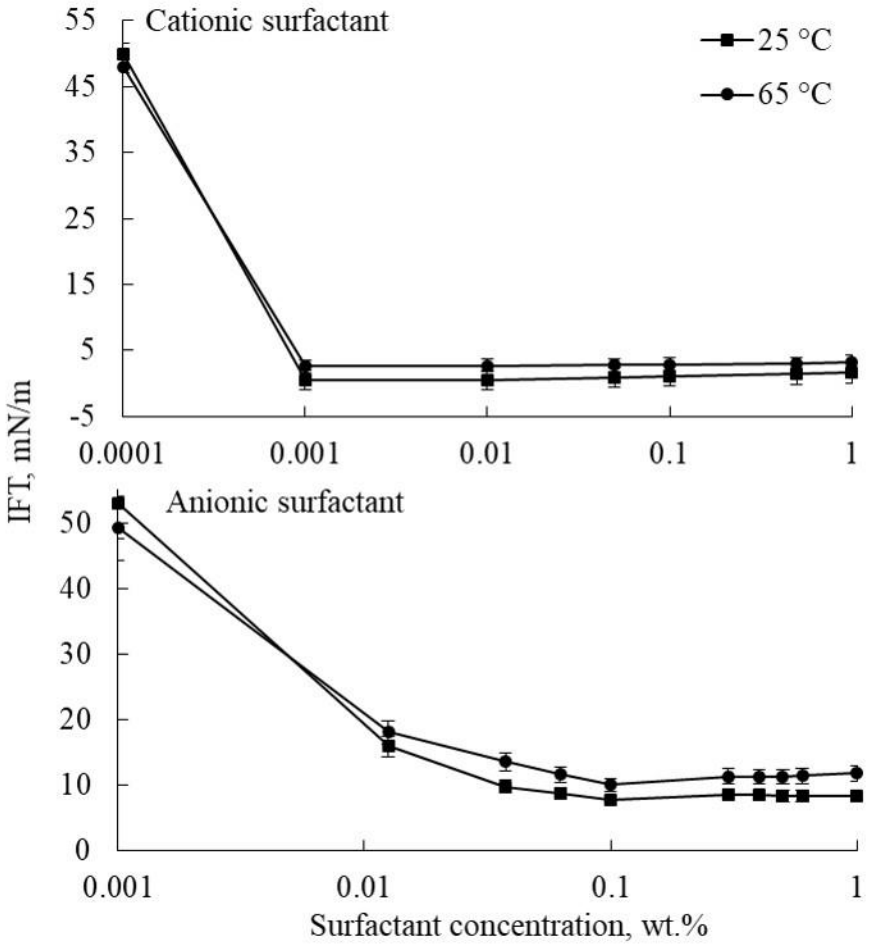

Figure 23. Interfacial tension of n-decane against aqueous surfactant solutions – EHAC (top) and SOS (bottom) as a function of surfactant concentration (at 25 (black squares) and 65 (black circles) °C).

Such IFT patterns are consistent with those obtained with the other surfactant types[108, 111]. Anionic and cationic surfactants caused dramatic IFT reductions of 88% and 98%, respectively, compared with pure water. Note that the IFT value between water and n-decane is 52.97 mN/m[159]. It should also be pointed out that the IFT decrease was far more significant when a cationic surfactant was added compared with the anionic surfactant at the same concentration (C = 0.1 wt.%) - 1.14 mN/m versus 7.7 mN/m, respectively.

However, IFT increased gradually with increasing temperature from 25 to 65 °C for all measured surfactant concentrations (Figure 23). In the literature, different observations have been reported about the temperature effect on IFT. For instance, Aoudia et al.[160] and Kamal et al.[161] reported that IFT between different anionic and amphoteric surfactant solutions and oil increased gradually with a temperature increase of up to 90 °C. In contrast, Saien and Akbari[143] reported a decrease in IFT of SDS – toluene systems when the temperature was increased. According to Gibbs's adsorption theory and the model developed in the work[162], the change in IFT (dγ) can be calculated as:

$$d\gamma = -RT \sum_i \Gamma_i \, d \ln C,$$

where R is the gas constant, T is temperature, Γ_i is the surface excess concentration, and C is the molar concentration of surfactant in bulk.

Thus, according to the equation an increase in temperature results in the decrease of IFT[163]. However, this contrasts some literature[160, 161], and our experimental results, where IFT clearly increased with temperature. The authors[66] explained such behavior with the complex composition of the used crude oil. This suggestion was supported by work conducted by El-Batanoney et al.[69], who demonstrated that aromatic, paraffinic, and naphthenic components of crude oil had different patterns of IFT dependence on temperature. As such, IFT between surfactant solution and naphthenic oil displayed a decrease with increasing temperature. For aromatic oil, the IFT remained almost unchangeable up to 50 °C and started to increase above this temperature. The effect of temperature on surfactant solution/paraffinic oil IFT was controversial compared to that of the aromatic oil. Hence, the minima in IFT with temperature can be explained by the synergetic effect of different oils[67].

In the present work, n-decane was used as a model oil, and thus, we suggest another explanation of the observed phenomenon. The ─OH groups in the EHAC and ─O groups in the SOS surfactant heads (Figure 22) can serve as donors and acceptors for hydrogen bond formation with the surrounding water molecules. It is known that, with increasing temperature, the number of hydrogen bonds in the system decreases[164]. Therefore, with increasing temperature, the hydrogen bonds between water and surfactant molecules are disrupted, resulting in a reduction of surfactant head solubility in water. Thus, EHAC and SOS surfactants become less soluble in water and exhibit more affinity to oil, and consequently, IFT increases.

3.3.2 Effect of nanoparticles on IFT between aqueous surfactant–n-decane systems

The effect of nanoparticles on IFT between aqueous surfactant solutions and n-decane with the selected SOS surfactant concentrations at ambient conditions is illustrated in Figure 24. Interfacial measurements were taken for concentrations below CMC 0.03 and 0.05 wt.%, near 0.1 wt.%, and above 0.5 wt.%.

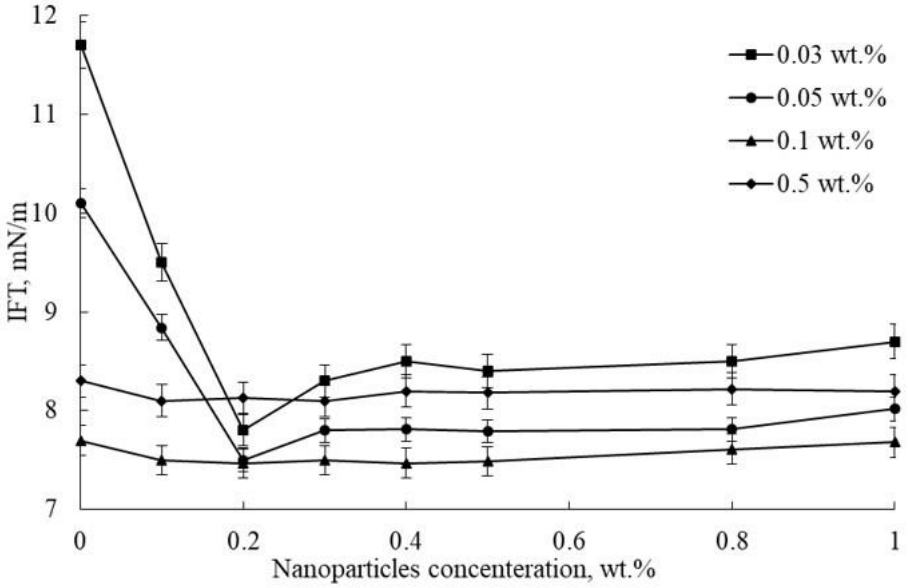

Figure 24. Interfacial tension of n-decane – SOS solutions with 0.03 wt.% (black squares), 0.05 wt.% (black circles), 0.1 wt.% (black triangles), and 0.5 wt.% (black rhombs) surfactant concentrations as a function of nanoparticle concentration (0–1 wt.%) at 25 °C.

It can be seen (Figure 24) that the addition of small nanoparticles concentration (< 0.2 wt.%) to aqueous surfactant solutions with 0.03 and 0.05 wt.% concentrations resulted in IFT reduction. Such an IFT reduction can be interpreted using several approaches. First, due to the Brownian motion and repulsion forces of similarly charged surfactant heads and nanoparticles, some nanoparticles could approach the interfacial zone and contribute to the IFT reduction. This suggestion is supported by experimental[108] and modeling[146] results, which showed that the inclusion of silica nanoparticles to water/n-decane systems had only a slight effect on the water/n-decane IFT in the absence of surfactant. On the other hand, due to the electrostatic repulsion between similarly charged surfactant molecules and nanoparticles, more surfactant molecules could move to the interfacial layer, resulting in further IFT reduction[111].

Further increase of nanoparticles concentration in 0.03 and 0.05 wt.%-concentrated surfactant solutions led to the slight increase of IFT values (Figure 24), which could be caused by nanoparticle agglomeration, which prevented them and surfactant molecules from reaching the interfacial zone[165]. It can also be seen in Figure 23 that the addition of nanoparticles to highly concentrated surfactant solutions (>0.1 wt.%) showed no impact on the IFT values. We hypothesize that, when surfactant concentration is higher than CMC, the interfacial zone consists mostly of surfactant molecules with no available space for nanoparticles. As such, nanoparticles mostly remained in the water phase and could not reach the interface and, thus, had no effect on IFT.

Cationic surfactant nanofluids showed more complex behavior, which could be caused by the intermolecular interactions between oppositely charged nanoparticles and surfactant molecules. As shown in the phase separation diagram (Figure 25), stable homogeneous surfactant nanoparticle formulations were obtained only when the surfactant concentration was above 0.7 wt.%, independent of nanoparticle concentration. This surfactant concentration was greater than CMC and corresponded to the semidilute regime of solutions[166].

Consequently, a 0.7 wt.% EHAC surfactant concentration was selected in order to test homogeneous solutions with respect to their IFT values against n-decane (Figure 26). Clearly, the IFT pattern resembled the IFT pattern of the anionic surfactant. We suggest that, at low surfactant concentrations (< 0.7 wt%), the majority of surfactant molecules rather adsorb onto nanoparticles (due to the attractive electrostatic forces) than approach the interface. However, a surfactant concentration below 0.7 wt.% was insufficient to prevent the aggregation and precipitation of

nanoparticles. Consequently, 0.7 wt.% was the surfactant threshold concentration for stabilizing the nanofluid. This value is higher than CMC because nanoparticles may need to be dispersed by forming a network with surfactant micelles[115].

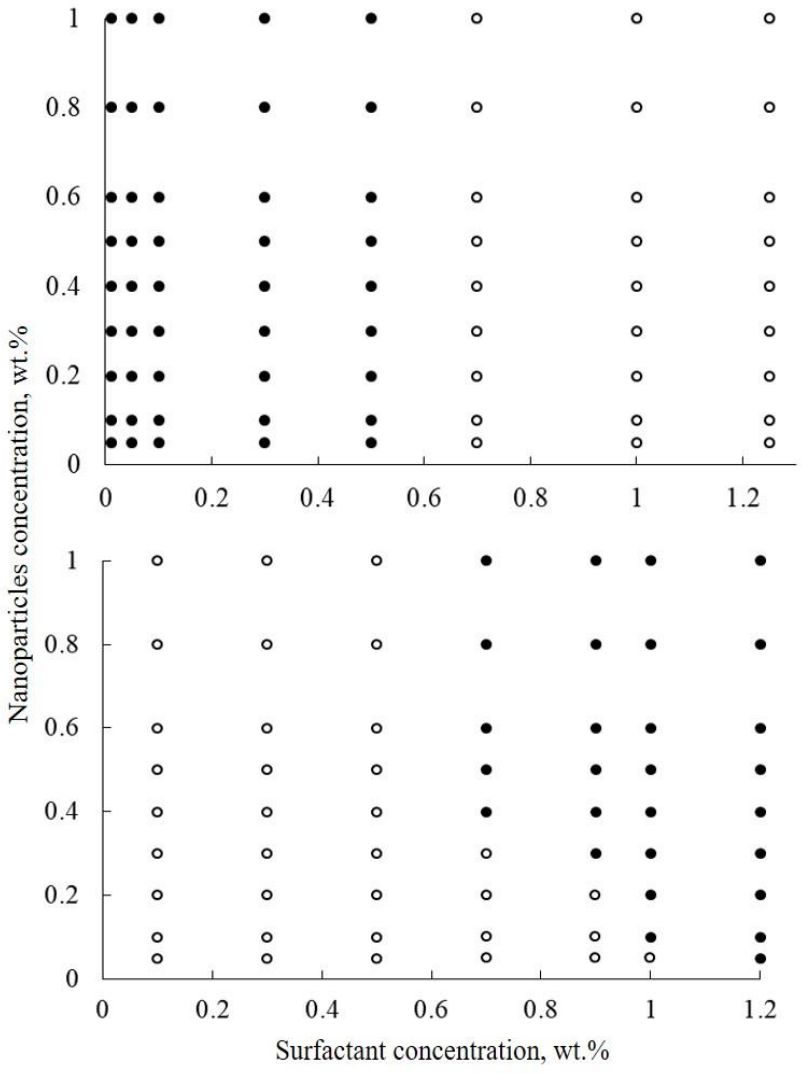

Figure 25. Phase diagrams of aqueous mixtures of cationic EHAC (top) and anionic SOS (bottom) surfactants with nanoparticles at 25 °C. Filled circles – heterogeneous solutions, open circles – homogeneous solutions.

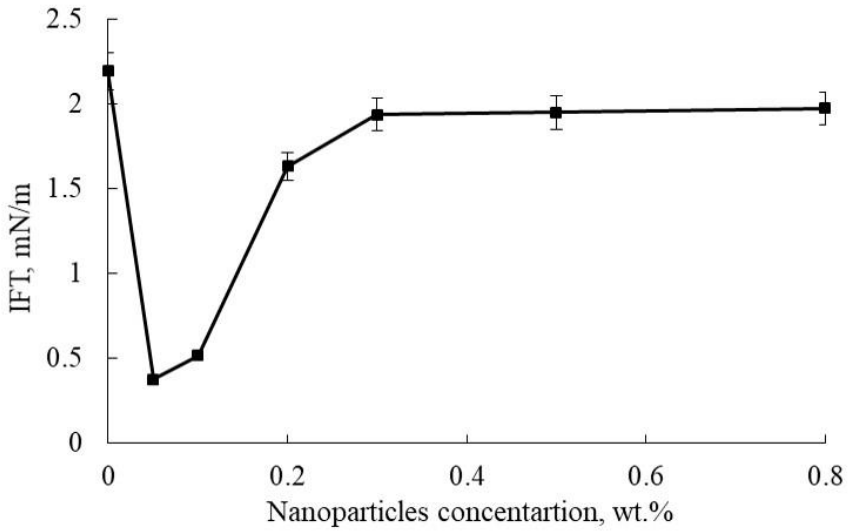

Figure 26. The interfacial tension between n-decane and 0.7 wt.% aqueous cationic surfactant solution as a function of nanoparticles concentration at 25 °C.

The minimum IFT (0.38 mN/m) was achieved when only 0.05 wt.% of nanoparticles were added to EHAC solutions. When nanoparticles concentration was above 0.05 wt.%, IFT started to increase, which implied that the number of surfactant molecules adsorbed at the interface decreased. Both descending and increasing trends of IFT can be explained in terms of attractive forces that act between the oppositely charged EHAC head group and nanoparticles. Indeed, at a low nanoparticle concentration (< 0.05 wt.%), the reduction of IFT can be explained by considering that nanoparticles, adsorbing the positively charged surfactant molecules, become more hydrophobic and, thus, move toward the interface carrying surfactant molecules[167]. It is worth noting that the observed phenomenon can also be attributed to the decrease of the negative surface charge of nanoparticles due to the adsorption of positively charged surfactant molecules.

Thus, nanoparticles serve as carriers of surfactant molecules into the interfacial zone due to Brownian motion, contributing to the IFT reduction. However, at high nanoparticle concentration (>0.05 wt.%), the IFT increase is related to the electrostatic interactions between surfactant molecules and nanoparticles in bulk. Consequently, fewer surfactant molecules can move to the interfacial zone and cause IFT reduction. Furthermore, at high nanoparticle concentration, nanoparticles can form a layer near the interface that prevents surfactant molecules from reaching the interface[165].

3.3.3 Effects of salinity and temperature on IFT

IFT of SOS and EHAC surfactant–nanoparticle formulations were studied over a wide range of salt concentrations (0–6 wt.% NaCl) and temperatures (25–65 °C). When nanoparticles were absent, the IFT was gradually reduced with increasing NaCl content (Figures 27 and 28), consistent with results for other surfactants-oil systems[168, 169].

It can be seen from Figures 27 and 28 that the addition of 6 wt.% NaCl had a significant effect on the IFT of 0.1 wt.% SOS solution (2.09 mN/m, a 58% reduction) and 0.1 wt. % EHAC solution (0.02 mN/m, an 89% reduction). We hypothesized the following explanation for this phenomenon.

Without salts, surfactant molecules were adsorbed at the interface randomly, suppressed by electrostatic forces between them. When salts were added to these ionic surfactant solutions, some salt cations and anions as counterions interacted with the polar surfactant heads, screening the electrostatic repulsion between the likely charged surfactant groups. By increasing the electrolyte content, more counterions were attracted to the polar surfactant heads, allowing them to approach each other. Consequently, surfactant molecules were packed more densely at the water-oil interface, and as a result, the IFT reduced rapidly.

It is interesting to point out that the IFT patterns of both surfactants in the presence of salt passed through a minimum with increasing temperature ("V" pattern). First, the IFT decreased and reached the minimum at 35 °C; then, above this temperature, IFT started to increase slightly. However, IFT values at 65 °C did not exceed the values at 25 °C and remained below 0.4 and 0.75 mN/m for anionic and cationic surfactants, respectively. The descending IFT pattern at temperatures below 35 °C can be explained by the closely packed surfactant layer at the interface, formed because of a counterion screening effect[80]. However, the increasing IFT trend above that temperature can be due to the decrease in the number of hydrogen bonds between the surfactant head groups and surrounding water molecules[72, 164]. Thus, surfactant heads become less soluble in water and exhibit a higher affinity to the oil phase and therefore diffuse further inside the oil phase, resulting in an IFT increase.

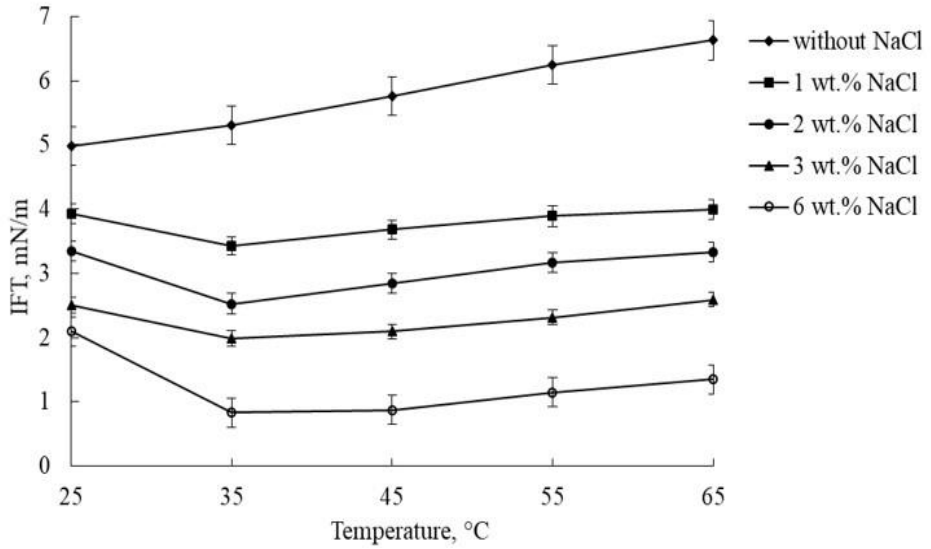

Figure 27. The interfacial tension between n-decane and SOS surfactant solution of 0.1 wt.% in distilled water (black rhombs) and 1 wt.% NaCl brine solution (black squares), 2 wt.% NaCl brine solution (black circles), 3 wt.% NaCl brine solution (black triangles), and 6 wt.% NaCl brine solution (open circles) as a function of temperature (25–65 °C).

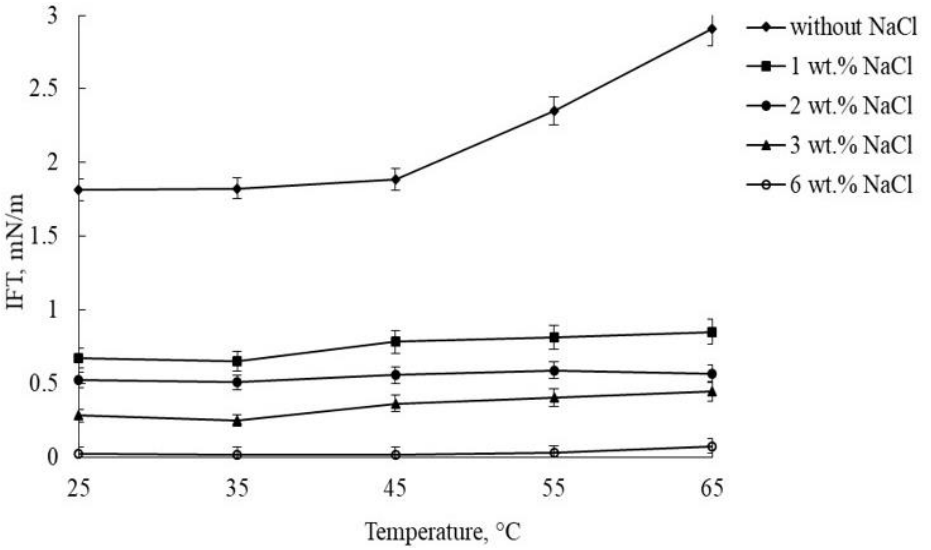

Figure 28. The interfacial tension between n-decane and EHAC surfactant solution of 0.1 wt.% in distilled water (black rhombs) and 1 wt.% NaCl brine solution (black squares), 2 wt.% NaCl brine solution (black circles), 3 wt.% NaCl brine solution (black triangles), and 6 wt.% NaCl brine solution (open circles) as function of temperature (25–65 °C).

Furthermore, it can be seen in Figure 29 that the general IFT pattern of SOS solutions with nanoparticles also had a well-defined minimum at the same temperature. Notably, silica nanoparticles had a slight effect on IFT in the presence of salt (Figure 29). Indeed, the addition of 0.1 wt.% SiO2 to 0.1 wt.% SOS surfactant brine solution (1 wt.% NaCl) further reduced IFT by up to 10% (in comparison with IFT of 0.1 wt.% SOS in 1 wt.% brine NaCl solution without nanoparticles) at 25 °C. With a further increase in temperature and salinity, the influence of nanoparticles on IFT became more insignificant as brine SOS solutions and nanoparticle-augmented brine SOS solutions had almost the same IFT values (Figures 27 and 29). Therefore, it can be stated that IFT reduction is related to the addition of electrolytes to solutions and, with a lesser impact, to nanoparticle content.

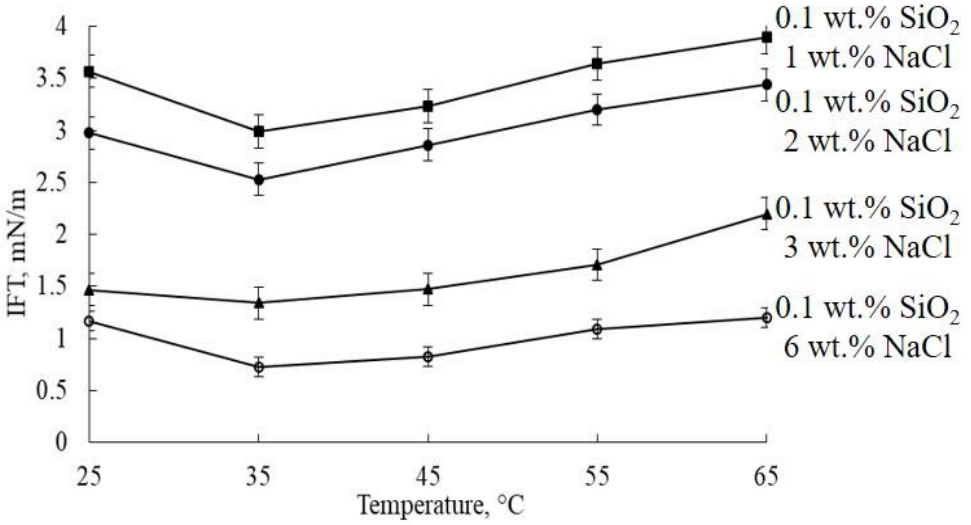

Figure 29. Interfacial tension of n-decane – Nanosurfactant formulations of 0.1 wt.% SOS and 0.1 wt.% nanoparticles in 1 wt.% NaCl brine solution (black squares), 2 wt.% NaCl brine solution (black circles), 3 wt.% NaCl brine solution (black triangles), and 6 wt.% NaCl brine solution (open circles) as a function of temperature.

3.3.4 The viscosity of Surfactant–Nanoparticle Formulations

The viscosity of aqueous and brine SOS and EHAC nanofluids were investigated. The effect of salt and nanoparticles on the viscosity of SOS surfactants solutions is presented in Figure 30. For comparison, the viscosity of pure 0.1 wt.% SOS solution, which was used for the preparation of brine nanoparticle-augmented solutions, is also presented. The inclusion of salt and nanoparticles had a slight effect on the viscosity, i.e., the viscosity of neat 0.1 wt.% SOS solution equaled 1.01 mPa*s, while the viscosity of 1.5 wt.% NaCl brine 0.1 wt.% SOS and 1.5 wt.% NaCl brine 0.1 wt.% SOS with 0.1 wt.% nanoparticles amounted to 1.1 mPa*s and 1.3 mPa*s, respectively. Viscosity was independent of shear rate within the measured interval (from 0.1 to 100 1/min); thus, SOS solutions in the presence of nanoparticles were Newtonian fluids that exhibited similar viscosity as water[170]. This phenomenon can be explained by taking into account the same negative charge of nanoparticles and surfactant molecules that prevent their interactions. In contrast, nanoparticle addition to 0.7 wt.% EHAC surfactant showed a significant effect on nanofluid viscosity (Figure 31). From Figure 30b, it can be seen that the neat 0.7 wt.% EHAC solution with 1.5 wt.% NaCl used for further preparations of the mixtures with nanoparticles had a relatively high viscosity (3500 mPa*s), which was higher than that of water and SOS solutions by 3 orders of magnitude. Such high viscosity of aqueous EHAC solutions with salt can be explained by taking into account the structural modification of surfactant spherical micelles to the long cylindrical micelles upon salt addition, which exhibits polymer-like behavior[166]. The viscosity of aqueous EHAC solution with 0.05 wt.% nanoparticles is also shown in Figure 31c. It can be seen that the mixture of nanoparticles with aqueous EHAC surfactant solution had a low viscosity (1.1 mPa*s), which is close to that of water[170]. In contrast to this, nanoparticle addition to 1.5 wt.% NaCl brine EHAC solution resulted in viscosity-increasing by 1 order of magnitude in comparison with that of brine EHAC solution without nanoparticles (Figure 31a). In the literature[117], it is suggested that nanoparticles mostly contribute to the screening effect of electrostatic repulsion of surfactant heads, acting as electrolytes without direct interaction with surfactant molecules. However, in this work, we show that the addition of nanoparticles to EHAC solutions led to a significant viscosity increase only in the presence of salt, whereas the viscosity of nanoparticle augmented EHAC solutions without salt remained low. Therefore, we suggest that nanoparticles had a lesser impact on the screening effect of charged surfactant heads than salt. Here, we propose the following explanation for the influence of nanoparticles on EHAC solution viscosity. In the absence of

electrolytes, oppositely charged surfactant molecules can adsorb on the particles, forming a double layer on them. Due to attraction forces and hydrophilic interactions between surfactant heads and nanoparticles, the formation of microemulsions (particle at the center with the outer layers of surfactant molecules) occurs, and thus, solutions exhibit low viscosity (Figure 31c).

On the other hand, when salt is added to an aqueous EHAC solution, salt counterions screen electrostatic repulsion of the surfactant heads; thus, surfactant molecules can approach close to each other, causing the formation of long cylindrical micelles in solution[166]. Finally, we suggest that, when nanoparticles are added to a surfactant solution with salt, some surfactant molecules interact with nanoparticles, forming microemulsions, while other surfactant molecules form cylindrical micelles. In this case, two types of aggregations are present in the solutions. Therefore, microemulsions can be involved in the formation of a network with cylindrical micelles, acting as bridging points between micelles (Figure 31) and, thus, further increasing solution viscosity.

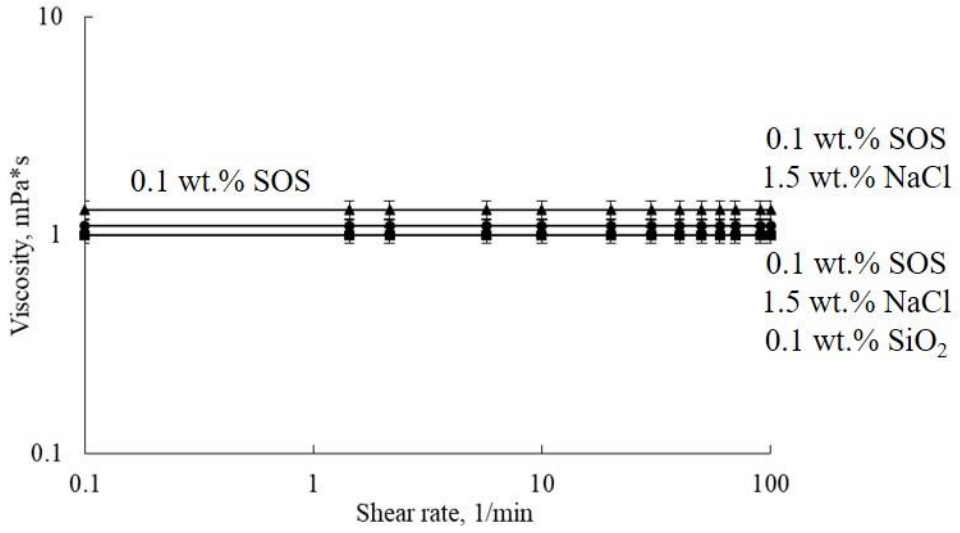

Figure 30. Viscosity of pure 0.1 wt.% SOS solutions (black squares), 0.1 wt.% SOS solution containing. 1.5 wt.% NaCl (black circles), and 0.1 wt.% SOS solutions containing 1.5 wt.% NaCl and 0.1 wt.% SiO2 (black triangles) at 25 °C.

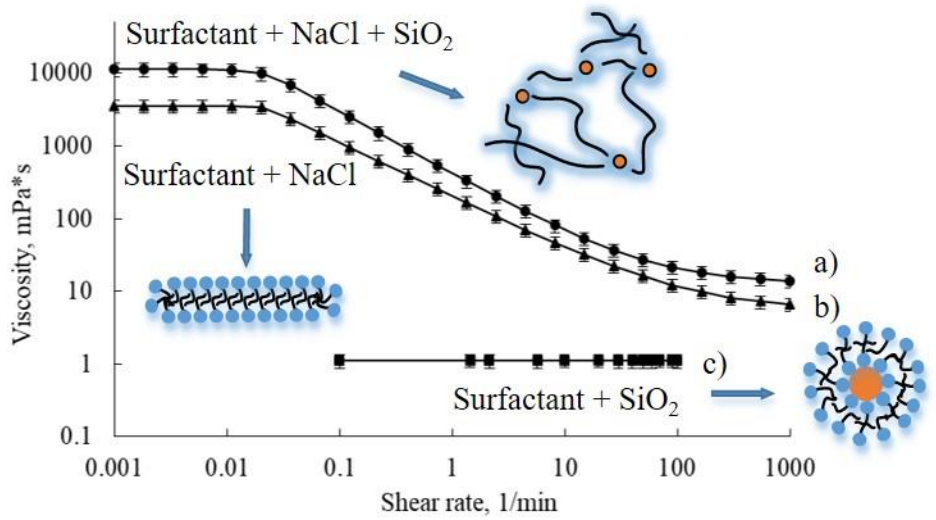

Figure 31. Viscosity of 0.7 wt.% aqueous EHAC at 25 °C with a) 1.5 wt.% NaCl and 0.05 wt.% SiO2; b) 1.5 wt.% NaCl; c) 0.05 wt.% SiO_2.

3.4 Summary

In this chapter, we systematically tested the influence of hydrophilic silica nanoparticles on the viscosity and interfacial properties of anionic (SOS) and cationic (EHAC) surfactant solutions. Based on the results obtained in this study, the main findings were stated:

1. The addition of nanoparticles to both cationic and anionic aqueous surfactant solutions further decreased IFT. However, the minimum of IFT was achieved when SOS surfactant concentration was less or near CMC, at low nanoparticle concentration (0.2 wt.%). However, a minimum of IFT for EHAC was observed when surfactant concentration was higher than CMC, and nanoparticle concentration was 0.05 wt.%.
2. IFT was strongly influenced by temperature and salt (NaCl). The IFT curves of brine SOS solutions with nanoparticles passed through a minimum with increasing temperature ("V" pattern). Furthermore, IFT reduction was more pronounced in solutions with salt than with nanoparticles. Thus, the IFT reduction is related to the addition of electrolytes to solutions and, with a lesser impact, to the addition of nanoparticles.
3. The impact of salt and nanoparticles on the bulk viscosity is cooperative. The addition of nanoparticles and salt to cationic surfactant solutions significantly increased solution viscosity (up to 10,000 mPa*s). Thus, nanoparticles can also serve as an effective viscosity modifier of injected fluids.

Overall, the results indicate that interactions between electrolytes and nanoparticles are competitive in the interfacial region and cooperative in the aqueous bulk. The contrast was more pronounced when the surfactant and particle had opposite charges. Results show that, for applications, an appropriate combination of surfactant/electrolytes/nanoparticles needs to be carefully selected to avoid negative synergism.

Chapter 4. Molecular insights in the temperature effect on adsorption of cationic surfactants at liquid/liquid interfaces

4.1 Motivation

As it was observed in the previous chapter, the experimental interfacial tension of the surfactants increased at high temperatures (65 °C). This interfacial behavior contradicts the well-known Gibbs theory that predicts the decrease of IFT with temperature increasing. According to Gibbs's theory, an increase in temperature results in an increase in the area per molecule, with a consequent decrease in the surface excess concentration of the surfactant[64]. Thus, IFT is expected to decrease with increasing temperature. However, there are a considerable number of experimental studies showing that IFT can also increase at high temperatures[65-68]. However, experimental investigations of temperature effect on liquid/liquid interfacial properties at microscale are challenging due to complexities associated with experimental procedures and limitations of experimental equipment to capture the structural properties of molecules at the interface. Therefore, an explanation of the deviation from Gibbs's theory is still not well understood.

Notably that in our previous chapter, we observed that EHAC surfactant significantly decreases IFT between water at room temperatures. Moreover, in the presence of salt, this surfactant forms wormlike micelles in the aqueous phase, thus causing remarkable viscoelasticity and high solution viscosity (~10^4 mPa*s). Therefore, EHAC can be used as a promising surfactant for either lowering water/oil IFT or increasing the viscosity of injected fluids when concentrations of surfactant and salt are correctly selected. However, the temperature influence on the interfacial properties of aqueous EHAC solutions remains unclear owing to the complex structure of the surfactant head in comparison with widely tested cationic surfactants.

MD simulation is one of the most effective approaches, which provides one with information about molecular insights into interactions and arrangements on the microlevel. Therefore, in this study, we aimed to examine the temperature effect on the adsorption process of the surfactant molecules (EHAC and cetyltrimethylammonium chloride (CTAC) at the water/n-decane interface. By studying cationic surfactants with different head structures but with identical counterion (Cl^-), we investigate the structural properties of surfactants at the interface. This study focuses on the following aspects: how the chemical structure of surfactants affects their packing at the interface

and how temperature influences on molecular arrangements between surfactant molecules and counterions at the interfacial zone. Thus, we demonstrate the connection between thermal and structural properties of cationic surfactants, and as a consequence, the hydrogen bonding role at the water-surfactant-n-decane zone.

4.2 Materials and Methods

4.2.1 Computational method

The liquid-liquid interfaces were simulated by the GROMACS 4.5.5 package[171] using a time step of 20 ns, as it was verified in the literature[85]. The molecular interaction parameters were computed using the GROMOS force field[172, 173]. Water was modeled by the implementation of a single point charge (SPC) model, which has been successfully used to obtain the best equilibrium distributions at the interface[75,174]. The molecular structures and topologies of EHAC and CTAC were obtained from PRODRG generator[175]. The charge distribution among atoms (Table 7) was selected and adjusted from that proposed in the literature[176], such that the system charge remained neutral. The simulation boxes were constructed by placing slabs of surfactant layers (2 nm each) around the n-decane layer (thickness 6 nm) and visualized using the visual molecular dynamics (VMD) tool[177]. The z dimension of the box with n-decane and surfactant molecules was increased to 18 nm to create regions for water molecules filling, as shown in Figure 32. Then, to obtain zero total charge of the systems, an appropriate number of counterions (Cl^-) were inserted by replacing the water molecules. The particle-mesh Ewald (PME) method of summation was used for careful and reliable computation of the electrostatic interactions[144]. The initial size of the simulation box was $4 \times 4 \times 18$ nm^3 for each system.

By taking into account that the EHAC head was bigger and more hydrophilic than that of CTAC (Figure 32), different numbers (4 EHAC and 6 CTAC surfactant molecules that corresponded to 0.4×10^{-6} mol/m^2 and 0.6×10^{-6} mol/m^2 respectively) were placed at each side of the box. These concentrations were less than critical micelle concentration (CMC) of EHAC (0.04 mM)[94] and CTAC (0.92 mM)[178], and were consistent with other simulation studies of cationic surfactants adsorption at liquid/oil interface[132, 179]. The simulations were carried out at atmospheric pressure (1 bar) and at different temperatures – 298 K, 318 K, 338 K, 353 K, and 368 K. After the simulation box was constructed, the energy minimization was performed by using the steepest descent method with the cut-off scheme for Coulomb and van der Walls forces of 0.9 nm.

The first simulation step was performed with a constant number of molecules and a volume and temperature (NVT) ensemble using a Berendsen barostat coupled with a simulation of a constant number of molecules, pressure, and temperature (NPT) with the time step of 400 ps. Then the productive simulations were run for 20 ns with a constant number of molecules, volume, and temperature (NVT) using the Nose-Hoover thermostat. The NVT and NPT simulation steps were consistently performed before the system production runs for all temperatures.

The interface tensions, density profiles, distribution functions of n-decane, ions, and surfactants, and number of hydrogen bonds were calculated using GROMACS.

4.2.2 Interfacial tension measurements

Interfacial tension measurements between n-decane and surfactant aqueous solutions were conducted using the spinning drop method (Kruss Tensiometer). Here, the drop of n-decane (less dense fluid) was placed inside the surfactant solution in the horizontal tube. Then the tube rotated, and the drop deformed into an elongated shape until it reached the equilibrium point. IFT was calculated when values remained unchanged (±4%) for half an hour. To avoid the influence of impurities on the results, before and after each experiment, the tube was cleaned with acetone and water then dried in an oven. The temperature was controlled and maintained with the high precision water thermostat supplied by Kruss, having an accuracy of ±0.1 °C.

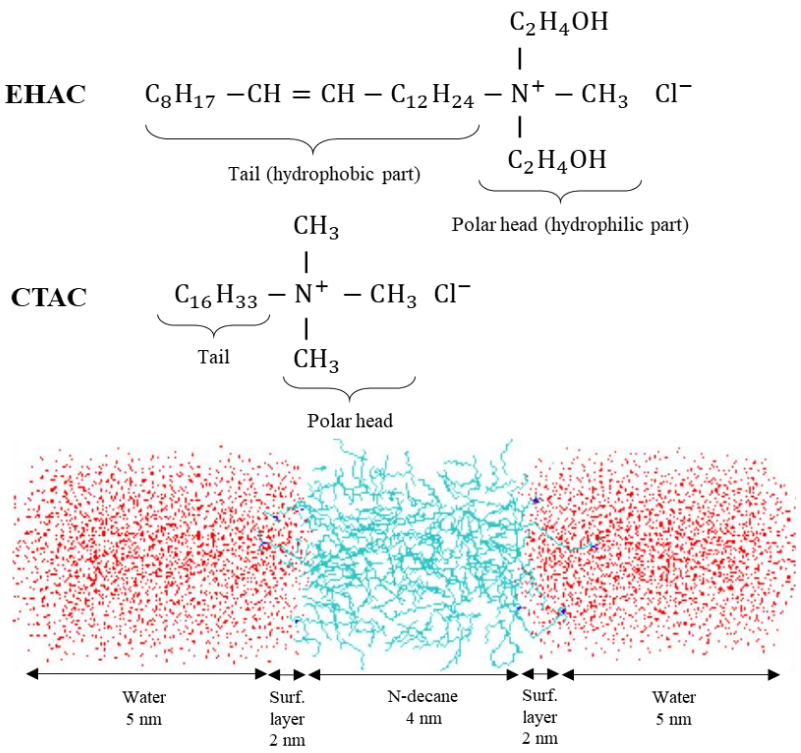

Figure 32. Surfactants used in this study: a) erucyl bis-(hydroxyethyl)-methylammonium chloride; b) cetyltrimethylammonium chloride and c) simulation box: red – oxygen, cyan – carbon, blue – nitrogen.

Table 7. Charge distribution of EHAC and CTAC surfactants and ions.

EHAC		CTAC	
Atoms	Charge (e)	Atoms	Charge (e)
CH_x	0	CH_x	0
α-CH_2	+0.250	α-CH_2	+0.250
O	- 0.700	CH_3 (-N)	+0.250
H	+0.435	Cl	-1
CH_2 (-N)	+0.250		
CH_2(-CH_2)	+0.265		
Cl	-1		

4.3 Results

4.3.1 Interfacial tension calculations

The simulation results for interfacial tension between water/n-decane in the presence of EHAC and CTAC surfactants at 298 K, 318 K, 338 K, 353 K, and 368 K are presented in Figure 32a, b, respectively. To achieve accurate values, the last 1000 ps of simulation data was used to calculate the interfacial tension (Figure 33c). The error bars were acquired by calculating the standard deviation of data over the last 1000 ps for every production run.

When the interface is perpendicular to the z-axis direction, the interfacial tension (γ) can be determined from[76]:

$$\gamma = -\int_0^{L_z} (p'(z) - p)dz,$$

where $p'(z)$ is the lateral pressure, p is the bulk pressure, L_z is the box length along the z-axis.

Assuming that in the bulk solution $p = p'(z)$ and taking into account that there are two interfaces (Figure 32), the integral (1) can be calculated by extending it to infinity[76]:

$$\gamma = -\frac{1}{2}\left(\frac{p_x+p_y}{2} - p_z\right)L_z,$$

where p_α represents the three diagonal elements of the pressure tensors $P_{\alpha\alpha}$ $(\alpha = x, y, z)$ along the axis.

As it can be clearly seen from Figure 33b, the IFT dropped with temperature increase in all simulations with CTAC surfactant, as it is predicted in Gibbs theory[163]. The same trends of IFT decrease with temperature increase were obtained experimentally for the SDS/toluene[148], SDS/n-decane[108,] and for CTAB/n-octane[63] systems. Interestingly, that surfactants with the same chemical structure but different counterions appeared to have similar interfacial behavior at high temperatures as it was shown for 1-alkyl-3-methylimidazolium cation in the presence of Br^- or BF_4^- [108].

However, the IFT of EHAC surfactant decreased with the temperature increase until 368 K and then started to increase with increasing temperature (Figure 33a). Notably, the IFT trend of EHAC obtained via molecular dynamics simulations is consistent with the experimental data, showing an increase in IFT with temperature increase (Figure 33c). In addition, there is an excellent match of IFT values obtained by simulations and experiments quantitatively. The precise numbers differ slightly, which can be due to the fact that we used the simple charge distribution model, where the surfactant is assumed to have a point unit charge at the headgroup, without consideration of the quantum chemical calculations for charge distribution throughout the molecule in the real system[176].

As the simulation box contained pure surfactant molecules and n-decane as a model oil, the influence of the impurities[71] or complex oil composition[69] on the observed phenomenon can be excluded. Thus, the observed behavior can be attributed to the emulsion inversion from oil-in-water (o/w) to water-in-oil (w/o), which occurred during temperature and/or salinity increase[181]. Such inversion is often explained in terms of Winsor phase behaviour[182]. When a surfactant is added to water/oil systems with roughly similar volumes of water and oil, the formation of microemulsions can occur in either the water or the oil phase, depending on temperature, brine salinity, and molecular structure of surfactant molecules. When a surfactant forms an oil-in-water emulsion in the water phase, it is referred to as a Winsor Type I system. On the other hand, a Winsor Type II is a system with water-in-oil emulsion formed in the oil phase. It is well known that Winsor I and II systems are unfavorable with respect to achieving ultra-low IFT, as in Winsor Type I surfactant molecules tend to remain in the water phase, whereas in Winsor Type II they remain in the oil phase[183, 184]. Instead, ultra-low IFT is reached when surfactant forms a continuous layer between the aqueous and oil phases, which contains the surfactant, water, and dissolved hydrocarbons referred to as a Winsor Type III phase behaviour[182]. Indeed, the emulsion type inversion was found to be the main factor that controls the interfacial behavior of toluene/aqueous NaCl systems in the presents of sugar surfactants at elevated temperatures[68]. Authors[68] reported that IFT passed through a minimum at the phase inversion temperature around which emulsions invert from o/w tow/o, in much the same way as for the systems with ethoxylate surfactants[185]. To the best of our knowledge, our study is one of the first, which demonstrates that systems with cationic surfactant can also exhibit the same behavioral inversion with the temperature increase.

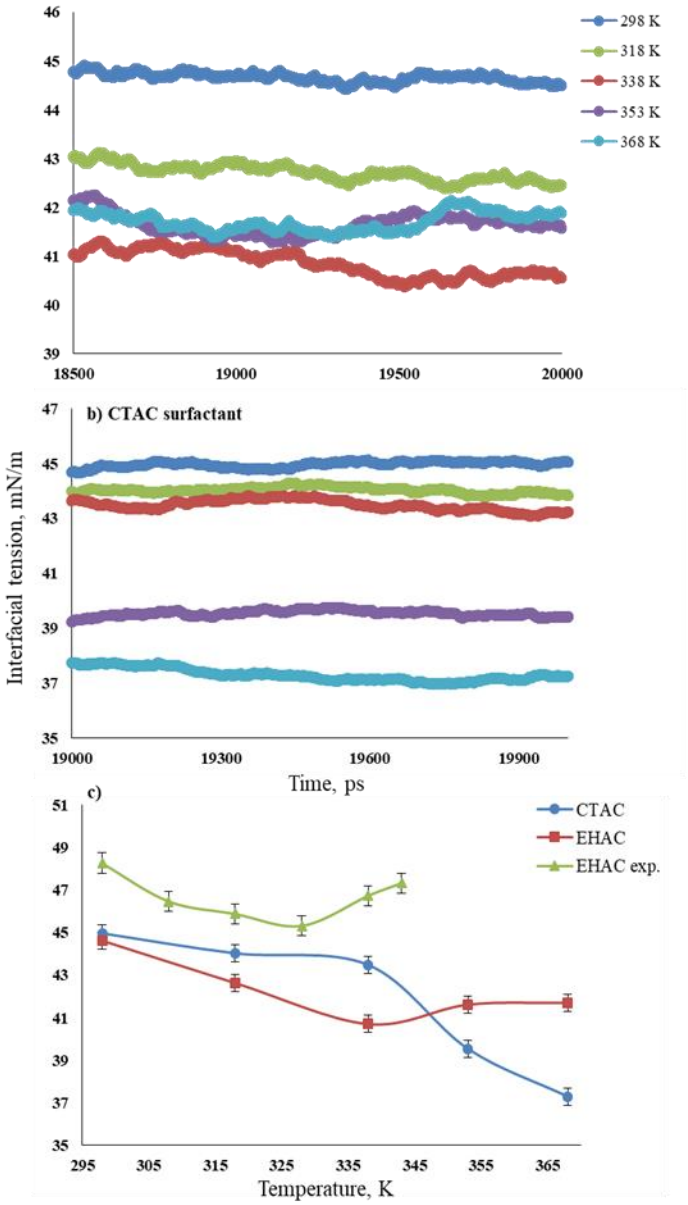

Figure 33. Simulation data for the interfacial tension of water/n-decane in the presence of a) EHAC surfactant and b) CTAC surfactant at different temperatures (blue – 298 K, green – 318 K, red – 338 K, green purple – 353 K, cyan – 368 K). c) Calculated interfacial tension between water/n-decane with EHAC (red line) and CTAC (blue line) and experimental data for 0.03 mM EHAC (green line) as a function of temperature.

Consequently, we suggest that water/n-decane systems containing EHAC surfactant are subject to behavioral inversion from Winsor type III to Winsor type II, governed by increasing temperature. At temperatures below 338 K, surfactant molecules formed a monolayer between

water and n-decane, resulting in decreasing IFT (Winsor type III). It was proposed in the literature that increasing temperature could modify the mutual solubility of water and oil, and thus, favor the IFT reduction[65]. However, up to now, this suggestion has not been verified due to the lack of information about the influence of structural properties of surfactant on its solubility at elevated temperatures. In our study, we hypothesize that the IFT minimum with increasing temperature is attributed mainly to the change of surfactant solubility rather than to the mutual solubility of solvents. Indeed, assuming that the EHAC surfactant has the hydroxyl groups in its head, we propose that increase in temperature (> 338 K) lead to the disruption of H-bonds between EHAC -OH groups and water molecules (see the section below), reducing surfactant solubility in water and increasing its affinity to the oil phase. As a result, when the temperature was around 338 K, slight diffusion of surfactant molecules into the hydrocarbon phase occurred, leading to an increase in IFT (Winsor Type II). The temperature associated with the minimum IFT is often referred to as phase inversion temperature[186]. Above this temperature, IFT increased again, revealing the inversion of emulsion type to w/o, i.e. from Winsor type III to Winsor Type II.

4.3.2 The density profiles

The average density profiles were obtained for all system components by calculating the density of the 300 slices perpendicular to the z-axis using the productive NVT simulation data. Figure 33 represents the results of the density distributions for models of CTAC surfactant, water, and n-decane at 298 K and 368 K. Two temperatures were chosen for this density analysis as they corresponded to both increasing and descending trends on the IFT curve (Figure 33c). From Figure 34, it can be seen that the water and n-decane densities had a well-defined sharp interface at both sides.

The surfactant molecules were clearly adsorbed at these interfaces, and there were no interactions between molecules from the different sides. The temperature increase from 298 K to 368 K led to a slight decrease of water and n-decane average densities – 4% and 8%, respectively, which is in good agreement with literature data for water and n-decane[187]. Furthermore, surfactant density changed with increasing temperature, indicating that molecules were distributed in a broader interfacial zone compared to the surfactant model at ambient temperature.

The water density distribution $\rho\,(z)$ was determined by fitting the simulation data with the error function[188]:

$$\rho\,(z) = \frac{\rho_0}{2}\left(1 - \mathrm{erf}\left(\frac{z - z_0}{\sqrt{2w}}\right)\right),$$

where ρ_0 is the density of water, z_0 is the position of Gibbs Dividing Plane (GDP), erf is an error function and w is the width of the interface.

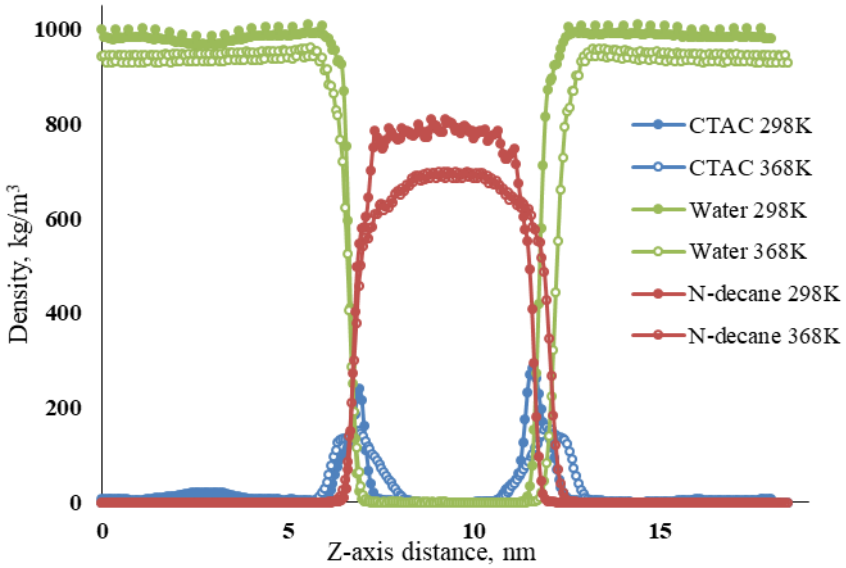

Figure 34. The density profiles of CTAC at 298 K (blue filled circles) and 368 K (blue open circles); water at 298 K (green filled circles) and 368 K (green open circles); n-decane at 298 K (red filled circles) and 368 K (red open circles). Pressure 1 bar.

The Gibbs dividing plane was determined for each temperature using water density profiles around the interfacial zone and plotted in Figure 35.

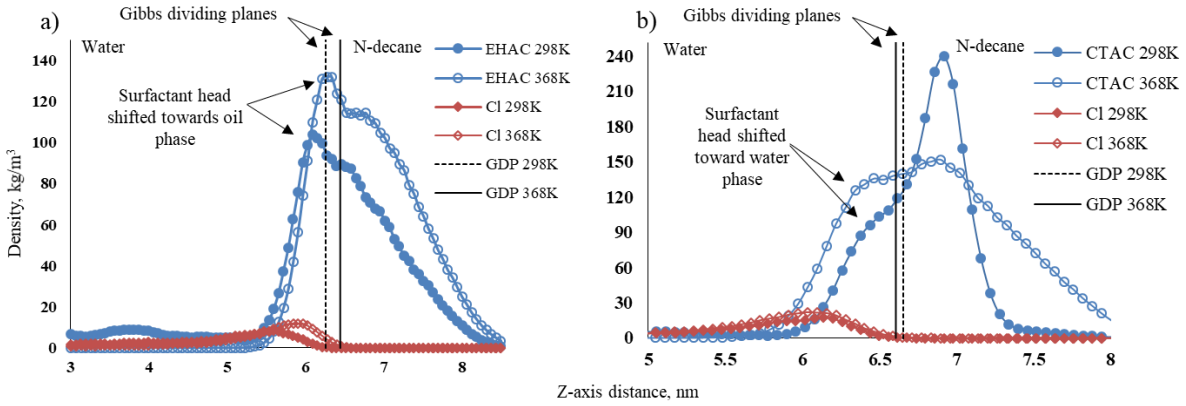

Figure 35. Surfactants and ions density distributions: a) EHAC surfactant and b) CTAC surfactant at two temperatures (298 K and 368 K).

It can be seen from Figure 35 that the surfactants' density profiles had two main peaks as expected. One peak corresponded to the head polar group of the surfactant and was close to the water phase, while the other peak represented the hydrophobic chain, which was oriented towards the n-decane phase. Here, it is interesting to point out that the Cl^- ions mainly concentrated near the hydrophilic group of both surfactants and could not approach the interface closer than 0.45 nm. This could be explained by taking into account that ions with the negative charge remained near to the hydrogen atoms of water, which had a partial positive charge. As a result, ions were covered by a monolayer of surrounding water molecules ("shell") caused by ion-dipole electrostatic interactions, which prevented them from reaching the interface more closely.

However, from Figure 35a, it can be seen that EHAC molecules moved close to the n-decane phase when the temperature was increased up to 368 K. Indeed, the density peak, which corresponded to the surfactant head groups, shifted closer to the n-decane phase from 0.17 nm at 298 K to 0.11 nm at 368 K. On the other hand (Figure 35b), the CTAC head group appeared to concentrate further inside the water phase when the temperature was raised, illustrating opposite behavior at the interfacial zone. This observation verified the hypothesis that EHAC solubility had been reduced with increasing temperature, as the affinity of the surfactant head to water decreased.

The other interesting fact to be pointed out is the arrangement of Cl^- ions around the surfactant polar heads. Figure 35b shows that the ions moved closer to the interface, from 0.52 nm at 298 K to 0.45 nm at 368 K. The existence of ions close to the interface could contribute to IFT reduction between water/n-decane with CTAC surfactant at higher temperatures[189]. Opposite to this, Cl^-

approached the hydrophilic EHAC surfactant head from a distance of 0.55 nm at 298 K to 0.49 nm at 368 K and resided in the same location relative to the interface.

4.3.3 Quantification of radial distribution functions and hydrogen bonds

Since the density profiles cannot explain arrangements between surfactant molecules, ions, and water molecules in the interfacial zone, the radial distribution functions (RDF) were analyzed. Radial distribution functions provide detailed information about the interactions between atoms, revealing insights into structural correlations between molecules. In this work, we coupled the RDF analysis with the calculation of the number of hydrogen bonds (H-bonds). This can help to determine the arrangements between surfactant molecules, water, and ions at the interfacial zone at different temperatures.

The main difference between the molecular structure of the two cationic surfactants was that the EHAC polar head contained two hydrophilic groups (-OH) in addition to N^+ and CH_3 groups (Figure 32). As such, for RDF and H-bonds calculations, the EHAC molecule was divided into three parts – tail, head, and two hydroxyl groups (-OH), whereas the CTAC molecule was divided into tail and head. Simulation results showed that the cationic head groups of both surfactants resided in the water phase with the tail (hydrophobic part) stretched perpendicular to the interface into the n-decane phase at all temperatures (Figure 36).

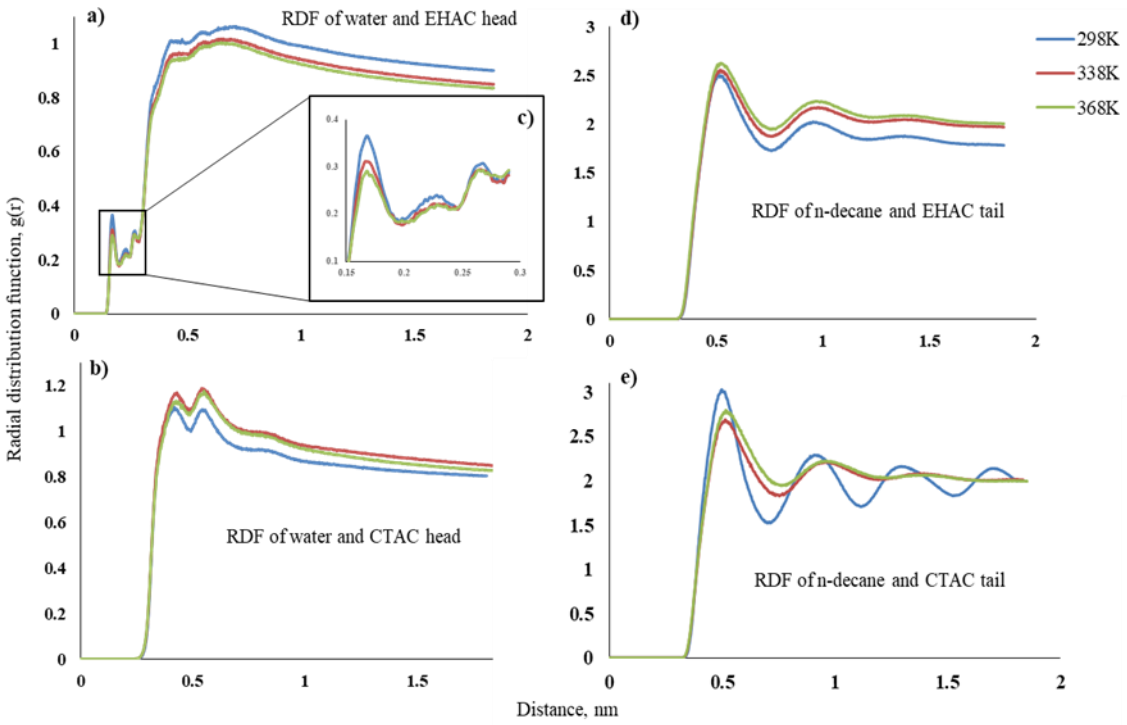

Figure 36. Radial distribution functions between water and surfactant heads – EHAC (a) and CTAC (b); (c) Zoom in to the RDFs between EHAC head and water from 0.15 to 0.3 nm; (d) and (e) - radial distribution functions between n-decane and EHAC and CTAC surfactant tails, respectively. Colours indicate temperatures - 298 K (blue), 338 K (red) and 368 K (green).

This observation illustrates the well-known ability of surfactants to orient at interfaces between two immiscible fluids and is consistent with SDS[135] and sulfobetaine-type zwitterionic[190] behavior at the water/oil interface. It can be seen from Figures 36d, e that the radial distribution functions of EHAC and CTAC surfactant tails/n-decane showed the same behavior patterns, while RDFs between surfactant heads and water had different patterns (Figures 36a, b). Indeed, the peaks on RDF plots of EHAC head and water were observed at 0.17 nm, 0.23 nm, and 0.27 nm (Figure 36a). This can be interpreted that hydrogen and oxygen atoms of the surfactant head served as donors and acceptors for the formation of H-bonds with near water molecules. The existence of three peaks indicates that oxygen atoms can be acceptors for two hydrogen atoms.

It is interesting to note that with the temperature increase, the intensity of these peaks decreased, which could be due to the reduction of the number of hydrogen bonds[73]. To verify this hypothesis, the average number of H-bonds (n_{HB}) between surfactant -OH groups and water

molecules was calculated at three temperatures within a cut-off distance of 0.35 nm, which was approximately the last peak of the RDF curves (Figure 36c). From Table 8, it can be seen that the average number of H-bonds per molecule decreased consistently with increasing temperature – from 3.43 at 298 K to 3.13 at 368 K.

Table 8. The average number of hydrogen bonds per molecule at different temperatures.

Temperature	298 K	338 K	368 K
n_{HB}	3.43	3.22	3.13

Hydrogen bonds play a critical role in controlling the solubilization of molecules containing oxygen and hydrogen in a water phase[164]. When the number of H-bonds around water molecules decreases with temperature, the solubility of the hydrophilic part of the surfactant in water also decreases, resulting in surfactant diffusion towards the hydrophobic phase. This is consistent with our result, which illustrated the shift in the density distribution of EHAC head close to the n-decane phase at 368 K (Figure 35a).

On the other hand, the peaks on the RDFs curves of CTAC head and water were observed only at 0.44 nm and 0.55 nm, showing that there were no interactions between molecules caused by H-bonding (Figure 36b). This could be explained by assuming the fact that the nitrogen atom in the CTAC head group shared all electrons with the -CH_3 groups, and thus, could not provide the lone pair of electrons to form bonds with water molecules.

A fundamental question of interest here is the potential connection between Cl^- ions and the polar head group of surfactants, which can influence surfactant molecules arrangements near the interface. For this reason, the radial distribution functions between Cl^- and a head group of surfactants were studied, as shown in Figure 37.

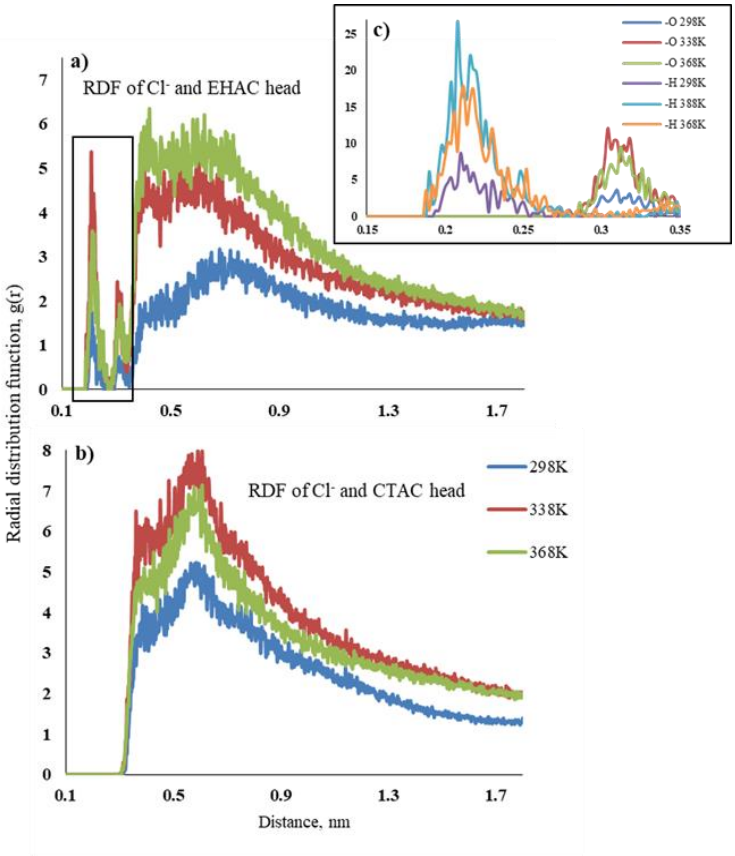

Figure 37. Radial distribution functions between Cl^- ions and surfactant heads – EHAC (a) and CTAC (b); (c) Radial distribution functions between Cl^- ions and oxygen and hydrogen atoms, respectively. The colours correspond to three temperatures: 298 K (blue), 338 K (red) and 368 K (green).

In Figure 37a, it can be seen that the RDF curves of EHAC head and ions had two sharp peaks within 0.35 nm range, whereas no peaks were observed for CTAC in the same distance. The peak, which appeared at 0.59 nm on RDF plots of both surfactants, could be referred to the electrostatic interactions between ions and positively charged $-CH_3$ and $-CH_2$ groups in the surfactant heads.

Furthermore, additional RDFs were calculated between separated oxygen and hydrogen atoms of surfactant and ions at different temperatures in order to provide the molecular origins of connection between Cl^- and EHAC head at distances <0.35 nm (Figure 37c). These graphs show an interesting behavior, as the first and second peaks revealed connections between both Cl^-/H^+ and Cl^-/O^- atoms. Such findings cannot be explained only by using the concept of electrostatic interactions between similarly charged atoms. Instead, one can consider the existence of the ion-

dipole forces between water and ions. In the literature, it has been reported that ions are surrounded by water molecules, which form a hydration layer ("shell") around them[191]. The existence of such hydration layers has also been reported for different ions, including Na^+, K^+, Ca^{2+}, Cl^- [192]. Hence, electropositive hydrogen atoms of the water molecules were attracted to the negative charge of the Cl^- by ion-dipole bonding. Further, these water molecules could serve as donors and acceptors for the formulation of the hydrogen bonds with hydrogen and oxygen atoms of surfactant head, contributing to the first and second peak of RDF plots, respectively (Figure 37c). Therefore, the existence of -OH groups caused the additional H-bonding network with ions, contributing to the surfactants' hydrophilic properties.

Notably, it was also shown that the presence of the carbonyl group in the surfactant head group resulted in the formation of hydrogen bonds between triacontanoic acid head groups and water at the water/hexane interface[193]. The authors demonstrated that the existence of hydrogen bonds affected the conformation of surfactant molecules at the interface leading to the change from disordered to ordered tail groups of surfactant. Interestingly that the difference in the conformation of alkyl chains was also observed for alkane- and alkylbenzenesulfonate surfactants[194]. The authors attributed the staggered tail geometry for dodecylbenzenesulfonate to the polarizable nature of the benzene ring. Arrangements between surfactant molecules, ions, and water at the interfacial zone are conceptually demonstrated in Figure 38.

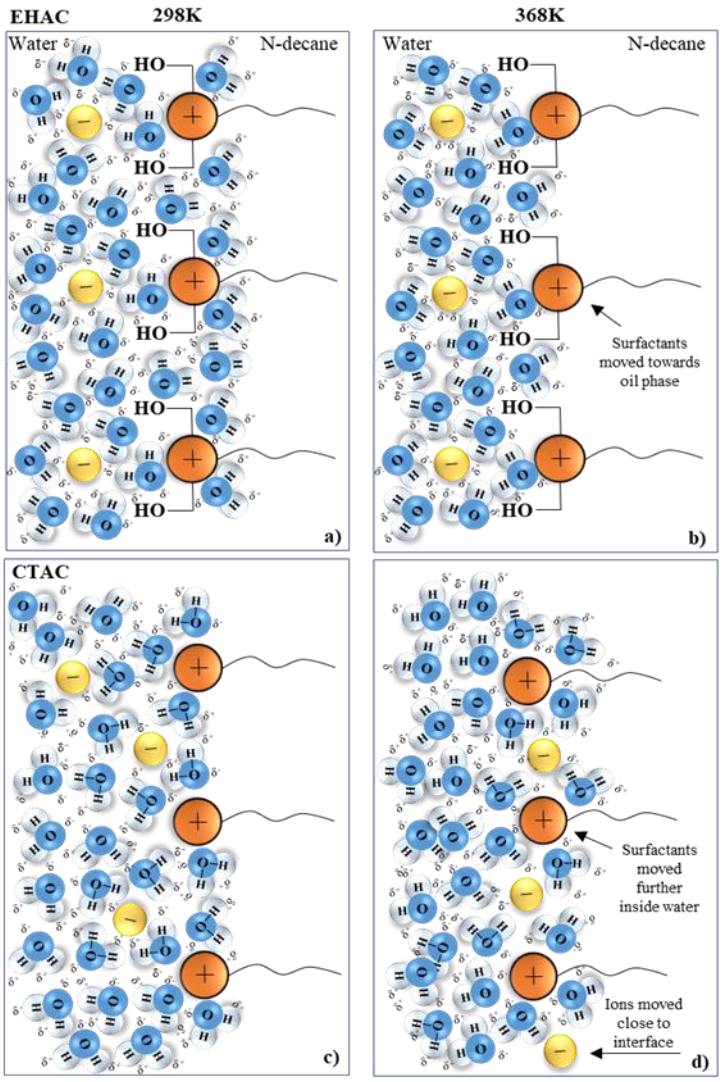

Figure 38. Arrangements between EHAC (a, b) and CTAC (c, d) surfactant molecules (orange color), ions (yellow color), and water molecules (blue and white colors) at the water/n-decane interface at 298K (a, c) and 368K (b, d).

Since the interactions between ions and -OH surfactant groups were observed at all temperatures (Figure 37a), we conclude that ions influenced the arrangements of the surfactant molecules at the interface, but they had an insignificant impact on interfacial tension increase at high temperatures. We also suggest that due to the chemical structure of EHAC molecules, ions could not approach the interface closely, and they remained mainly near the polar surfactant heads in the aqueous phase (Figures 38a, b). The CTAC head, in contrast, was smaller than the EHAC

head, thus some Cl^- ions could get closer to the interface, supporting interfacial tension reduction when the temperature was increased (Figures 38c, d)[188].

4.4 Summary

Self-assembly of surfactant molecules at a water/oil interface controls the IFT, and as a consequence, plays a key role in an effective oil production[183]. The majority of surfactant studies are dedicated to searching for the best formulations for EOR, including IFT measurements, wettability alteration, and core flood tests[39]. However, there is still a serious lack of information regarding the surfactant molecules packing at the interfacial zone that directly influences the IFT properties.

Thus, this study investigates the adsorption of two cationic surfactants with different molecular structures at the water/n-decane interface at different temperatures: 298 K, 318 K, 338 K, 353 K, and 368 K. We showed that surfactants had different IFT when the temperature was increased. As expected, the IFT of CTAC surfactant decreased with the temperature according to the Gibbs theory. Whereas the IFT of EHAC went through a minimum at 338 K and then started to increase.

Such behavior cannot be explained by the implementation of the conventional Gibbs adsorption equation. From this study, we suggest the following explanation for the seen phenomena.

The existence of hydroxyl groups in the EHAC surfactant head resulted in the formation of additional hydrogen bonds with the nearest water molecules. As the temperature was increased to 368 K, the number of hydrogen bonds in the system decreased up to 10%. As a result, the EHAC polar head became less soluble in water and displayed more affinity to the oil phase. The slight diffusion of EHAC surfactant head further into the oil phase at high temperatures was also verified by density distribution profiles. This led to emulsion type inversion from oil-in-water to water-in-oil, i.e. from Winsor type III to Winsor Type II, with a consistent IFT increase. Therefore, we hypothesize that hydrogen bonding between surfactant and water plays an important role at the liquid/liquid interfaces and controls the interfacial behavior of surfactant at elevated temperatures. We thus, also propose that the observed IFT - temperature dependence can be generalized for other surfactants containing head groups that can form hydrogen bonds with surrounding water molecules. Our results showed that Cl^- ions interact with -OH groups of EHAC surfactant by ion-dipole forces and resided rather more close to the surfactant head than to the interface (at all

temperatures). Therefore, we conclude that the presence of Cl^- was unlikely responsible for the IFT increase with temperature.

On the other hand, due to the small head group of CTAC surfactant, Cl^- ions positioned closer to the interface when the temperature was high, contributing to the IFT decrease. The obtained results provide an important basis for the understanding of deviations from the Gibbs theory of surfactant adsorption at the interfacial zone. Thus, the findings of this work can be used for further modification of the existed theory by taking into account the chemical structure of surfactants.

Chapter 5. Molecular dynamics study of ions effect on surfactant – hydrocarbon interfaces

5.1 Motivation

The brine-oil interface is of broad research interest in the petroleum industry and geochemistry. Indeed, the functionality and effectiveness of surfactant formulations, and consequently oil recovery efficiency, strongly depend on the concentration and type of ions present in the formation brine[46]. In general, the presence of salt in natural brines causes a decrease in the solubility of surfactants in the aqueous phase due to the salting-out effect[78,79]. Thus, more surfactant molecules are forced to approach the interface closely, which leads to the brine/oil IFT decrease. However, as it was shown in many studies[60, 80, 82, 84], IFT can pass through a minimum, illustrating the so-called "V"- shape pattern. However, despite a considerable number of experimental studies, the existence of two different IFT-salinity patterns cannot be satisfactorily explained. For instance, while the descending IFT trend can be attributed to the surfactant molecules packing tightly at the interface, the ascending IFT trend is not well understood. Bera et al.[60] suggested that IFT starts to increase at the point where the accumulation of surface active-agents terminates. Another promising explanation is the partitioning of surfactant molecules into the oil phase as salinity increases, with a consequent formation of micelles in the oil phase[84].

However, due to complexities associated with the experimental procedures and limitations of experimental equipment, it is challenging to investigate the effect of ions at the atomic scale in such systems and to capture their precise molecular arrangements at the interface, especially in the presence of surfactants[85]. Recently, it was shown that molecular modeling approaches such as molecular dynamics (MD) and Monte Carlo (MC) can be used for detailed studies of the molecular interactions and orientations at liquid/vapor[85, 133, 134, 195] and liquid/liquid[135, 139, 196] interfaces at an atomic scale. Thus, these methods have been effective tools for providing detailed atomistic and molecular information about such interfaces, including hydrogen bonds correlation functions[144] and interfacial thicknesses[197].

Although there are simulations addressed the influence of ions on brine/oil[198] and surfactant/brine/oil IFT[142], to our knowledge, no systematic MD study has been performed to investigate the effect of ions and temperature on the interfacial properties of surfactants with different molecular architecture at the oil/water interfaces.

Therefore, to address this deficiency, we present MD simulation studies on ions and temperature effects to resolve the adsorption process of surfactants at the water/n-decane interface. The surfactants used in this study are both cationic (erucylbis-(hydroxyethyl)-methylammonium chloride, EHAC, and cetyltrimethylammonium chloride, CTAC) (the same as in the previous chapter). EHAC has two hydroxyl groups (Figure 31), and thus, can combine features of both cationic and non-ionic surfactants. This study focuses on the following aspects: how surfactant packing at the water/oil interface is affected by ions specific effects, and how temperature influences the molecular arrangements and interactions of surfactant molecules at the interfacial zone in the presence of ions.

5.2 Computational method

The interfacial behavior of the cationic surfactants CTAC and EHAC has been studied by molecular dynamics. Simulation boxes were built by placing slabs of surfactant layers (2 nm each) around an n-decane layer (thickness 6 nm). The model system consisted of two n-decane–aqueous phase interfaces as this has been shown to be advantageous for liquid/liquid interfacial studies[76]. The box with surfactant and n-decane molecules was stretched along the Z direction to 18 nm to create space for water molecules. Owing to the fact that formation water is usually enriched mainly with NaCl salt[199], different numbers of Na^+ and Cl^- ions were inserted by replacing water molecules so that prescribed concentrations were reached (i.e. NaCl concentrations of 0.01, 0.02, 0.03, 0.07, 0.1, 0.2, 0.4, 0.6 and 1 M). This range of NaCl concentrations accounts for low salinity brine (5 wt.%) and for typical reservoir brine salinity[198]. The number of surfactant molecules in each slab was set in such a way that area density for EHAC equaled to 0.25 molecule / nm^2, while for CTAC 0.38 molecule / nm^2. These values are adopted from the previous simulation studies and are consistent with other researches, where interfacial behavior has been investigated[132, 179, 196, 200], and was constant in all simulation runs. Since in our study we are focusing on molecular interactions at the interface and not on the bulk properties of surfactants, the concentrations considered in this study are within a reasonable range to mimic the adsorption behavior and chemical interactions properly.

The partial charge distribution among atoms and ions (Figure 39) was taken from data proposed in the literature[176], which was successfully used for the computation of similar systems[179]. The molecular potentials between atoms of both surfactants were described using the

GROMOS force field[172, 173]. The SPC/E model was employed to model the water potential[174], and the particle-mesh Ewald (PME) method of summation was implemented to compute the electrostatic interactions[144]. The initial size of the simulation box was 4 × 4 × 18 nm3 for each system.

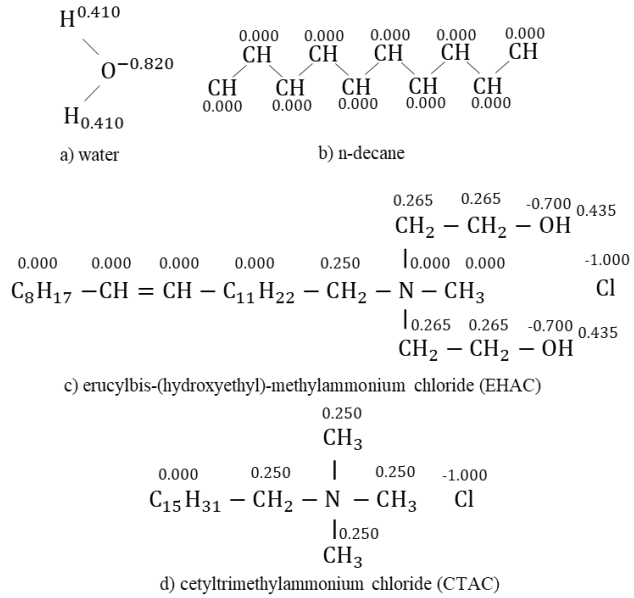

Figure 39. Chemical structures and charge distribution models used in this study: a) water; b) n-decane; c) erucylbis-(hydroxyethyl)-methylammonium chloride and d) cetyltrimethylammonium chloride.

All molecular dynamic simulations were carried out using the GROMACS 4.5.5 package[171] at atmospheric pressure (1 bar) and two temperatures (298 K and 343 K). The steepest descent method with the cut-off scheme for Coulomb and van der Walls forces of 0.9 nm was used for energy minimization to ensure that the system had no steric clashes. The first step of equilibration was conducted under an NVT ensemble (constant Number of particles, Volume, and Temperature) using a Berendsen thermostat[171]. Equilibration of the pressure, and thus also density, was performed under an NPT ensemble (constant Number of particles, Pressure, and Temperature) using the Parrinello-Rahman barostat[171]. The calculated densities of n-decane (0.726 g/ml) and water (0.994 g/ml) are in a good agreement with experimental values – 0.725 g/ml and 0.997 g/ml for n-decane and water, respectively[159, 187, 201]. Both NVT and NPT equilibration steps were carried

out at 1 bar and the temperature studied (i.e. 298 K or 343 K), followed by 20 ns of production runs in the NVT ensemble using the Nose-Hoover thermostat[171]. The interfacial tensions, density profiles, distribution functions of n-decane, ions and surfactants, and the number of hydrogen bonds were calculated by analyzing the atomic trajectories recorded at 0.5 ps intervals.

5.3 Results

5.3.1 Ions effect on interfacial behavior of surfactants: the impact of molecular structure

The interfacial tension (γ) can be determined from the following, as the interface between the phases is perpendicular to the Z-axis direction[76]:

$$\gamma = -\int_0^{L_z}(p'(z) - p)dz,$$

where L_z is the box length along the z-axis, $p'(z)$ is the lateral pressure, and p is the bulk pressure.

The integral can be calculated using the fact that in the bulk solution $p = p'(z)$ and taking into consideration that there are two interfaces in our system[76]:

$$\gamma = -\frac{1}{2}\left(\frac{p_x+p_y}{2} - p_z\right)L_z,$$

where p_α describes the three diagonal elements of the pressure tensors $P_{\alpha\alpha}$ $(\alpha = x, y, z)$ along the axis.

Hence, the simulation data for the water/n-decane interfacial tensions in the presence of EHAC and CTAC surfactants at different NaCl concentrations are presented in Figures 40a, b. To obtain accurate values, only the last 2 ns of simulation data was used for IFT calculation (Figures 40c, d). For each salt concentration, three simulation boxes were built independently for the standard deviation calculation.

In Figure 40c it can be seen that the interfacial tension of EHAC went through a minimum at 0.03 M NaCl concentration, illustrating a "V"- shaped pattern at 298 K and 343 K. On the other

hand, the interfacial tension of CTAC increased within the range of all tested NaCl concentrations at 298 K and 343 K (Figure 40d).

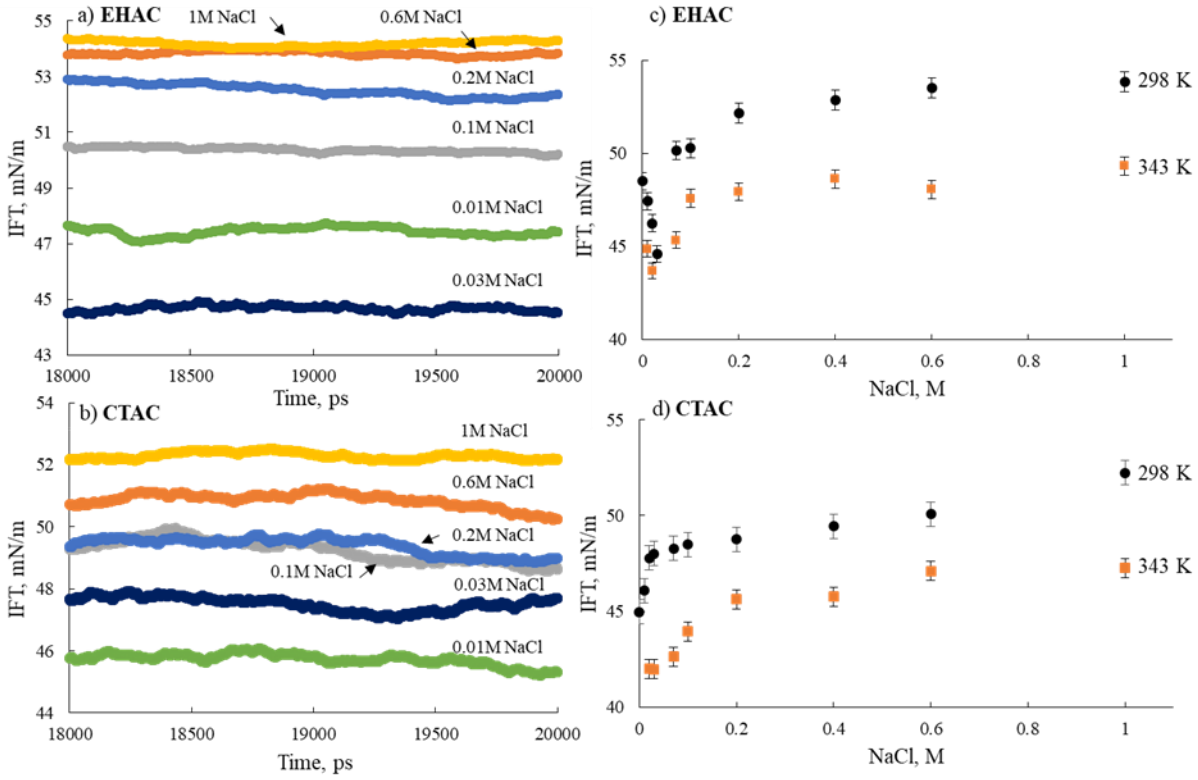

Figure 40. Simulation data for the water/n-decane interfacial tension in the presence of (a) EHAC surfactant and (b) CTAC surfactant at different NaCl concentrations; calculated IFT values for EHAC (c) and CTAC (d) surfactants as a function of NaCl concentration at two different temperatures – 298 K (black circles) and 343 K (orange squares). Colors in (a) and (b) represent different salt concentrations.

Here, we exclude the influence of impurities or synergy effects of different hydrocarbons on interfacial behavior as all simulations were performed with the pure components. Therefore, one of the main reasons for the observed ascending IFT trend for CTAC could be related to an emulsion inversion from oil-in-water (o/w) to water-in-oil (w/o), which is caused by an increase in salt concentration. Indeed, this behavior is usually described in terms of the Winsor phase types[163, 182]. As such, if surfactant forms an o/w emulsion in the aqueous phase, it is affiliated with a Winsor I system; on the contrary, a system with w/o emulsion formed in the oleic phase is referred to as

Winsor II type. However, Winsor I or Winsor II emulsions exhibit high IFT values[182], as surfactant molecules are mostly retained in bulk (water or oil) phases rather than approach the interface. Instead, low IFT values can be reached when there is a continuous layer of surfactant molecules between aqueous and oleic phases, referred to as Winsor Type III behavior. Previously it was reported that without salt, all CTAC molecules tend to adsorb at the interface, representing Winsor Type III behavior[196]. In this context, we suggest that water/CTAC/n-decane systems in the presence of electrolytes endured the behavioral inversion from a Winsor III (when all CTAC molecules were adsorbed at the interface) to a Winsor II system. Such a salting-out effect can be governed by temperature[196, 202] and/or salinity[181]. Therefore, the solubility of CTAC in the water phase is lowered due to an increase in salt content, and, as a result, CTAC affinity to the oil phase is increased. This is also verified by the observation of slight diffusion of CTAC molecules further inside the oil phase (see below sections). Consequently, IFT increased upon salt addition.

It is worth mentioning that in our study, we used NaCl concentrations between 0.01 - 1 M. Although this is consistent with the NaCl content in the reservoir brines[198], even the lowest tested NaCl concentration may be too high to observe the descending IFT trend of CTAC. For instance, Zhang et al.[203] experimentally showed that emulsion inversion in systems containing a sorbitan oleate surfactant occurred at significantly lower NaCl concentrations, around 5 mM.

Interestingly, the IFT of water/n-decane/EHAC systems exhibits different behavior (Figure 40c). By now, in some experimental studies on the influence of electrolytes on aqueous surfactant solution/oil IFT, the IFT has been found to pass through a minimum with salinity increasing[80, 82, 83]. However, in these previous studies, only two regions were observed. As such, the first region illustrates a decrease in IFT values upon the addition of salt up to the optimal salt concentration. The second region shows an increase in IFT with further salt concentration increase. The descending and ascending trends on the IFT curve illustrate a “V” - shaped pattern.

In our study, the existence of a third region on the IFT curve has also been proposed. This region corresponds to the part of the curve where IFT values remained almost unchanged at higher salt concentrations (Figure 40c). Indeed, when NaCl concentration was higher than 0.4 M, the IFT remained almost constant and varied in the range 52.16 – 54.27 mN/m (Figure 40c). This range is consistent with experimental data of the interfacial tensions between brine solutions and hydrocarbons[204]. Therefore, we suggest that this phenomenon is attributed to the repelling of almost all surfactant molecules from the interface into the bulk due to the presence of ions near

the interface. To substantiate this further, we calculated the density distribution profiles and studied micelle formation in bulk (see below sections).

Notably, for EOR applications, reservoirs with a temperature range from 343 K to 393 K are considered to be promising candidates for surfactant flooding[205]. Therefore, in our study, we investigated the effect of one of the typical reservoir temperatures (343 K) on interfacial properties. Clearly, the IFT patterns for both surfactants at 343 K follow the same trend obtained at 298 K, and with the temperature increase IFT decreased for all NaCl concentrations tested (Figures 40c,d).

It is interesting to point out that surface tension between water and air in the presence of electrolytes also passes through a minimum at very low salt concentrations (1-2 mM)[206]. This effect is known as the Jones-Ray effect and has been considered an experimental artifact until recent experiments, including non-resonant second harmonic scattering and surface ion resonant second-harmonic reflection techniques, confirmed its existence[206]. Okur et al.[206] attributed this effect to the increase of the orientational order of water molecules in bulk induced by the addition of ions, which in turn increased the entropic penalty that caused the reduction of the surface tension.

Thus, following Okur et al.[206], we suggest that the descending trend of EHAC IFT at low salt concentrations (< 30 mM) originates from the increased orientational order of water molecules due to ion-dipole electrostatic interactions either in bulk or near to the interface. In this study, the orientation of water molecules at the n-decane/water interface in the presence of EHAC and different NaCl concentrations was analyzed considering the water dipole order parameter, cos (θ), where θ is the angle between Z-axis and water dipole moment[207]. The simulation box was divided into slices, with each water molecule assigned to a slice per time frame, and the average orientation per slice was calculated. Figure 41 illustrates the computed average cos (θ) as a function of distance along the Z-axis. The results demonstrated that values of cos (θ) remained positive at the interfacial zone, forming a peak, while the bulk angle equaled zero due to the random distribution of water molecules (Figure 41). The same trends of cos (θ) were observed for ethanol and methanol at the water/air interface[208].

It was shown[209] that near the interface, water molecules had a two-layer orientation; namely, in one layer, the water molecules pointed towards the water phase, while they pointed towards the oil phase in the second layer. The presence of surfactant molecules and ions near the interface disrupted this molecular water molecule arrangement. Therefore, water molecules at the outmost

layer tended to reorient (more pointing towards the water phase) to comfort EHAC molecules and ions[207]. In Figure 41 it can be seen that the positive peak increased and shifted further inside the n-decane phase with increasing NaCl concentrations up to 0.03 M, which suggests an increase in the orientational order of water molecules. This shift of peak in the water dipole order distribution curve has been correlated with surface tension reduction[209]. Thus, the decrease of IFT upon the addition of NaCl below 0.03 M can also be attributed to the increase of the orientational order of water.

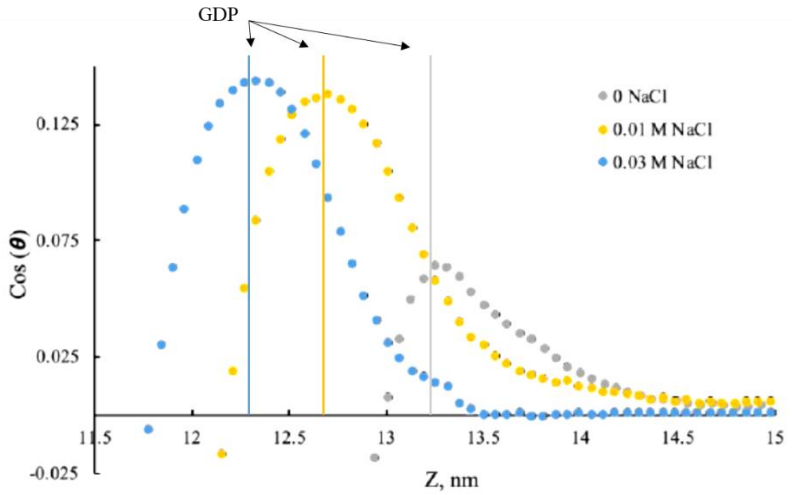

Figure 41. Water dipole order parameter in the presence of EHAC molecules and different NaCl concentrations. Colors represent 0 NaCl (grey), 0.01 M NaCl (yellow) and 0.03 M NaCl (blue).

5.3.2 Density distribution profiles of surfactants, n-decane, ions and water

The average density distribution profiles were obtained for water, n-decane, either EHAC or CTAC surfactants, Na^+ and Cl^- ions by calculating the density values over 300 slices perpendicular to the Z-axis. The bulk density of water was found to increase slightly with the increase of NaCl concentration, while the bulk density of n-decane was calculated to be 726 kg/m^3, both are in good agreement with literature data[187].

From Figure 42 it can be seen that EHAC and CTAC surfactant molecules were oriented around the water/n-decane interface with two well-defined sharp peaks. The right peak represented

the surfactants' head polar groups anchored in the water phase, while the left peak corresponded to the hydrophobic tail, which resided inside the n-decane phase.

Interestingly, at low salt concentrations (< 0.03 M), no EHAC molecules were observed in the bulk phase, whereas CTAC molecules were located both at the interface and in bulk, illustrating a different behavior (Figure 42b). Note that in the absence of salt, CTAC surfactant molecules are adsorbed only at the water/n-decane interface[196].

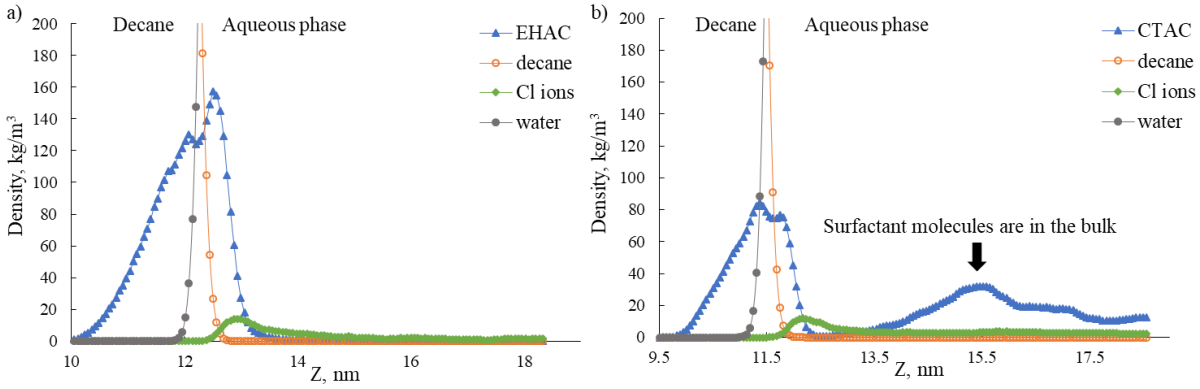

Figure 42. Density profiles of water/n-decane systems containing (a) EHAC surfactant, and (b) CTAC surfactant, in the presence of 0.01 M NaCl.

Therefore, to describe the interfacial behavior of these surfactant molecules, we analyzed the distributions of surfactant tails and heads at the interface at different salt concentrations (Figure 43). The Gibbs dividing planes were determined for each salt concentration by fitting the simulated water density data of the interfacial zone with the error function[188]:

$$\rho\,(z) = \frac{\rho_0}{2}\left(1 - \mathrm{erf}\left(\frac{z - z_0}{\sqrt{2w}}\right)\right), \qquad (3)$$

where ρ_0 is the water density, z_0 is the position of the Gibbs Dividing Plane (GDP), erf is an error function and w is the interface width.

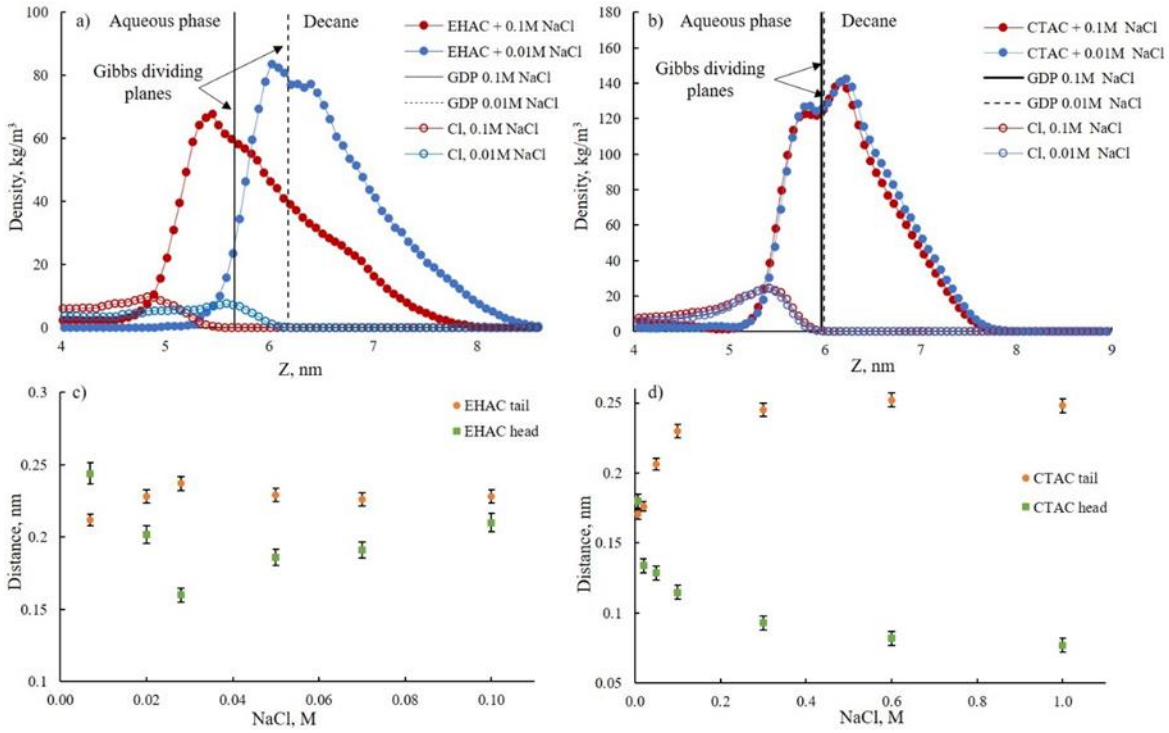

Figure 43. Surfactant and ion density distributions: (a) EHAC surfactant and (b) CTAC surfactant in the presence of 0.1 M NaCl (red circles) and 0.01 M NaCl (blue circles); distance of surfactant tail and head relative to the GDP position as a function of NaCl concentration: (c) EHAC surfactant and (d) CTAC surfactant.

The density profiles of surfactants and Cl^- ions in 0.01 M and 0.1 M NaCl brines are shown in Figures 43a, b. The distances of surfactant tails and heads relative to the GDP position are plotted as a function of NaCl concentration in Figures 43c, d.

As it can be seen in Figure 43, EHAC and CTAC molecules showed different arrangements at the interfacial zone when salt concentration was increased. As such, the polar heads of EHAC approached closely to the interface from 0.24 nm to 0.16 nm when NaCl concentration was below 0.03 M and moved further inside the aqueous phase when NaCl was above 0.03 M (Figure 43c). This trend clearly follows the IFT "V" pattern (Figure 40c), and thus, the decrease in IFT at low salt concentrations can be attributed to the optimal packing of surfactant heads at the interface that allows more surfactant molecules to adsorb. However, with further NaCl concentration increase, the distance between head and interface started to increase, whereas the distance between tail and interface decreased gradually. Therefore, we conclude that some surfactant molecules desorbed

from the interface, and thus, fewer surfactant molecules were presented at the interface, resulting in the IFT increase. When almost no surfactant molecules were left at the interface, IFT values were identical to experimental values for the NaCl brine/hydrocarbons system within the experimental error[210].

In contrast, an increase in NaCl concentration in water/n-decane systems containing CTAC showed the opposite behavior. While the distance between the surfactant head and interface decreased, the distance between the tail and interface increased (Figure 43d). We conclude that surfactant molecules penetrated further inside the oil phase with increasing NaCl content. As a result, IFT increased for all NaCl concentrations investigated (Figure 40d). The same behavior was experimentally observed for the IFT between anionic decylmethylnaphthalene sulfonate surfactant and crude oil[84]. It was suggested[84] that at high salinity (> 0.4 M), surfactant molecules started to partition into the oil phase, resulting in the formation of reverse micelles.

Taking into account that CTAC surfactant cannot form hydrogen bonds with water molecules (see below section for an explanation), we propose that the main reason for the IFT increase in the presence of salt is that the hydrophobic interactions become stronger than the solute-solvent interactions, and thus, surfactant molecules migrate into the oil phase.

The different interfacial arrangements of EHAC and CTAC are also visualized in Figure 44. In Figures 44c, it can be seen that at 1 M NaCl concentration, all EHAC molecules associated with each other and formed micelle, while no CTAC micelle was observed either in the oil or in the aqueous phase. This can be explained by the different molecular surfactant structure, which results in different critical micelle concentrations (CMC), which are 0.03 mM for EHAC[94] and 0.92 mM for CTAC[178]. Besides, CMC is found to decrease with the addition of salt[163], which also facilitates EHAC micelle formation in the bulk phases. However, in Figures 44d, e, f, it can be seen that although no CTAC micelles were found in the oleic phase, surfactant molecules moved further inside the hydrocarbon phase.

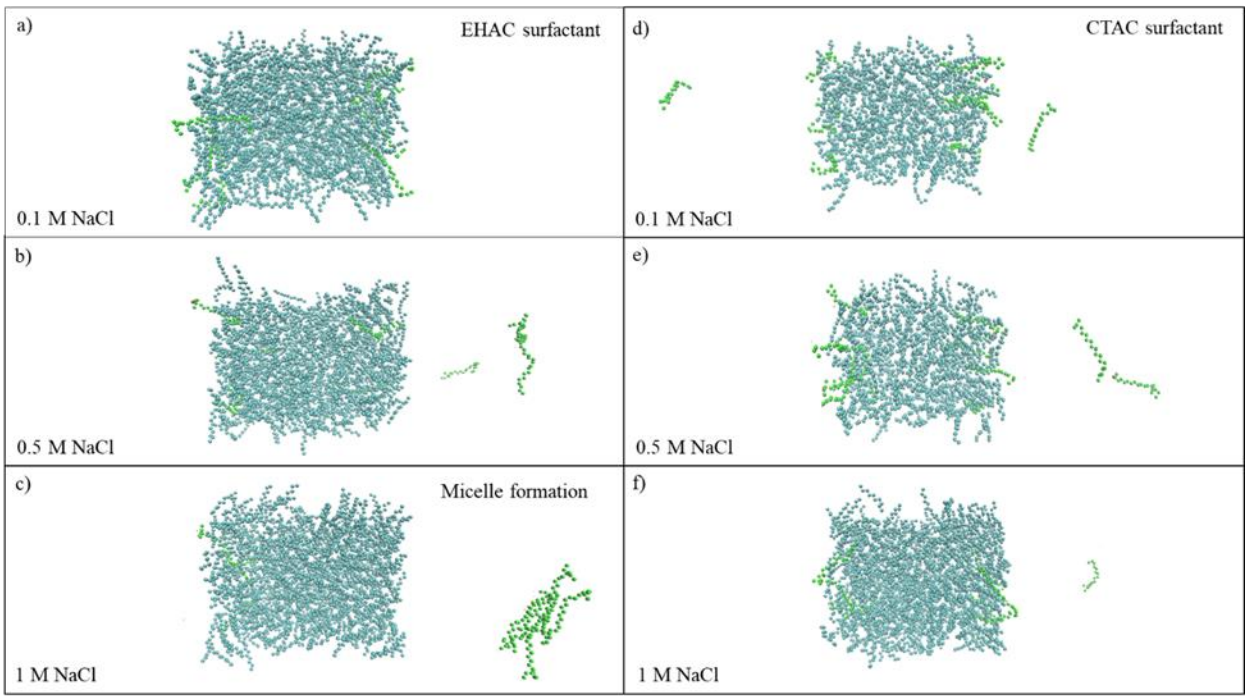

Figure 44. Snapshots (obtained using VMD[177]) of the simulation box containing EHAC surfactant with (a) 0.1 M NaCl, (b) 0.5 M NaCl and (c) 1 M NaCl brine; CTAC surfactant with (d) 0.1 M NaCl, (e) 0.5 M NaCl and (f) 1 M NaCl brine. Colors: cyan – carbon in n-decane, green – carbon in surfactant. Water molecules and ions are removed for better visualization.

A fundamental question of interest here is the Na^+ ion distribution, which we hypothesize to be the main reason for the surfactant molecules being repelled from the interface. To verify this hypothesis, we calculated and analyzed the density distribution profiles of Na^+ at different NaCl concentrations relative to the Gibbs dividing plane (Figure 45).

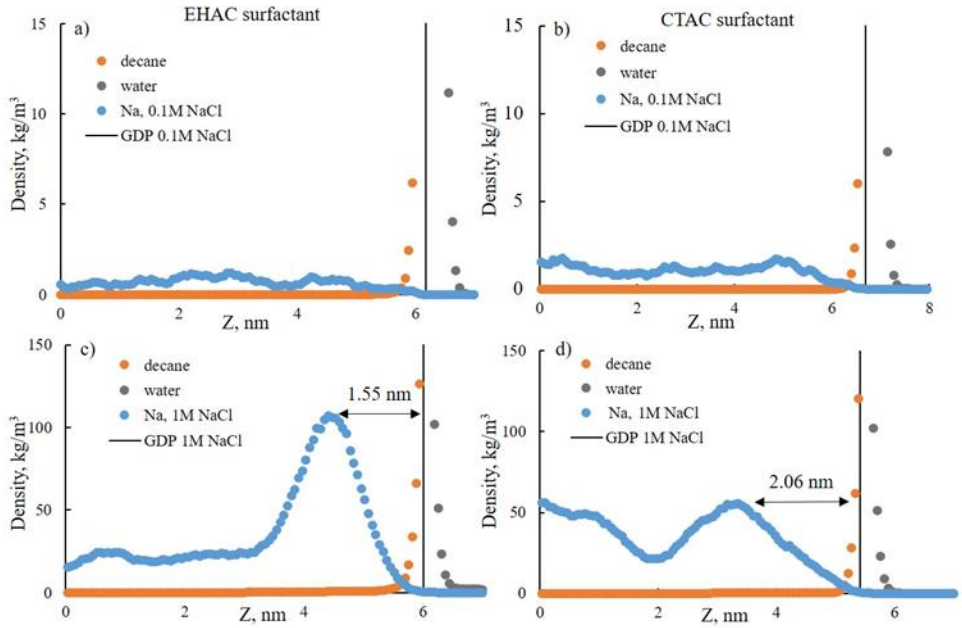

Figure 45. Average density distributions of decane (orange circles), water (grey circles) and Na^+ ions (blue circles) for EHAC (a, c) and CTAC (b, d). Note that NaCl concentration is 0.1 M in (a), (b) and 1 M in (c), (d).

Interestingly (Figures 45c, d), that at high NaCl concentration (1 M), Na^+ ions approached the interface more closely in the presence of EHAC (1.55 nm distance) than of CTAC (2.06 nm distance) molecules. On the contrary (Figures 45a, b), at low NaCl concentration (0.1 M), Na^+ ions were distributed homogeneously in bulk for both surfactants.

It is known that positively charged surfactant headgroups adsorbed at the interface facilitated the adsorption of negatively charged Cl^- ions in the Stern layer at the same Helmholtz plane[211]. Furthermore, adsorbed ions can be shared by several headgroups, and thus the Stern layer can be considered to be not electroneutral. The charge of the Stern layer (i.e. the sum of charges of adsorbed surfactant headgroups and ions) determines the potential of the diffuse layer. Thus, as outlined above, with increasing salt concentration, Na^+ ions can approach closer to the interface (out of the diffuse layer), contributing to the overall positive interfacial charge density. As a result, surfactant molecules will be repelled from the interface due to the increased positive charge density. These results are conceptionally presented in Figure 46.

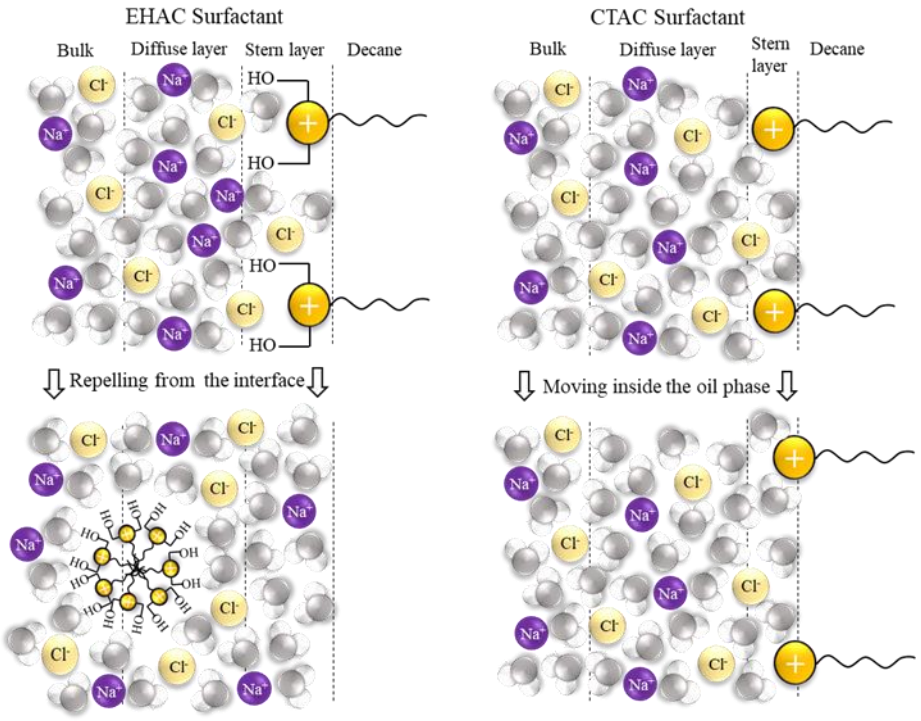

Figure 46. Schematic representation of ion and surfactant molecule arrangements at the interface and in the diffuse layer and bulk at high salt concentrations. Colors represent: water molecules (white and grey), Na^+ (purple), Cl^- (yellow), surfactant head (orange).

Clearly, the interfacial behavior of CTAC differs from that of EHAC. One can suggest two reasons for this. First, the surfactants have different chemical head and tail structures, which impact interfacial arrangement and orientation. Second, the studied CTAC concentration and salt range (0.01 – 1 M) may be insufficient for observing the CTAC micelle formation. However, according to the density distribution profiles (Figure 43), we suggest that CTAC molecules diffused slightly into the oil phase due to the salting-out effect, resulting in a decrease of the affinity of the surfactant towards the aqueous phase.

5.3.3 The interfacial thickness of aqueous, hydrocarbon, and surfactant phases

On the basis of the density distribution profiles (Figure 45), we calculated and analyzed the interfacial thicknesses between the different phases of the system. Figure 46a presents the density distribution profiles of n-decane, water, EHAC surfactant, and Cl- ions (NaCl concentration corresponded to 0.01 M) along the Z-axis. According to the "90-90" criterion[197], the oil/water interfacial thickness (h_{total}) can be found as the distance between two points where the densities of

oil and water are 90% of their bulk densities (which are 725 kg/m^3 [159, 163] and 997 kg/m^3 [201] for n-decane and water, respectively). Generally, for an oil/water interface, a "10-90" criterion is used for calculation of the interfacial thicknesses between the oil (h_{oil}) and water (h_{water}) phases by measuring the distance between two points where the density differs from 10 to 90% of the bulk phase. The presence of surfactant at the interface results not only in the formation of two sub-interfaces (oil/surfactant and water/surfactant) but also in a surfactant monolayer (h_{surf})[197]. Thus, the total thickness of the interface is considered as the sum of the three components, namely toil and h_{water} (defined by the "10-90" criterion) and h_{surf}, thus $h_{surf} = h_{total}-h_{oil}-h_{water}$ as illustrated in Figure 47 for EHAC. The same criteria were used for the thickness calculations of CTAC systems.

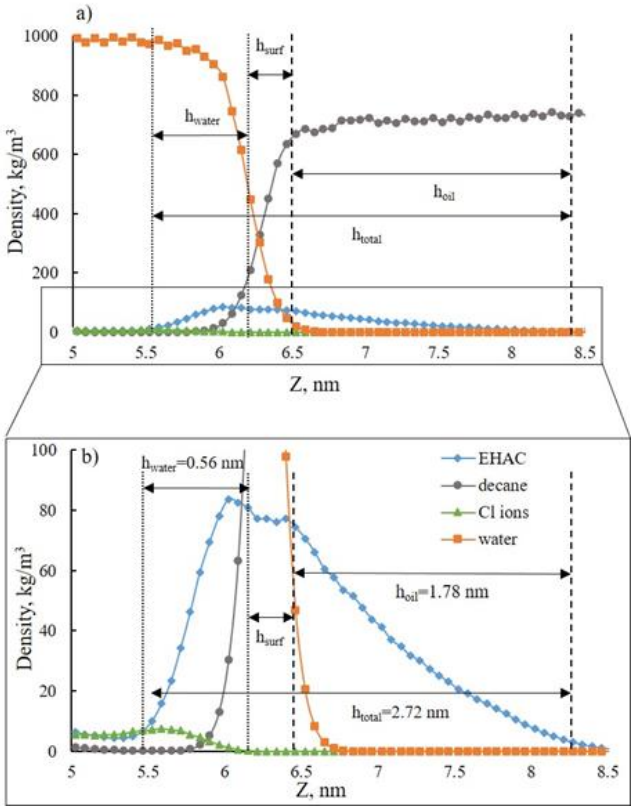

Figure 47. a) Density profiles of n-decane, water, EHAC surfactant and Cl ions; b) Zoom into area highlighted by the black square in (a) (note that the NaCl concentration was 0.01 M).

Using the "10-90" criterion the total interfacial thickness of the n-decane/water system without surfactant was found to be 0.49 nm, which is in good agreement with the experimentally measured value (0.46 nm)[212], and independent MD simulations[76]. Thicknesses of oil (h_{oil}) and water (h_{water}) interfaces were 0.41 nm and 0.46 nm, respectively.

From Figure 47, it is seen that the addition of EHAC surfactant resulted in broadening of t_{oil} by 1.37 nm and h_{water} by 0.10 nm, with a consequent increase in h_{total} by 2.23 nm. Such an increase illustrates the well-known surfactant property of self-assembly at the oil/water interface when hydrophobic tails orient towards the oil phase while hydrophilic headgroups align towards the water phase. Thus, n-decane and water molecules can penetrate the hydrophobic and hydrophilic parts of a surfactant layer at the interface, leading to an increase in interfacial thicknesses.

Calculated values of h_{total}, h_{water} and h_{oil} for EHAC and CTAC at different NaCl concentrations are shown in Figure 48. Interestingly the observed patterns were different for both surfactants. Indeed, the interfacial thickness (h_{total}) of water/EHAC/n-decane systems did not vary monotonically as a function of added salt, instead h_{total} clearly showed an inverse pattern to IFT (Figure 48a); whereas h_{total} of water/CTAC/n-decane systems decreased gradually in all brines (Figure 48d).

Different results were reported in the literature regarding the dependence of IFT on the h_{total}. For instance, it is generally accepted that an increase in interfacial thickness leads to an increase in the miscibility of two phases, with a consequent IFT reduction[163]. However, in the work of Qu et al.[190] it was shown that the thickness of water/surfactant/n-decane systems remained unchanged when temperature and salinity were increased, while IFT decreased. The authors explained this IFT descending trend with the reduction of the non-bonded potentials between water and surfactant molecules that led to a decrease of intermolecular forces[190]. Contrary to this, Jang et al.[197] reported a strong correlation between the interfacial thickness and the interfacial tension for n-decane/water interfaces in the presence of anionic surfactants. As such, the maximum broadening of the interfacial thickness in the presence of a surfactant was observed when IFT reached the minimum value. The authors inferred that the low IFT was due to an increase of the phases' miscibility when surfactant was added.

To explain the trends obtained in our work, we further analyzed h_{water} and h_{oil} as a function of NaCl content (Figures 48b-f). As it can be seen in Figure 48c, h_{water} of the water/EHAC/n-decane system broadened at low salt concentrations. This can be explained by taking into account that counterions penetrated into the headgroup layer adsorbed at the interface (Stern layer). Notably, the same approach was used for predicting the adsorption of SDS and CTAB surfactant molecules in the presence of KCl[213] and NaCl[211]. Furthermore, the co-adsorption of counter-ions together

with surfactant molecules at the interface was also supported by analyzing the average number of hydrogen bonds (n_{hb}) between surfactant head groups and water molecules (Figure 49).

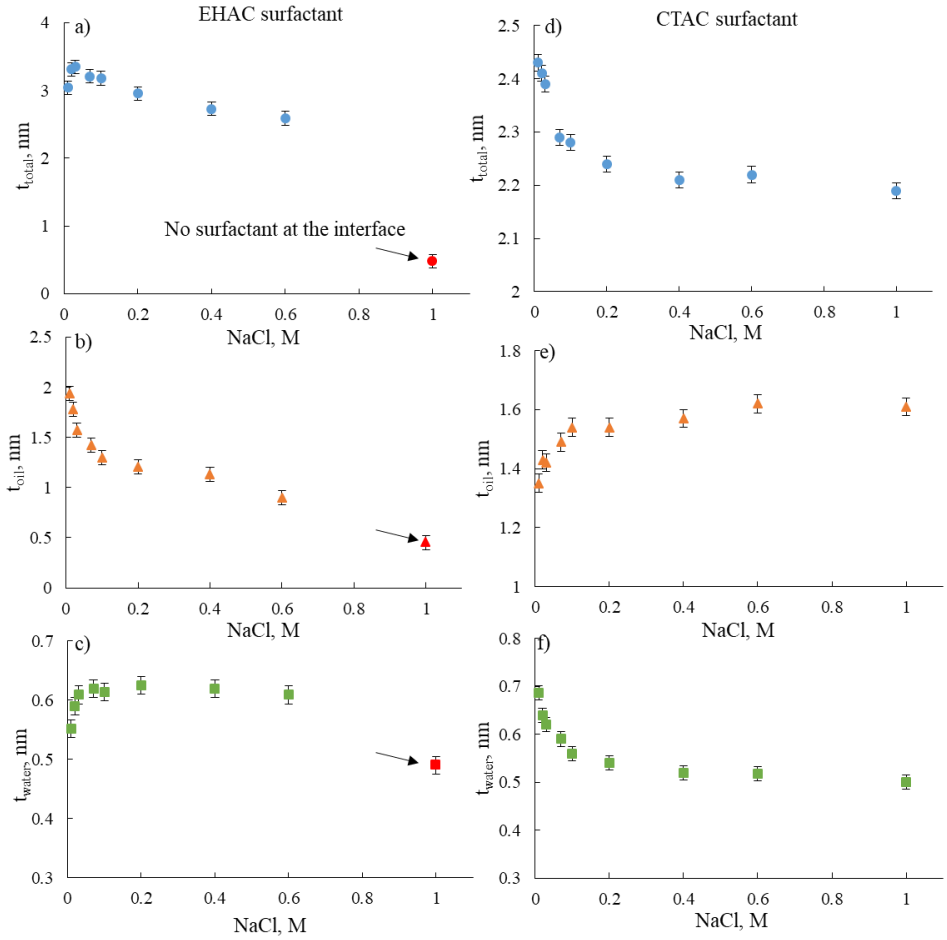

Figure 48. Interfacial thickness as a function of NaCl concentration: total thickness (blue circles); oil thickness (orange triangles) and water thickness (green squares); (a)-(c) EHAC surfactant; (d)-(f) CTAC surfactant.

As can be seen from Figure 49, the number of hydrogen bonds decreased rapidly with increasing salinity. Thus, one can suggest that counter-ions bind with surrounding water molecules by ion-dipole interactions, leaving fewer water molecules to form bonds with the head groups. Therefore, the existence of counter-ions at the interface (when NaCl < 0.03 M) screens the electrostatic repulsion, and surfactant molecules are packed more tightly, resulting in the IFT decrease.

Interestingly, a further increase in NaCl concentration led to a decrease of n_{hb}, which indicates that fewer water molecules can form bonds with surfactant polar heads (Figure 49). Notably, no hydrogen bonds were found between CTAC surfactant and water molecules, which is due to the fact that the nitrogen atom in the CTAC head group could not provide the lone pair of electrons for bond formation.

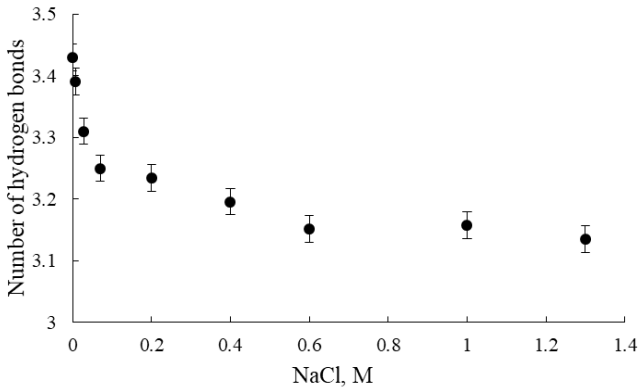

Figure 49. The average number of hydrogen bonds (n_{hb}) between EHAC surfactant heads and water molecules as a function of NaCl concentration.

Moreover, h_{total} started to decrease when NaCl concentration exceeded 0.03 M (Figure 48a). The same descending trend of Stern layer thickness was reported for fluid/solid adsorption as a function of NaCl concentration (up to 0.15 M[214]).

In the case of CTAC, h_{total} and h_{oil} both decreased for all NaCl concentrations, while h_{water} showed an increasing trend (Figure 48f). These findings illustrate the incremental partitioning of CTAC molecules into the oil phase with increasing NaCl concentration.

5.4 Summary

While testing surfactants as candidates for surfactant flooding, one should consider reservoir brine composition and temperature as important factors that affect surfactant adsorption at the oil-water interface, and consequently, oil production[215]. Screening the surfactant properties at high salinity and temperature is thus essential to avoid failure of the whole recovery process.

Therefore, this study investigates the influence of typical reservoir salinities and temperature on the adsorption process of two different cationic surfactants at the water/n-decane interface at

the molecular level. We showed that surfactants had different IFT patterns as a function of salinity due to different headgroup architectures. So far, experimental studies[60, 80, 82] showed IFT passes through a minimum, illustrating two behavioral regions. From our work, we propose that the IFT trend of EHAC can be categorized into three regions, namely the first region where surfactant molecules adsorb at the interface, the second region where surfactant molecules desorb, and a third region where no surfactant molecules are left at the interface (and where thus micelle formation is facilitated). The reason of the increasing IFT trend (second region) was due to Na^+ ions positioned closer to the Stern layer. These Na^+ ions then contributed to the positive interfacial charge, resulting in the repelling of surfactant molecules from the interface until no surfactant was left at the interface (third region).

However, the IFT of CTAC solutions increased for all salt concentrations examined. We attribute this to the decrease of CTAC solubility in the aqueous phase caused by the salting-out effect. The slight migration of CTAC further into the oil phase was also verified by the interfacial thickness analysis.

Moreover, temperature increase led to a decrease in IFT for all salt concentrations. However, IFT-salinity patterns resembled those measured at ambient temperature.

These results indicate that interactions between ions and surfactant molecules are competitive at the interface and cooperative in the bulk phase. The findings of this study thus provide important insights into the understanding of the influence of ions in the interfacial zone and thus can be used for screening surfactants that are favorable for enhanced oil recovery, ultimately leading to improved productivity.

Chapter 6. Molecular dynamics study of surfactant – hydrocarbon interface in the presence of nanoparticles

6.1 Motivation

As it was observed in chapter 2 and supported by a literature survey, silicon nanoparticles (SiO_2) are promising agents for improving the surfactant properties, such as IFT reduction, viscosity increase, and wettability alteration of carbonate surfaces. As such, it has been regarded as a potential additive to surfactant injection fluid for chemical EOR. However, as it was shown in the previous chapters, the properties of surfactant and its mixtures with nanoparticles highly depend on salinity and temperature conditions. Moreover, results showed that, for practical applications, an appropriate combination of surfactant/electrolytes/nanoparticles needs to be carefully selected to avoid the negative synergism and undesirable performance during EOR.

Despite many experimental studies that have been published recently, the effect of nanoparticles at the surfactant – hydrocarbon interfaces remains controversial and poorly understood due to the difficulty of studying their interactions solely with experiments. Moreover, no optimal concentration of nanoparticles or surfactant has been proposed to be economically and technically effective for EOR methods. Therefore, we aim to establish the models of interactions of surfactants in the presence of nanoparticles using MD that would aid in the screening process of these chemicals for a future application for wettability alteration of carbonates and thus enhance oil recovery.

6.2 Materials and Methods

6.2.1 Nanoparticles preparation

The amorphous silicon nanoparticles have been obtained by cutting the spherical shape of 3 nm diameter out of the amorphous silica model. In turn, the amorphous silica model has been prepared by following the procedure suggested in Litton et al[216].

In general, a crystalline silica model can be built by replicating the silica unit cell to fill the cubic volume. For instance, it can be performed using VMD modeling tool[177]. Then amorphous silica can be prepared by the annealing process, which involves three steps – heating up to 8000 K in order to achieve the randomization of the crystalline silica structure, then cooling silica to room temperature (300 K), and then relaxation process for system's volume adaptation.

It is interesting to point out that the melting temperature of silica is approximately 1723 K. However, in order to reduce the computational time, a high temperature, such as 8000 K, is utilized in MD.

Notably, that one can also obtain the amorphous structures by using commercial software Cerius with specialized force fields[217].

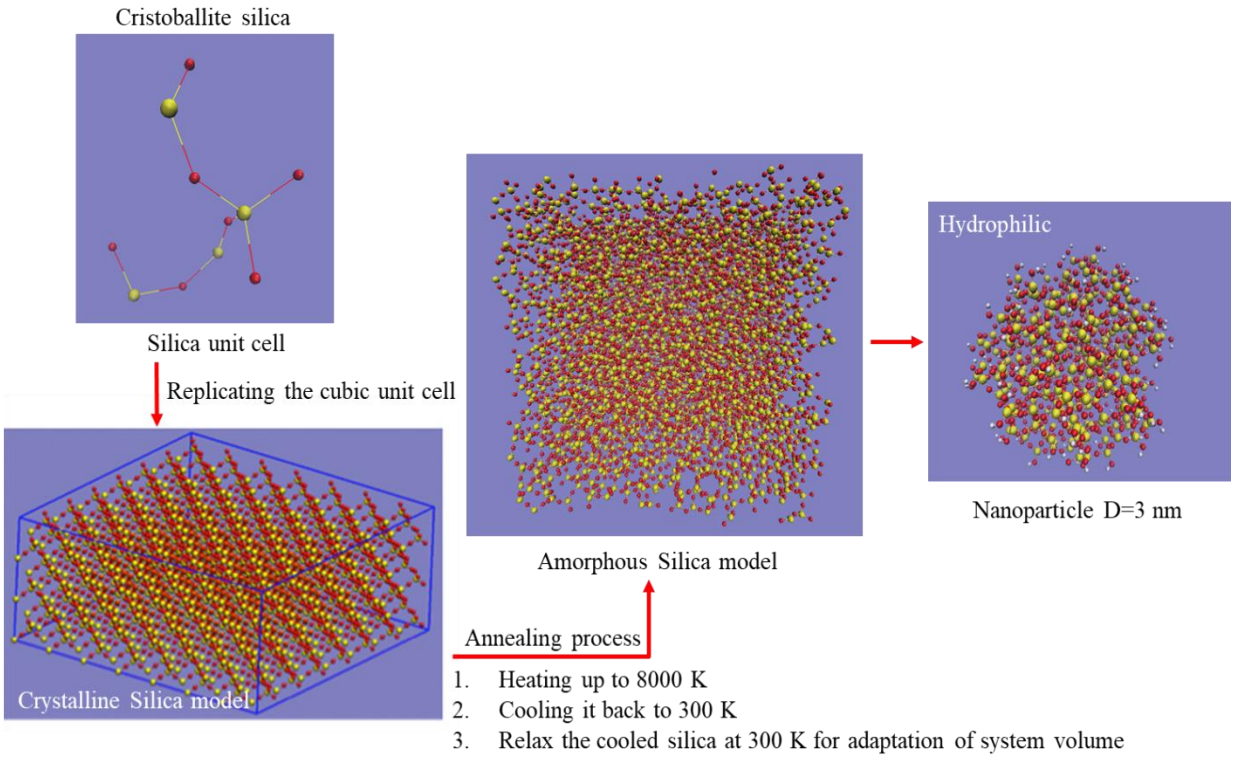

Figure 50. Schematic representation of the nanoparticle preparation process. Colors represent silicon atom – yellow, oxygen atom – red and hydrogen – white.

In this study, the diameter of the studied nanoparticle was taken 3 nm, which is several times less than the real size of SiO_2 nanoparticles (∼12 nm). However, as it was shown in the work of Fan et al.[146], this diameter is reasonable to capture the effects of nanoparticles at the interface, and on the other hand, is feasible in terms of computational resources.

In order to obtain a hydrophilic nanoparticle, the unsaturated atoms from the nanoparticle surface have been deleted, and then, non-bridging oxygen atoms have been saturated with a hydrogen atom (Figure 50).

In the MD simulation study, we used the same surfactants as in experiments (please refer to chapter 2) – cationic EHAC and anionic SOS (Figure 51). Figure 51 represents the molecular structures of surfactants and the snapshot of the simulation box containing nanoparticles and either EHAC or SOS surfactant molecules. In all simulation runs, the surface density of OH groups equaled 4.5 groups per nm^2, which is in good agreement with the experimental data - 4.6 groups per nm^2 [146].

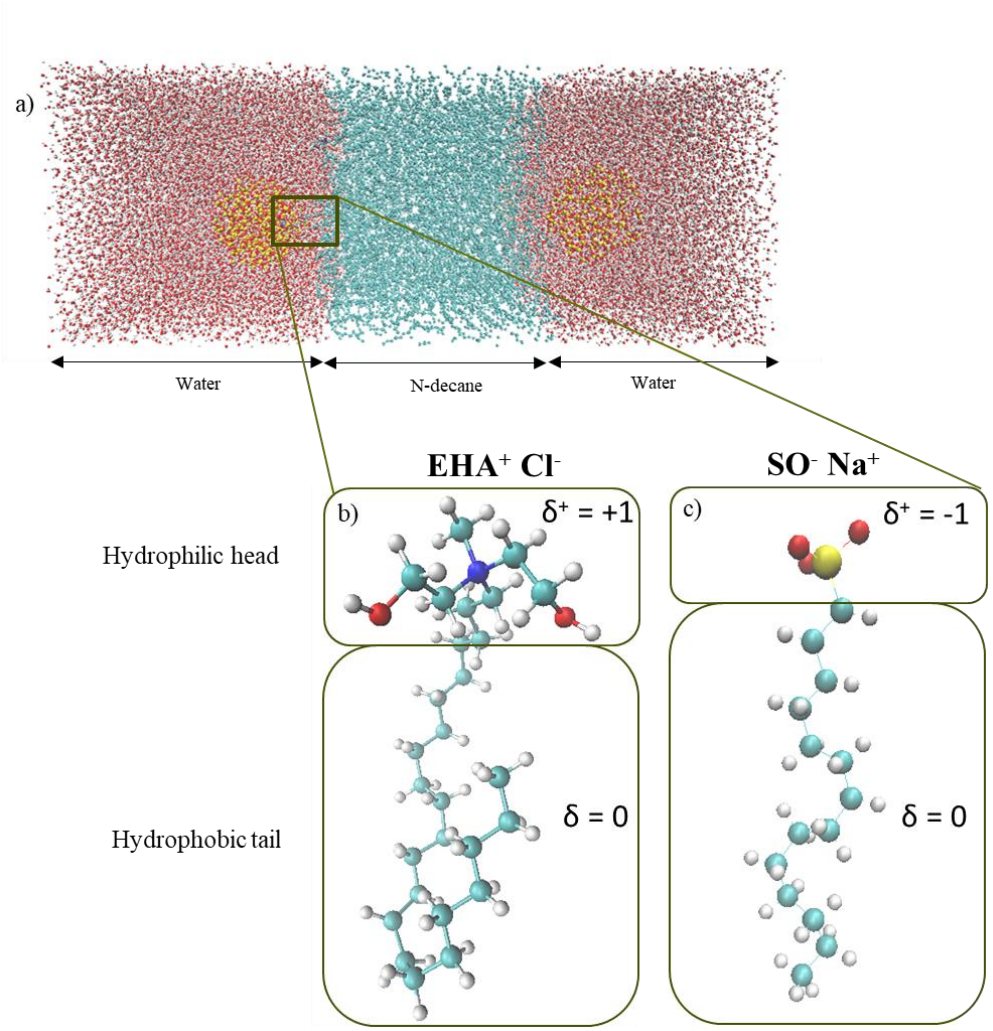

Figure 51. a) Simulation box containing nanoparticles and surfactants – b) cationic surfactant (EHAC) and b) anionic surfactant (SOS)

6.2.2 Computational method

The liquid-liquid interfaces were simulated by the GROMACS 4.5.5 package[171] with an application of the leapfrog algorithm for Newton's equations integration. Water was modeled by

the implementation of a single point charge/ extended (SPC/E) model, which has been successfully used to obtain the best equilibrium distributions at the interface [174, 196]. The charge distribution among surfactant atoms (Figure 51) was selected and adjusted from that proposed in the literature[176], such that the system charge remained neutral.

The molecular interaction parameters between silica atoms were computed using the CLAYFF force field[218]. Table 9 shows the force field parameters used in this study for modeling silica nanoparticles. The Transferable Potentials for Phase Equilibria (TraPPE) force field was applied for computing the n-decane phase. The Chemistry at Harvard Macromolecular Mechanics (CHARMM) force field was used for modeling the surfactants. The dispersive interactions between nanoparticles and water and/or n-decane were modeled by a 12-6 Lennard-Jones potential. The Lennard-Jones parameters were calculated with a Lorentz-Berthelot mixing rules[219]. The particle-mesh Ewald (PME) method of summation was implemented to compute the electrostatic interactions[173].

Table 9. Force field parameters for silica nanoparticles.

Force field parameters:				
	Si	O_b (bringing oxygen)	O_w (Non-bringing oxygen)	H
ε (kJ/mol)	$7.7007*10^{-6}$	0.6502	0.6502	0.0000
σ (nm)	0.3302	0.3166	0.3166	0.0000
charge (e)	2.100	-1.0500	-0.9500	0.4250
K_b (kJ/mol/nm^2)	463700			
K_θ (kJ/mol/rad^2)	251.04			
b_0 (nm)	0.1			
θ_0 (deg)	109.47			

The simulation boxes with nanoparticles were constructed by placing slabs of surfactant layers (2 nm each) and nanoparticles (3.5 nm each) around the n-decane layer (thickness 5 nm) and visualized using the visual molecular dynamics (VMD) tool[177]. The z dimension of the box with n-decane, surfactant molecules, and nanoparticles was increased to 25 nm create regions for water

molecules filling as shown in Figure 50a. The initial size of the simulation box was $8 \times 8 \times 25$ nm^3 for each system. Periodic boundary conditions (PBC) were set in three dimensions.

Two surfactants have been chosen from experimental data presented in Chapter 2. The number of surfactant molecules in each slab was set in such a way that area density for EHAC equaled to 0.18 molecule / nm^2 and 0.25 molecule / nm^2, while for SOS - 0.22 molecule / nm^2 and 0.31 molecule / nm^2. These values are adopted from the previous simulation studies and are consistent with other researches, where interfacial behavior has been investigated[132, 179, 196, 200]. Since in our study we are focusing on molecular interactions at the interface and not on the bulk properties of surfactants and nanoparticles, the concentrations considered in this study are within a reasonable range to mimic the adsorption behavior and chemical interactions properly.

Then, to obtain zero total charge of the systems, an appropriate number of counterions (Cl^- and Na^+) were inserted by replacing the water molecules. The number of nanoparticles used in this study corresponded to concentrations of 0.002 M, 0.004 M, and 0.006M that were feasible in terms of the computational resources.

The simulations were carried out at atmospheric pressure (1 bar) and 300 K. After the simulation box was constructed, the energy minimization was performed by using the steepest descent method with the cut-off scheme for Coulomb and van der Walls forces of 1.4 nm. The first equilibration step was performed with a constant number of molecules and a volume and temperature (NVT) ensemble using a Berendsen barostat coupled with a simulation of a constant number of molecules, pressure, and temperature (NPT) for 1 ns. Then the productive simulations were run for 30 ns with a constant number of molecules, volume, and temperature (NVT) using Nose-Hoover thermostat. The simulation data obtained from the last 15 ns of the production run was used to calculate parameters.

6.3 Results

6.3.1 Nanoparticles effect on interfacial behavior of surfactants: the influence of nanoparticles concentration

As it was shown in works[146, 220], it is important to study simple systems first, e.g. water/n-decane, water/surfactant/n-decane, water/nanoparticles/n-decane in order to test the chosen force fields for reliable results analysis and accurate IFT calculation of the whole system.

The interfacial tension (γ) can be determined as following, as the interface between the phases is perpendicular to the Z-axis direction[76]:

$$\gamma = -\int_0^{L_z}(p'(z) - p)dz,$$

where L_z is the box length along the z-axis, $p'(z)$ is the lateral pressure, and p is the bulk pressure.

The integral can be calculated using the fact that in the bulk solution $p = p'(z)$ and taking into consideration that there are two interfaces in our system[76]:

$$\gamma = -\frac{1}{2}\left(\frac{p_x+p_y}{2} - p_z\right)L_z,$$

where p_α describes the three diagonal elements of the pressure tensors $P_{\alpha\alpha}$ $(\alpha = x, y, z)$ along the axis.

The results calculated for the water/n-decane interface and water/n-decane in the presence of nanoparticles are presented in Table 10. Then, the computed interfacial tensions of the water/n-decane system with and without nanoparticles were compared to the experimental data obtained at 300 K. The experimental IFT data was taken from the work of Zeppeiri et al.[159], processed by extrapolating the data using the correlation on temperature.

Table 10. Comparison of computed IFT values with the experimental data from literature[108, 159].

System	Computed IFT values	Experimental IFT data
Water/n-decane	52.5 ± 1.5	51.7[159]
Water/nanoparticles (0.002 M)/n-decane	48.4 ± 0.8	50.1[108]

As can be seen from Table 10, the computed IFT values for all systems are in good agreement with available experimental data. Therefore, the same force field parameters have been used for other simulations with more complex systems, i.e. including both nanoparticles and surfactants.

Notably, the simulation results showed that interfacial tension between water and n-decane had changed slightly when nanoparticles were added (Table 10). This result illustrates the hydrophilic nature of SiO_2 nanoparticles computed in our study. As such, nanoparticles tend to stay in the aqueous phase rather than approach closer to the interface. However, the slight reduction of IFT can be explained by considering the increase of the orientational order of water molecules near to the interface when nanoparticles were presented near the interface.

Once the force field parameters have been tested on relatively simple systems, the water/n-decane system, including nanoparticles and surfactants, were computed. The results for computed IFT values between surfactant and n-decane in the presence of different numbers of nanoparticles are shown in Figure 52.

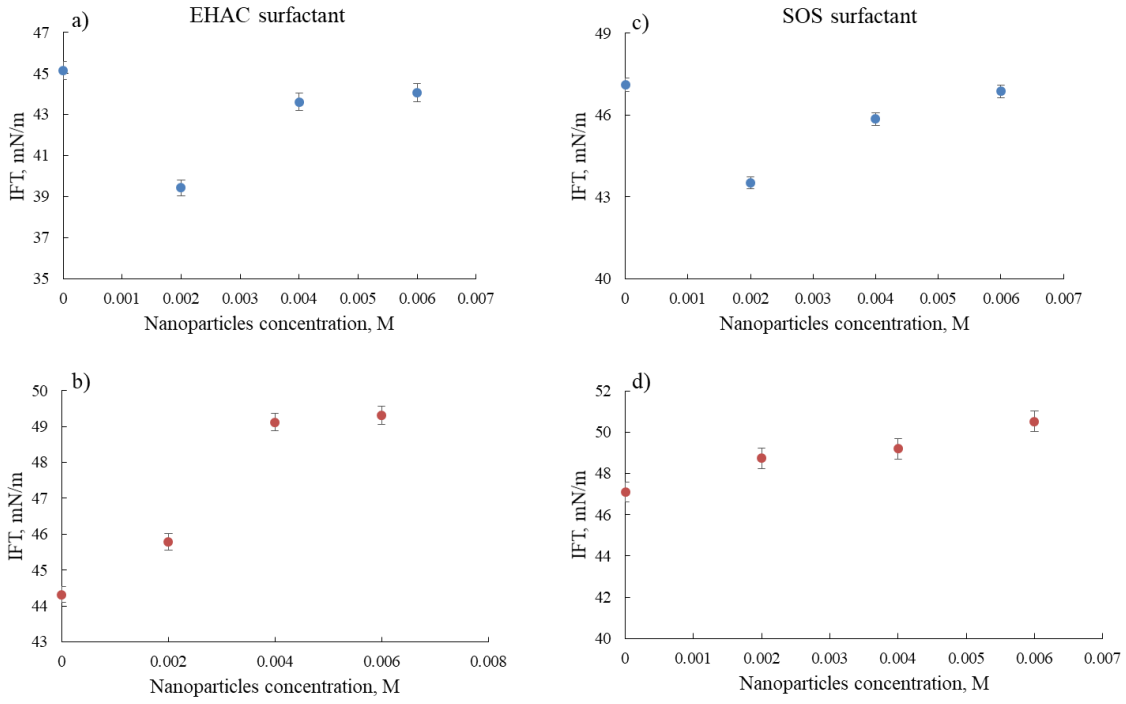

Figure 52. Computed IFT values for EHAC: a) 0.18 molecule / nm^2; b) 0.25 molecule / nm^2 and SOS: c) 0.22 molecule / nm^2; d) 0.31 molecule / nm^2 as a function of nanoparticles concentration.

As it can be seen from Figure 52, the addition of a small number of nanoparticles (0.002 M) to the less concentrated surfactant solutions resulted in a modest decrease of IFT values (Figure 52a, c). Further, with the increase of nanoparticles content in the system, the IFT started to grow. On the other hand, nanoparticles addition to more concentrated surfactant solutions led to an IFT increase in all ranges of nanoparticles concentrations. The obtained trend agrees with a number of experimental results illustrating that there is an optimal amount of nanoparticles that aid in the IFT reduction of surfactants[95, 96, 108, 221].

From the simulation results, we propose that when nanoparticles concentration is small, nanoparticles locate near the interfacial zone interacting with surfactant molecules via electrostatic forces. However, when the concentration is relatively high, nanoparticles tend to remain in the bulk phase, detaching some surfactant molecules from the interface. Consequently, fewer surfactant molecules can move to the interfacial zone and cause IFT reduction. As a result, IFT raises up to values that are close to the values of the water/n-decane system without surfactant (Figure 52). This hypothesis is supported by analyzation of density distribution profiles of nanoparticles, water, and n-decane (Figure 53). The Gibbs Dividing Planes have been calculated for all systems using the same procedure presented in Chapters 4, 5. In Figure 53, it can be seen that when nanoparticles concentration was 0.002 M, nanoparticles resided in close proximity to the interface – 1.82 nm, and thus, indicating the impact on interfacial behavior of surfactants and interfacial water molecules. However, at 0.004 M concentration nanoparticles moved further inside the aqueous phase, showing no effect at the interface.

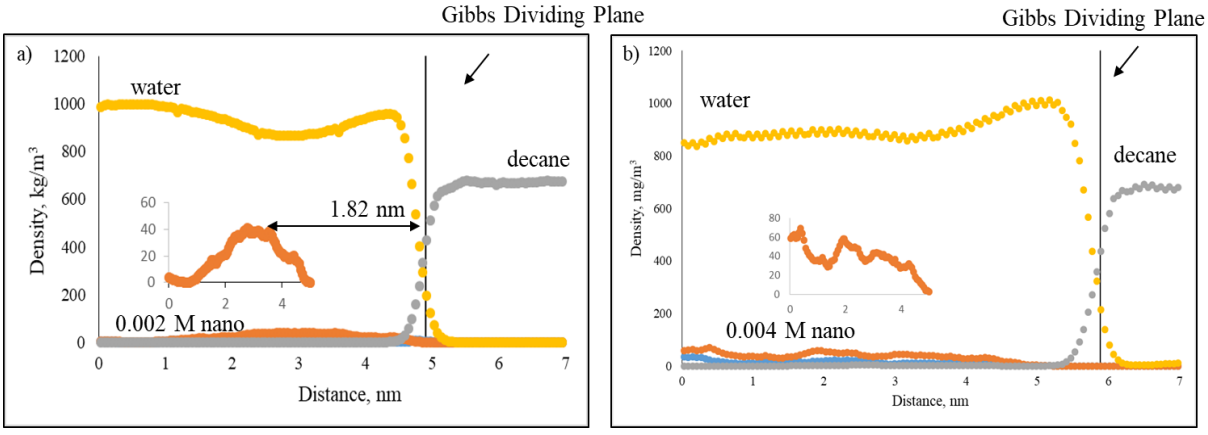

Figure 53. The density distribution profiles: a) nanoparticles concentration – 0.002 M; b) nanoparticles concentration – 0.004 M.

Notably, at a higher number of surfactants in the system, the IFT increase has been observed for all nanoparticle concentrations. We hypothesize that, when surfactant concentration is high, the interfacial zone consists mostly of surfactant molecules with no available space for nanoparticles. As such, nanoparticles mostly remained in the water phase and could not reach the interface and, thus, had no effect on IFT (Figure 54). It is worth to note that simulation trends are in good agreement with the experimental trends presented in Chapter 2. Therefore, the models developed in this chapter are reliable, and thus, can be used for other surfactants to make the screening process more convenient.

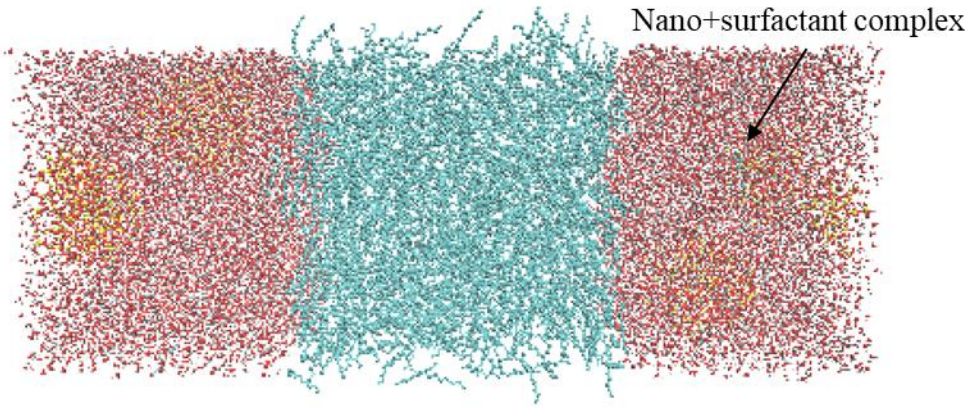

Figure 54. Snapshot of simulation box containing 0.004 M nanoparticles and EHAC surfactant. Colors represent - carbon (cyan), oxygen (red), silica (yellow), hydrogen (white).

6.4 Summary

In this chapter, we analyzed surfactant – nanoparticles systems using the MD simulation tool. The models of their interactions at the water/n-decane surface have been developed. Further, models were validated with the experimental trends presented in the previous chapter and with available literature data. As a result, the developed procedure can be modified further for studying other surfactants with regard to use them in nanoEOR.

From the simulation study, it was shown that optical concentrations of nanoparticles and surfactant should be chosen accurately in order to achieve the synergism in IFT reduction. Our results illustrated that the range of optimal concentrations is represented by rather small amounts

of surfactant and nanoparticles than high. This fact makes nanoparticles application in EOR methods economically attractive.

It should be pointed out that this study aids in the prediction of interfacial properties of the mixture of surfactants and nanoparticles using the MD tool, which in turn can help in predicting the overall performance of nanoparticles augmented surfactant solutions' performance as an injected fluid.

Conclusions

In this thesis, we performed a systematic study of the systems involving different surfactants and nanoparticles and explored their interactions by experimental and modeling evaluations. Starting from the study of the reasons for oil-wet wettability of carbonate rocks and going all the way to completed nano-surfactant solutions for wettability alteration, we investigated a number of important parameters and characteristics and featured the most promising nano-surfactant suspension potentially applicable for use in EOR techniques in carbonates.

A comparative analysis of micro-scale wettability of 12 carbonate samples in 2 different extraction states provided important information on the wetting state of carbonate rocks and revealed the reason for oil wetting preferences of carbonates. We developed the methodology for measuring the contact angle between water and carbonate surfaces at the microscale by using the ESEM approach. Further, the advanced microscopic technologies were first applied to identify the organic layers on carbonate surfaces. We discovered that the surface covered by hydrocarbon layers had hydrophobic wetting properties, while pure calcite exhibited hydrophilic. This result was also confirmed by EDXS analysis in the corresponding points of the surface. Furthermore, we studied the properties of the first adsorbed layer on the surface by combining the Cryo-FIB approach with S/TEM experiments. The calculated thickness of the hydrophobic organic layer was 180 ± 12 nm and can be used in fluids displacement models for evaluation in the more accurate way the critical parameters of fluids multi-phase flow through pore throats, such as capillary pressure curves. The EELS results revealed the bond nature between the layer and surface. As such, we propose that asphaltenes react with calcium ions by the ionic bond between calcium (Ca^{2+}) and oxygen (O^{-}) from the carboxyl group (COO^{-}). Then, on the surface of this organic layer, other hydrocarbons from oil start to adsorb.

Knowing that the reason for oil wetness stems from the chemical adsorption of organic components from oil, we further studied potential solutions consisted of surfactants and nanoparticles that can desorb those layers from the carbonate surfaces. A systematic experimental study of 2 potential surfactants and a mixture thereof with SiO_2 at high temperature and high salinity conditions provided essential information on the factors governing their effectiveness in terms of stability, IFT, and viscosity properties. We found that the addition of nanoparticles to surfactant solutions aids in IFT reduction. The minimum of IFT was achieved for EHAC surfactant when surfactant concentration was higher than CMC, and nanoparticle concentration was 0.05

wt.%. We further observed that IFT was strongly influenced by temperature and salt (NaCl). The results revealed that the IFT reduction is related to the addition of electrolytes to solutions and, with a lesser impact, to the addition of nanoparticles. We observed that the impact of salt and nanoparticles on the bulk viscosity is cooperative. The addition of nanoparticles and salt to cationic surfactant solutions significantly increased solution viscosity (up to 10,000 mPa*s), illustrating that nanoparticles can also serve as an effective viscosity modifier of injected fluids. The results indicated that interactions between electrolytes and nanoparticles are competitive in the interfacial region and cooperative in the aqueous bulk. The contrast was more pronounced when the surfactant and particle had opposite charges. Results show that, for applications, an appropriate combination of surfactant/electrolytes/nanoparticles needs to be carefully selected to avoid negative synergism.

Further, we studied important phenomena of surfactant interfacial behavior that can not be explained by conventional theories at the microscale using MD simulations. We investigated the adsorption of 2 surfactants (EHAC and CTAC) with different molecular structures at the water/n-decane interface at different temperatures: 298 K, 318 K, 338 K, 353 K, and 368 K. We showed that surfactants had different IFT patterns when the temperature was increased. As expected, the IFT of CTAC surfactant decreased with the temperature according to the Gibbs theory. Whereas the IFT of EHAC went through a minimum at 338 K and then started to increase. From the results, we proposed that hydrogen bonding between surfactant and water molecules plays an important role at the liquid/liquid interfaces and controls the interfacial behavior of surfactant at elevated temperatures. We thus, also suggest that the observed IFT - temperature dependence can be generalized for other surfactants containing head groups that can form hydrogen bonds with surrounding water molecules. The obtained results provided an important basis for the understanding of deviations from the Gibbs theory of surfactant adsorption at the interfacial zone. Thus, the findings of this work can be used for further modification of the existed theory by taking into account the chemical structure of surfactants.

We studied the salinity effect on surfactants interfacial behavior owing to the fact that reservoirs contain high concentrated brines. Screening the surfactant properties at high salinity and temperature is thus essential to avoid failure of the whole recovery process. We investigated 2 surfactants (EHAC and CTAC) and showed that surfactants had different IFT patterns as a function of salinity due to different headgroup architectures. So far, experimental studies[60, 80, 82] showed IFT passes through a minimum, illustrating two behavioral regions. From our work, we propose that

the IFT trend of EHAC can be categorized into three regions, namely the first region where surfactant molecules adsorb at the interface, the second region where surfactant molecules desorb, and a third region where no surfactant molecules are left at the interface (and where thus micelle formation is facilitated). The reason for the increasing IFT trend (second region) was due to Na^+ ions positioned closer to the Stern layer. These Na^+ ions then contributed to the positive interfacial charge, resulting in the repelling of surfactant molecules from the interface until almost no surfactant was left at the interface (third region). The findings of this study thus provide important insights into the understanding of the influence of ions in the interfacial zone and thus can be used for screening surfactants that are favorable for enhanced oil recovery, ultimately leading to improved productivity.

With the existing controversial trends of nanoparticles' influence on surfactant properties, such as their ability to reduce water/hydrocarbon IFT, it is important to study their interactions at the atomic level. Therefore, we developed the models of their interactions at the water/n-decane interface. Further, models were validated with the experimental trends presented in the previous chapter and with available literature data. We revealed that in all cases, the optical concentrations of nanoparticles and surfactants should be chosen accurately in order to achieve the synergism in IFT reduction. As a result, the developed procedure can be modified further for studying other surfactants with regard to use them in nanoEOR.

The research finding of this thesis points out also new challenges to be investigated in future projects. One of them is to develop the procedure of the contact angle calculation at a micro-scale using micro-tomography images. This information will help to reveal the three-phase contact angle in the presence of surfactants and nanoparticles. To address this issue, one can develop the procedure using mCT scanner and build a special core holder that allows obtaining images with a resolution of 1-3 μm.

Finally, it is worthy to point out that the application of nanoparticles in surfactant EOR is still a hot and ongoing topic in science and industry and raises challenges to researchers from all over the world. We believe that our study contributes significantly to this area and represents an important step forward for applying this technology in the real oil field project.

Bibliography

1. Klemme, H., Ulmishek, G. F. Effective petroleum source rocks of the world: stratigraphic distribution and controlling depositional factors. AAPG Bulletin 75, 1809–1851 (1991)
2. Characterization of Fractured Reservoirs. Schlumberger market analysis 2007. https://www.slb.com/-/media/files/theme/brochure/cb-characterization-09os0003.ashx
3. Burchette, T. Carbonate rocks and petroleum reservoirs: A geological perspective from the industry. Geological Society London Special Publications 370, 17-37 (2012). 10.1144/SP370.14
4. Muriel, H., Madland, M.V., Korsnes, R. I. Evolution of wetting index over time in mixed wet kansas chalk using triaxial cells. Thesis for Master of Science (2017). https://uis.brage.unit.no/uis-xmlui/handle/11250/2463444
5. Al-Hadhrami, H. S., Blunt, M. J. Thermally induced wettability alteration to improve oil recovery in fractured reservoirs. SPE (2000). 10.2118/59289-MS
6. Chilingar, G.V., Yen, T. "Some notes on wettability and relative permeabilities of carbonate reservoir rocks, II". Energy Sources 65-75 (1983)
7. Jadhunandan, P.P, Morrow, N.R. Effect of wettability on waterflood recovery for crude oil/brine/rock systems. Paper SPE 22597 prepared for presentation at the 66th Annual Technical Conference and Exhibition, Dallas, TX (1991)
8. Tabary, R., Fornari, A., Bazin, B., Bourbiaux, B. J., Dalmazzone, C. S. H. Improved Oil Recovery with Chemicals in Fractured Carbonate Formations. SPE (2009). 10.2118/121668-MS
9. Abdallah, W., Buckley, J.S., Carnegie, J., Edwards, J., Fordham, B.H.E., Graue, A., Habashy, T., Seleznev, N., Signer, C., Hussain, H., Montaron, B., and Ziauddin, M., Fundamentals of wettability, Oilfield Rev., 19, 44-61 (2007)
10. Ivanova, A.A., Mitiurev, N.A., Shilobreeva, S. N., Cheremisin, A. NExperimental Methods for Studying the Wetting Properties of Oil Reservoirs: A Review. Izv., Phys. Solid Earth 55, 496–508 (2019). https://doi.org/10.1134/S1069351319030042
11. Yuan, Y. and Lee, T.R., Contact angle and wetting properties, Surf. Sci. Tech. 51, 3–34 (2013)
12. Anderson, W.G., Wettability literature survey—Part 5: The effects of wettability on relative permeability, J. Pet. Technol. 39, 1453–1468 (1987b)
13. Buckey, J. S., Liu, Y., Monsterleet, S. Mechanisms of wetting alteration by crude oils. SPE J. 3, 54–61 (1998). https://doi.org/10.2118/37230-pa
14. Madsen, L., Lind, I. Adsorption of carboxylic acids on reservoir minerals from organic and aqueous phase. SPE Reserv. Eval. Eng. 47–51 (1998). https://doi.org/10.2118/37292-PA

15. Thomas, M. M., Clouse, J. A., Longo, J. M. Adsorption of organic compounds on carbonate minerals: 1. Model compounds and their influence on mineral wettability. Chem. Geol. 109, 201–213 (1993). https://doi.org/10.1016/0009-2541(93)90070-Y
16. Amott, E. Observations relating to the wettability of porous rock. Pet. Trans. AIMB 216, 156–162 (1959)
17. Donaldson, E. C., Thomas, R. D., Lorenz, P. B. Wettability determination and its effect on recovery efficiency. J. Soc. Pet. Eng. 13–20 (1969). https://doi.org/10.2118/2338-PA
18. Donaldson, E. C. Oil-water-rock wettability measurement. ACS Symp. Chem. Eng. Comb. Depos. Conf., Atlanta, USA, 29 March – 3 April (1981)
19. Yuan, Y. & Lee, T. R. Contact angle and wetting properties. Surf. Sci. Technol. 51, 3–34 (2013). https://doi.org/10.1007/978-3-642-34243-1_1
20. Cuiec, L.E., Determination of the Wettability of a Sample of Reservoir Rock, Revue de l'Institut Francais du Petrole (translation no, pp. 81-13920-81), 33, 705–728 (1978)
21. Tul'bovich, B.I., Method for Determination of Wettability in Hydrocarbon-Bearing Rocks: OST 39-180-85), Moscow: Nedra, (1979)
22. Rudakovskaya, S.Yu. Determination of rock wettability by NMR, All-Russ. Research and Practice Conf. "Nuclear-Magnetic Logging and Analytical Methods as Part of GIS for Solving the Rock-Physics, Geophysical, and Geological Problems at Oil and Gas Fields. 206–221 (2014)
23. Anderson, W. Wettability literature survey- part 2: wettability measurement. J. Pet. Technol. 38, 1246–1262 (1986). https://doi.org/10.2118/13933-PA
24. Kowalewski, E., Boassen, T., and Torsaeter, O., Wettability alterations due to aging in crude oil; wettability and Cryo-ESEM analysis, J. Pet. Sci. Eng., 39, 377–388 (2003) https://doi.org/10.1016/S0920-4105(03)00076-7
25. Park, J., Han, H.S., Kim, Y.C., Ahn, J.P., Ok, M.R., Lee, K.E., Lee, J.W., Cha, P.R., Seok, H.K., Jeon, H., Direct and accurate measurement of size dependent wetting behaviors for sessile water droplets, Sci. Rep., 5, 2015. https://doi.org/10.1038/srep18150
26. Ensikat, H., Schulte, A.J., Koch, K., Barthlott, W., Droplets on super hydrophobic surfaces: visualization of the contact area by cryo-scanning electron microscopy, Langmuir, 25, 13077–13083 (2009). https://doi.org/10.1021/la9017536
27. Ruidiaz, E. M., Winter, A. & Trevisan, O. V. Oil recovery and wettability alteration in carbonates due to carbonate water injection. J. Petrol. Explor. Prod. Technol. 8, 249–258 (2018). https://doi.org/10.1007/s13202-017-0345-z
28. Eral, H. B., Mannetje, D. J. C. M. & Oh, J. M. Contact angle hysteresis: A review of fundamentals and applications. Colloid Polym. Sci. 291, 247–260 (2013). https://doi.org/10.1007/s00396-012-2796-6

29. Lan, Q., Dehghanpour, H., Wood, J. & Sanei, H. Wettability of the Montney tight gas formation. SPE Reserv. Eval. Eng. 417–431 (2015). https://doi.org/10.2118/171620-PA
30. Ma, S., Zhang, X., Morrow, N. & Zhou, X. Characterization of wettability from spontaneous imbibition measurements. J. Can. Pet. Technol. 38, 1–8 (1999). https://doi.org/10.2118/99-13-49
31. Treiber, L. E. & Owens, W. W. A Laboratory evaluation of the wettability of fifty oil-producing reservoirs. J. Soc. Pet. Eng. 12, 531–540 (1972). https://doi.org/10.2118/3526-PA
32. Puntervold, T., Strand, S. & Austad, T. Water flooding of carbonate reservoirs: effects of a model base and natural crude oil bases on chalk wettability. Energy Fuels 21, 1606–1616 (2007). https://doi.org/10.1021/ef060624b
33. Shehata, A. M., Alotaibi, M. B., Nasr-El-Din, H. A. Waterflooding in carbonate reservoirs: does the salinity matter? SPE Reserv. Eval. Eng. 304–313 (2014). https://doi.org/10.2118/170254-PA
34. Kasiri, N., Bashiri, A. Wettability and its effects on oil recovery in fractured and conventional reservoirs. J. Pet. Sci. Eng. 29, 1324–1333 (2011). https://doi.org/10.1080/10916460903515540
35. Manrique, E. J., Muci, V. E., & Gurfinkel, M. E. EOR field experiences in carbonate reservoirs in the united states. SPE. 10, (2007). https://doi.org/10.2118/100063-PA
36. Moore, G., Mehta, R., Ursenbach, M. Air injection for oil recovery. J. Can. Petrol. Tech. 41 16-19, (2002)
37. Iglauer, S., Wu, Y., Shuler, P.J., Blanko, M., Tang, Y., Goddard III, W.A. Alkyl poly-glycoside surfactants for improved oil recovery. Paper SPE 89472 presented at the SPE/DOE Symposium on Improved Oil Recovery, (2004). https://doi.org/10.2118/89472-MS
38. Xie, X., Weiss, W.W., Tong, Z., and Morrow, N.R. Improved oil recovery from carbonate reservoirs by chemical stimulation. SPE J 10 276-285, (2005). SPE-89424-PA. doi: 10.2118/89424-PA.
39. Sheng, J.J. Status of surfactant EOR technology. Petroleum 1 97-105, (2015). https://doi.org/10.1016/j.petlm.2015.07.003
40. Sheng, J.J. Review of surfactant enhanced oil recovery in carbonate reservoirs. Adv. Pet. Explor. Dev., 6 1-10, (2013). Doi:10.3968/j.aped.1925543820130601.1582
41. Standnes, D. C., Austad, T. Wettability alteration in chalk. SPE J, 28, 123–143 (2000). doi:10.1016/s0920-4105(00)00084-x
42. Jarrahian, Kh., Seiedi, O., Sheykhan, M., Vafaie Sefti, M., Ayatollahi, Sh. Wettability alteration of carbonate rocks by surfactants: A mechanistic study. Colloids and Surfaces A: Physicochemical and Engineering Aspects, 410 1–10 (2012). doi:10.1016/j.colsurfa.2012.06.007
43. Kumar, A., Mandal A. Critical investigation of zwitterionic surfactant for enhanced oil recovery from both sandstone and carbonate reservoirs: Adsorption, wettability alteration and imbibition studies. Chem. Eng, Science, 209, 115-222 (2019). https://doi.org/10.1016/j.ces.2019.115222

44. Souraki, Y., Hosseini, E., Yaghodous, A. Wettability alteration of carbonate reservoir rock using amphoteric and cationic surfactants: Experimental investigation, Energy Sources, Part A: Recovery, Utilization, and Environmental Effects, 41, 349-359 (2019). https://doi.org/10.1080/15567036.2018.1518353
45. Souayeh, M., Al-Maamari, R.S., Aoudia, M., Karimi, M., Hadji, M. Experimental investigation of wettability alteration of oil-wet carbonates by a non-ionic surfactant. Energy Fuels. 32, 11222–11233 (2018). https://doi.org/10.1021/acs.energyfuels.8b02373
46. Kamal, M.S., Hussein, I.A., Sultan, A.S. Review on surfactant flooding: phase behavior, retention, IFT, and field applications. Energy Fuels. 31, 7701-7720 (2017). https://doi.org/10.1021/acs.energyfuels.7b00353
47. Negin, C., Ali, S., Xie, Q. Most common surfactants employed in chemical enhanced oil recovery. Petroleum. 3, 197-211 (2017). https://doi.org/10.1016/j.petlm.2016.11.007
48. Weiss, W.W., Xie, X., Weiss, J., Subramanium, V., Taylor, A., Edens, F. Artificial intelligence used to evaluate 23 single-well surfactant-soak treatments SPEREE. 9, 209-216 (2006). https://doi.org/10.2118/89457-PA
49. Xie, X., Weiss, W.W., Tong, Z., Morrow, N.R. Improved oil recovery from carbonate. SPE J 10, (2005). https://doi.org/10.2118/89424-PA
50. Chen, H.L., Lucas, L.R., Nogaret, L.A.D., Yang, H.D., Kenyon, D.E. Laboratory monitoring of surfactant imbibition with computerized tomography. SPEREE. 16-25 (2000). https://doi.org/10.2118/59006-MS
51. Yang, H.D., Wadleigh, E.E. Dilute surfactant IOR – design improvement for massive, fractured carbonate applications. Paper SPE 59009 presented at the SPE International Petroleum Conference and Exhibition. (2000). https://doi.org/10.2118/59009-MS
52. Rilian, N.A., Sumestry, M., Wahyuningsih, W. surfactant stimulation to increase reserves in carbonate reservoir “a case study in semoga field”. Paper SPE 130060 presented at the SPE EUROPEC/EAGE Annual Conference and Exhibition. (2010). https://doi.org/10.2118/130060-MS
53. Sheng, J.J. Review of surfactant enhanced oil recovery in carbonate reservoirs. Adv. Pet. Explor. Dev., 6, 1-10 (2013)
54. Xie, X., Weiss, W.W., Tong, Z., Morrow, N.R. Improved Oil Recovery From CarbonateReservoirs by Chemical Stimulation. J SPE. 10, 276-285 (2005). https://doi.org/10.2118/89424-PA
55. Iglauer, S., Wülling, W., Pentland, C. H., Al-Mansoori, S. K., Blunt, M. J. Capillary-trapping capacity of sandstones and sandpacks. SPE. 16, 778–783 (2011). https://doi.org/10.2118/120960-PA

56. Melrose, J. C. Role of capillary forces in determining microscopic displacement efficiency for oil recovery by waterflooding. Journal of Canadian Petroleum Technology. 13, 54–62 (2010). https://doi.org/10.2118/74-04-05
57. Fulcher, R. A., Ertekin, T., & Stahl, C. D. Effect of capillary number and its constituents on two - phase relative permeability curves. J Pet. Tech., 37, 249–260 (1985). https://doi.org/10.2118/12170-PA
58. Morrow, N. R. Interplay of capillary, viscous and buoyancy forces in the mobilization of residual oil. J. Pet. Tech. 18, 35–46 (1979).
59. Yuan, C.D., Pu, W.F., Wang, X.C., Sun, L., Zhang, Y.C., Cheng, S. Effects of interfacial tension, emulsification, and surfactant concentration on oil recovery in surfactant flooding process for high temperature and high salinity reservoirs. Energy Fuels. 29, 6165-6176 (2015). https://doi.org/10.1021/acs.energyfuels.5b01393
60. Bera, A., Mandal, A., Guha, B.B. Synergistic effect of surfactant and salt mixture on interfacial tension reduction between crude oil and water in enhanced oil recovery. J. Chem. Eng. Data. 59, 89-96 (2014). https://doi.org/10.1021/je400850c
61. Y. He, P. Yazhgur, A. Salonen, D. Langevin, Adsorption–desorption kinetics of surfactants at liquid surfaces, Adv. Colloid Interface Sci. 222, 377-384 (2015). https://doi.org/10.1016/j.cis.2014.09.002
62. W. Karnanda, M.S. Benzagouta, A. AlQuraishi, M.M. Amro, Effect of temperature, pressure, salinity, and surfactant concentration on IFT for surfactant flooding optimization, Arab. J. Geosci. 6, 3535-3544 (2013). https://doi.org/10.1007/s12517-012-0605-7
63. T. Al-Sahhaf, A. Elkamel, A. Suttar Ahmed, A.R. Knan, The influence of temperature, pressure, salinity, and surfactant concentration on the interfacial tension of the n-octane-water system, Chem. Eng. Comm. 192, 667-684 (2005). https://doi.org/10.1080/009864490510644
64. L.A. Girifalco, R.J. Good, A theory for the estimation of surface and interfacial energies. Derivation and application to interfacial tension, J. Phys. Chem. 61, 904–909 (1957). https://doi.org/10.1021/j150553a013
65. Z. Ye, F. Zhang, L. Han, P. Luo, J. Yang, H. Chen, The effect of temperature on the interfacial tension between crude oil and gemini surfactant solution, Colloids Surfaces A Physicochem. Eng. Asp. 322, 138–141 (2008). https://doi.org/10.1016/j.colsurfa.2008.02.043
66. M. Aoudia, M. N. Al-Shibli, L. H. Al-Kasimi, R. Al-Maamari, A. Al-Bemani, Novel surfactants for ultralow interfacial tension in a wide range of surfactant concentration and temperature. J. Surfactants Deterg. 9, 287-293 (2006). https://doi.org/10.1007/s11743-006-5009-9
67. A. Mosayebi, M.T. Angaji, P.Khadiv-Parsi, The effect of temperature on the interfacial tension between crude oil and ethoxylated nonylphenols, Pet. Sci. Technol. 34, 1315-1322 (2016). https://doi.org/10.1080/10916466.2011.601506

68. R. Aveyard, B.P. Binks, J. Chen, J. Esquena, P.D.I. Fletcher, Surface and colloid chemistry of systems containing pure sugar surfactant, Langmuir 14, 4699-4709 (1998). https://doi.org/10.1021/la980519x
69. M. El-Batanoney, Th. Abdel-Moghny, M.Ramzi, The effect of mixed surfactants on enhancing oil recovery, J. Surfactants Deterg. 2, 201-205 2 (1999). https://doi.org/10.1007/s11743-999-0074-7
70. R.A. Mohammed, A.L. Bailey, P.F. Luckham, S.E. Taylor, Dewatering of crude oil emulsions 2. Interfacial properties of the asphaltic constituents of crude oil, Colloids Surfaces A Physicochem. Eng. Asp. 80, 237-242 (1993). https://doi.org/10.1016/0927-7757(93)80203-Q
71. G.M. Ataev, Anomalous Temperature Dependence of Interfacial Tension in Water–Hydrocarbon Mixtures, Russ. J. Phys. Chem. A. 81, 2094-2095 (2007). https://doi.org/10.1134/S003602440712031X
72. P. Wernet, D. Nordlund, U. Bergmann, M. Cavalleri, M. H. Ogasawara, L. A. Naslund, T. K. Hirsch, L. Ojamae, P. Glatzel, L. G. Pettersson, A. Nilsson, The structure of the first coordination shell in liquid water, Science 304, 995-999 (2004). 10.1126/science.1096205
73. A. Rastogi, A.K. Ghosh, S.J. Suresh, Hydrogen bond interactions between water molecules in bulk liquid, near electrode surfaces and around ions, in: J.C.M. Piraján (Eds.), Thermodynamics - Physical Chemistry of Aqueous Systems, open access, 2011. 10.5772/21074
74. D.C. Rapaport, Hydrogen bonds in water, J. Mol. Phys. 50, 1151-1162 (1983). 10.1080/00268978300102931
75. P. Fenter, S. Kerisit, P. Raiteri, J. D. Gale, Is the calcite−water interface understood? Direct comparisons of molecular dynamics simulations with specular X-ray reflectivity data, J. Phys. Chem. C. 117, 5028−5042 (2013). 10.1021/jp310943s
76. A.R. van Buuren, S.J. Marrink, H.J.C. Berendsen, A molecular dynamics study of the decane/water interface, J. Phys. Chem. 97, 9206-9212 (1993).
77. C.V. Nguyen, C.M. Phan, H. Nakahara, O. Shibata, Surface Structure of Sodium Chloride Solution. J. Mol. Liq. 248, 1039-1043 (2017). 10.1016/j.molliq.2017.10.138
78. L.C. Price, Aqueous solubility of petroleum as applied to its origin and primary migration, AAPG Bulletin 60, 213-244 (1976). 10.1306/83D922A8-16C7-11D7-8645000102C1865D
79. A.Z. Hezave, S. Dorostkar, S. Ayatollahi, M. Nabipour, B. Hemmateenejad, Dynamic interfacial tension behavior between heavy crude oil and ionic liquid solution (1-dodecyl-3-methylimidazolium chloride ([C12mim] [Cl] + distilled or saline water/heavy crude oil)) as a new surfactant, J. Mol. Liq. 187, 83-89 (2013). 10.1016/j.molliq.2013.05.007
80. S. Kumar, A. Mandal, Studies on interfacial behavior and wettability change phenomena by ionic and nonionic surfactants in presence of alkalis and salt for enhanced oil recovery, Appl. Surf. Sci. 372, 42-51 (2016). 10.1016/j.apsusc.2016.03.024

81. L.S.C. Wan, P.K.C. Poon, Effect of salts on the surface/interfacial tension and critical micelle concentration of surfactants, J. Pharm. Sci. 58, 1562-1567 (1969). 10.1002/jps.2600581238
82. Z. Liu, L. Zhang, X. Cao, X. Song, Z. Jin, L. Zhang, S. Zhao, Effect of electrolytes on interfacial tensions of alkyl ether carboxylate solutions, Energy and Fuels, 27, 3122-3129 (2013). 10.1021/ef400458q
83. J.M. Bai , W.Y. Fan , G.Z. Nan , S.P. Li, B.S. Yu, Influence of interaction between heavy oil components and petroleum sulfonate on the oil–water interfacial tension, J. Disper. Sci. Technol. 31, 551-556 (2010). 10.1080/01932690903167475
84. Z. Zhao, C. Bi, Z. Li, W. Qiao, L. Cheng, Interfacial tension between crude oil and decylmethylnaphthalene sulfonate surfactant alkali-free flooding systems, Colloids Surfaces A Physicochem. Eng. Asp. 276, 186-191 (2006). 10.1016/j.colsurfa.2005.10.036
85. G. Liu, R. Li, Y. Wei, F. Gao, H. Wang, S. Yuan, C. Liu, Molecular dynamics simulations on tetraalkylammonium interactions with dodecyl sulfate micelles at the air/water interface, J. Mol. Liq. 222, 1085-1090 (2016). 10.1016/j.molliq.2016.08.009
86. D.L. Zhang, S. Liu, M. Puerto, C.A. Miller, G.J. Hirasaki, Wettability alteration and spontaneous imbibition in oil-wet carbonate formations, J. Pet. Sci. Eng. 52 213-226 (2006). https://doi.org/10.1016/j.petrol.2006.03.009
87. Nwidee, L. N., Lebedev, M., Barifcani, A., Sarmadivaleh, M., Iglauer, S.. Wettability alteration of oil-wet limestone using surfactant-nanoparticle formulation. Journal of Colloid and Interface Science 504, 334–345 (2017). 10.1016/j.jcis.2017.04.078
88. Bai, S., Kubelka, J., Piri, M. Atomistic molecular dynamics simulations of surfactant-induced wettability alteration in crevices of calcite nanopores. Energy Fuels. 34, 3135-3143 (2020). https://doi.org/10.1021/acs.energyfuels.9b04528
89. Mannhardt, K., Schramm, L.L. and Novosad, J.J. Effect of Rock Type and Brine Composition on Adsorption of Two Foam-Surfactants. Paper SPE 20463 presented at the 1990 SPE Annual Technical Conference and Exhibition. (1990).
90. Zhang, P., Austad, T. Wettability and oil recovery from carbonates: Effects of temperature and potential determining ions. Colloids and Surfaces A: Physicochemical and Engineering Aspects. 279, 179-187 (2006). https://doi.org/10.1016/j.colsurfa.2006.01.009
91. Jian, G., Puerto, M., Wehowsky, A., Miller, C., Hirasaki, G. J., Biswal, S.L. Characterizing adsorption of associating surfactants on carbonates surfaces. Journal of Colloid and Interface Science. 513, 684-692 (2018). https://doi.org/10.1016/j.jcis.2017.11.041

92. ShamsiJazeyi, H., Verduzco, R., Hirasaki, G. J. Reducing adsorption of anionic surfactant for enhanced oil recovery: Part II. Applied aspects, Colloids Surf. A: Physicochem. Eng. Aspects (2014). http://dx.doi.org/10.1016/j.colsurfa.2014.02.021
93. S.M. Mohnot, J.H. Bae, W.L. Foley. A study of mineral/alkali reactions, Soc. Petrol. Eng. 2, 653–663 (1987).
94. A.A. Ivanova, A.N. Cheremisin, M.Y. Spasennykh, Application of nanoparticles in chemical EOR, EAGE conference proceedings (2017). 10.3997/2214-4609.201700247
95. Cheraghian, G., Hendraningrat, L. A review on applications of nanotechnology in the enhanced oil recovery part a: Effects of nanoparticles on interfacial tension. International Nano Letters, 6, 129–138 (2016). https://doi.org/10.1007/s40089-015-0173-4
96. Ogolo, N. A., Olafuyi, O. A., Onyekonwu, M. O. Enhanced oil recovery using nanoparticles. SPE. 1–9 (2012). https://doi.org/10.2118/160847-MS
97. Nettesheim, F., Liberatore, M. W., Hodgdon, T. K., Wagner, N. J., Kaler, E. W., & Vethamuthu, M. Influence of nanoparticle addition on the properties of wormlike micellar solutions. Langmuir. 24, 7718–7726 (2008). https://doi.org/10.1021/la800271m
98. Morrow, L., Potter, D.K., Barron, A.R. Detection of magnetic nanoparticles against proppant and shale reservoir rocks. Journal of Experimental Nanoscience. 10, 1028-1041 2015. https://doi.org/10.1080/17458080.2014.951412
99. White, R.J., Luque, R., Budarin, V.L., Clark, J.H., Macquarrie, D.J. Supported metal nanoparticles on porous materials, methods and applications. Chemical Society Reviews. 38, 481-494 2009. 10.1039/B802654H
100. Fedele, L., Colla, L., Bobbo, S., Barison, S., Agresti, F. Experimental stability analysis of different water-based nanofluids. Nanoscale Res Lett. 6 (2011). https://doi.org/10.1186/1556-276X-6-300
101. Hendraningrat, L., Torsæter, O. Metal oxide-based nanoparticles: Revealing their potential to enhance oil recovery in different wettability systems. Applied Nanoscience. 5, 181-199 (2015). https://doi.org/10.1007/s13204-014-0305-6
102. Yu.W., France, D.M., Routbort, J.L., Choi, S.U. Review and comparison of nanofluid thermal conductivity and heat transfer enhancements. Heat Transfer Engineering. 29, 432-460 (2009). https://doi.org/10.1080/01457630701850851
103. Sun, X., Zhang, Y., Chen, G., Gai, Z. Application of nanoparticles in enhanced oil recovery: a critical review of recent progress. Energies, 10 (2017). https://doi.org/10.3390/en10030345
104. Esmaeilzadeh, P., Fakhroueian, Z., Bahramian, A., Arya, S. Influence of ZrO2 nanoparticles including SDS and CTAB surfactants assembly on the interfacial properties of liquid-liquid, liquid-air

and liquid-solid surface layers. Journal of Nano Research. 21, 15–21 (2012). https://doi.org/10.4028/www.scientific.net/jnanor.21.15

105. Esmaeilzadeh, P., Hosseinpour, N., Bahramian, A., Fakhroueian, Z., Arya, S. Effect of ZrO2 nanoparticles on the interfacial behavior of surfactant solutions at air-water and n-heptane-water interfaces. Fluid Phase Equilibria. 361, 289–295 (2014). https://doi.org/10.1016/j.fluid.2013.11.014

106. Mirchi, V., Saraji, S., Goual, L., Piri, M. Dynamic interfacial tension and wettability of shale in the presence of surfactants at reservoir conditions. Fuel. 148, 127–138 (2015). https://doi.org/10.1016/j.fuel.2015.01.077

107. Ravera, F., Santini, E., Loglio, G., Ferrari, M., Liggieri, L. Effect of nanoparticles on the interfacial properties of liquid/liquid and liquid/air surface layers. Journal of Physical Chemistry B. 110, 19543–19551 (2006). https://doi.org/10.1021/jp0636468

108. Al-Anssari, S., Wang, S., Barifcani, A., Iglauer, S. Oil-water interfacial tensions of silica nanoparticle-surfactant formulations. Tenside, Surfactants, Detergents. 54, 334–341 (2017). https://doi.org/10.3139/113.110511

109. Lan, Q., Yang, F., Zhang, S., Liu, S., Xu, J., Sun, D. Synergistic effect of silica nanoparticle and cetyltrimethyl ammonium bromide on the stabilization of O/W emulsions. Colloids and Surfaces A: Physicochemical and Engineering Aspects. 302, 126–135 (2007). https://doi.org/10.1016/J.COLSURFA.2007.02.010

110. Ma, H., Luo, M., Dai, L. L. Influences of surfactant and nanoparticle assembly on effective interfacial tensions. Physical Chemistry Chemical Physics. 10, 2207–2213 (2008). https://doi.org/10.1039/b718427c

111. Zargartalebi, M., Barati, N., Kharrat, R. Influences of hydrophilic and hydrophobic silica nanoparticles on anionic surfactant properties: Interfacial and adsorption behaviors. Journal of Petroleum Science and Engineering. 119, 36–43 (2015). https://doi.org/10.1016/j.petrol.2014.04.010

112. Biswal, N.R., Singh, J.K. Interfacial behavior of nonionic Tween 20 surfactant at oil–water interfaces in the presence of different types of nanoparticlesRSC Adv. 6, 113307–113314 (2016). 10.1039/c6ra23093h

113. Kazemzadeh, Y., Dehdari, B., Etemadan, Z., Riazi, M., Sharifi, M. Experimental investigation into Fe3O4/SiO2 nanoparticle performance and comparison with other nanofluids in enhanced oil recovery. Pet. Sci. 16, 578–590 (2019). https://doi.org/10.1007/s12182-019-0314-x

114. Shah, R. D. Application of nanoparticle saturated injectant gases for EOR of heavy oils. SPE Annual Technical Conference and Exhibition. (2009). doi:10.2118/129539-stu

115. Helgeson, M. E., Hodgdon, T. K., Kaler, E. W., Wagner, N. J., Vethamuthu, M., Ananthapadmanabhan, K. P. Formation and rheology of viscoelastic “double networks” in wormlike micelle-nanoparticle mixtures. Langmuir. 26, 8049–8060 (2010). https://doi.org/10.1021/la100026d

116. Nettesheim, F., Liberatore, M. W., Hodgdon, T. K., Wagner, N. J., Kaler, E. W., Vethamuthu, M. Influence of nanoparticle addition on the properties of wormlike micellar solutions. Langmuir. 24, 7718–7726 (2008). https://doi.org/10.1021/la800271m

117. Bandyopadhyay, R., Sood, A. K. Effect of silica colloids on the rheology of viscoelastic gels formed by the surfactant cetyl trimethylammonium tosylate. Journal of Colloid and Interface Science. 283, 585–591 (2005). https://doi.org/10.1016/j.jcis.2004.09.038

118. Ragab, A.M. Hannora, A.E. A Comparative investigation of nano particle effects for improved oil recovery–experimental work. In Proceedings of the SPE Kuwait Oil and Gas Show and Conference, (2015). https://doi.org/10.2118/175395-MS

119. Al-Anssari, S., Nwidee, L. N., Arif, M., Wang, S., Barifcani, A., Lebedev, M., Iglauer, S. Wettability alteration of carbonate rocks via nanoparticle-anionic surfactant flooding at reservoirs conditions. SPE Symposium: Production Enhancement and Cost Optimisation. (2017). doi:10.2118/189203-ms

120. Omidi, A., Manshad, A. K., Moradi, S., Ali, J. A., Sajadi, S. M., Keshavarz, A. Smart- and nano-hybrid chemical EOR flooding using Fe3O4/eggshell nanocomposites. Journal of Molecular Liquids. (2020). doi:10.1016/j.molliq.2020.113880

121. Bayat, E. A. Junin, R. Samsuri, A. Piroozian, A. Hokmabadi, M. Impact of metal oxide nanoparticles on enhanced oil recovery from limestone media at several temperatures. Energy Fuels. 28, 6255-6266 (2014). https://doi.org/10.1021/ef5013616

122. Li, Y. Dai, C. Zhou, H. Wang, X. LV W. Zhao, M. Investigation of Spontaneous Imbibition by Using a Surfactant-Free Active Silica Water-Based Nanofluid for Enhanced Oil Recovery. Energy Fuels. 32, 287–293 (2017). https://doi.org/10.1021/acs.energyfuels.7b03132

123. Roustaei, A. Moghadasi, J. Bagherzadeh, H. Shahrabadi, A. An experimental investigation of polysilicon nanoparticles' recovery efficiencies through changes in interfacial tension and wettability alteration. SPE Int. Oilfield Nanotechnology Conference Exhibition. (2012). https://doi.org/10.2118/156976-MS

124. Saha, R. Uppaluri, R. V. Tiwari, P. Silica nanoparticle assisted polymer flooding of heavy crude oil: emulsification, rheology, and wettability alteration characteristics. Industrial Eng. Chem. Res. 57, 6364–6376 (2018). https://doi.org/10.1021/acs.iecr.8b00540

125. Kazemzadeh, Y.; Sharifi, M.; Riazi, M.; Rezvani, H.; Tabaei, M. Potential effects of metal oxide/SiO2 nanocomposites in EOR processes at different pressures. Colloids and Surfaces A: Physicochemical Eng. Aspects. 559, 372–384 (2018). https://doi.org/10.1016/j.colsurfa.2018.09.068

126. Rezvani, H. Riazi, M. Tabaei, M.; Kazemzadeh, Y. Sharifi, M. Experimental investigation of interfacial properties in the EOR mechanisms by the novel synthesized Fe3O4/Chitosan nanocomposites, Colloids and Surfaces A: Physicochemical Eng. Aspects. 544, 15-27 (2018). https://doi.org/10.1016/j.colsurfa.2018.02.012

127. Ali, J. A.; Kolo, K.; Manshad, A. K; Stephen, K. D. Potential application of low-salinity polymeric-nanofluid in carbonate oil reservoirs: IFT reduction, wettability alteration, rheology and emulsification characteristics. J. Mol. Liquids. 284, 735-747 (2019b). doi:10.1016/j.molliq.2019.04.053

128. Dahkaee, K. P.; Sadeghi, M. T.; Fakhroueian, Z.; Esmaeilzadeh, P. Effect of NiO/SiO2 nanofluids on the ultra-interfacial tension reduction between heavy oil and aqueous solution and their use for wettability alteration of carbonate rocks. J. Petrol. Sci. Eng. 176, 11–26 (2019). https://doi.org/10.1016/j.petrol.2019.01.024

129. Asl, H. F.; Zargar, G.; Manshad, A. K.; Takassi, M. A.; Ali, J. A.; Keshavarz, A. Effect of SiO2 nanoparticles on the performance of L-Arg and L-Cys surfactants for enhanced oil recovery in carbonate porous media. J. Molecular Liquids. 300, (2020). https://doi.org/10.1016/j.molliq.2019.112290

130. Nikolov, A., Kondiparty, K., Wasan, D. Nanoparticle self-structuring in a nanofluid film spreading on a solid surface. Langmuir. 26, 7665-7670 (2010). https://doi.org/10.1021/la100928t

131. Wasan, D., Nikolov, A., Kondiparty, K. The wetting and spreading of nanofluids on solids: Role of the structural disjoining pressure. Current Opinion in Colloid & Interface Science. 16, 344-349 (2011). https://doi.org/10.1016/j.cocis.2011.02.001

132. C.M. Phan, C.V. Nguyen, S.I. Yusa, N.L. Yamada, Synergistic adsorption of mibc/ctab mixture at the air/water interface and applicability of Gibbs adsorption equation, Langmuir. 30, 5790–5796 (2014). 10.1021/la500721d

133. G. Gao, C.V. Nguyen, C.M. Phan, Molecular arrangement between electrolyte and alcohol at the air/water interface, J. Mol. Liq. 242, 859-867 (2017). 10.1016/j.molliq.2017.07.083.

134. H. Kuhn, H. Rehage, Molecular orientation of monododecyl pentaethylene glycol at water/air and water/oil interfaces. A molecular dynamics computer simulation study, Colloid Polym. Sci. 278, 114-118 (2000). 10.1007/s003960050019.

135. H. Dominguez, Computer simulations of surfactant mixtures at the liquid/liquid interface, J. Phys. Chem. B. 106, 5915-5924 (2002). 10.1021/jp014403c.

136. Allen, M.P. Introduction to molecular dynamics simulation. Computational Soft Matter: From Synthetic Polymers to Proteins, Lecture Notes. 23, 1-28 (2004). https://dasher.wustl.edu/chem430/readings/md-intro-2.pdf

137. Boas, F.E., Harbury, P.B. Potential energy functions for protein design. Current opinion in structural biology. 17, 199-204 (2007). 10.1016/j.sbi.2007.03.006

138. Y. Li, X.J. He, X.L. Cao, Y.H. Shao, Z.Q. Li, F.L. Dong. Mesoscopic simulation study on the efficiency of surfactants adsorbed at the liquid/liquid interface, Mol. Simul. 31, 1027-1033 (2005). 0.1080/08927020500411948

139. K. J. Schweighofer, U. Essmann, M. Berkowitz. Structure and dynamics of water in the presence of charged surfactant monolayers at the water−CCl4 interface. A molecular dynamics study, J. Phys. Chem. B. 101, 10775-10780 (1997). 10.1021/jp971865a

140. F. L. Dong, Y. Li, P. Zhang, Mesoscopic simulation study on the orientation of surfactants adsorbed at the liquid/liquid interface, J. Chem. Phys. Let. 399, 215-219 (2004). 10.1016/j.cplett.2004.10.022

141. N.M. Van Os, L. A. M. Rupert, B. Smit, P. A. J. Hilbers, K. Esselink, M. R. Böhmer, L. K. Koopal, Surfactant adsorption at liquid/liquid interfaces. Comparison of experimental results with self-consistent field lattice calculations and molecular dynamics simulations, Colloids Surfaces A Physicochem. Eng. Asp. 81, 217-229 (1993). 10.1016/0927-7757(93)80249-E

142. F. Goodarzi, S. Zendehboudi. Effects of salt and surfactant on interfacial characteristics of water/oil systems: molecular dynamic simulations and dissipative particle dynamics. Ind. Eng. Chem. Res. 58, 8817-8834 (2019). 10.1021/acs.iecr.9b00504

143. J. Saien, S. Akbari, Interfacial tension of toluene + water + sodium dodecyl sulfate from (20 to 50) °C and pH between 4 and 9, J. Chem. Eng. Data. 51, 1832-1835 (2006). 10.1021/je060204g

144. C.D. Bruce, M.L. Berkowitz, L. Perera, D.E. Forbes, Molecular dynamics simulation of sodium dodecyl sulfate micelle in water: micellar structural characteristics and counterion distribution, J. Phys. Chem. B 106, 3788-3793 (2002). 10.1021/jp013616z

145. S. Chowdhuri, A. Chandra, Molecular dynamics simulations of aqueous NaCl and KCl solutions: Effects of ion concentration on the single-particle, pair, and collective dynamical properties of ions and water molecules, J. Chem. Phys. 115, 3732-3741 (2001). 10.1063/1.1387447

146. Fan, H., Resasco, D.E., Striolo, A. Amphiphilic silica nanoparticles at the decanewater interface: insights from atomistic simulations. Langmuir. 27, 5264-5274 (2011). dx.doi.org/10.1021/la200428r

147. Goldstein, J., Newbury, D.E., Echlin, P., Joy, D.C., Romig Jr., A.D., Lyman, C.E., Fiori, C., and Lifshin, E., Scanning Electron Microscopy and X-Ray Microanalysis, New York: Plenum, 1981

148. Garvie, L. A. J., Craven, A. J., Brydson, R. Use of electron-energy loss near-edge fine structure in the study of minerals. Am. Mineral. 79, 411–425 (1994)

149. Schindelin, J. et al. Fiji: an open-source platform for biological-image analysis. Nat. Methods 9, 676–682 (2012). https://doi.org/10.1038/nmetAloisih.2019

150. Deglint, H., Clarkson, C. R., DeBuhr, C. & Ghanizadeh, A. Live imaging of micro-wettability experiments performed for low-permeability oil reservoirs. Sci. Rep. 7, (2017). https://doi.org/10.1038/s41598-017-04239-x

151. Robin, M., Combes, R., Degreve, F., Cuiec, L. Wettability of porous media from environmental scanning electron microscopy: from model to reservoir rocks. SPE Int. Symp. Oilfield Chem. (1997). https://doi.org/10.2118/37235-MS

152. Rossi, A. L. et al. Long-range crystalline order in spicules from the calcareous sponge Paraleucilla magna (Porifera, Calcarea). Acta Biomater. 10, 3875–3884 (2014) https://doi.org/10.1016/j.actbio.2014.01.023

153. Aloisi, G. et al. Nucleation of calcium carbonate on bacterial nanoglobules. Geology. 34, 1017–1020 (2006). https://doi.org/10.1130/G22986A.1

154. Gomari, S. R., Hamouda, A. A. Effect of fatty acids, water composition and pH on the wettability alteration of calcite surface. J. Pet. Sci. Eng. 50, 140–150 (2006). https://doi.org/10.1016/j.petrol.2005.10.007

155. Legens, C., Toulhoat, H., Cuiec, L., Villieras, F. & Palermo, T. Wettability change related to adsorption of organic acids on calcite: experimental and ab initio computational studies. J. Soc. Pet. Eng. 4, 328–333 (1999). https://doi.org/10.2118/57721-PA

156. Viades-Trejo, J., Gracia-Fadrique, J. Spinning drop method. From Young-Laplace to Vonnegut. Colloids and Surfaces A: Physicochemical and Engineering Aspects. 302, 549–552 (2007). https://doi.org/10.1016/j.colsurfa.2007.03.033

157. Cao, Y., Zhao, R. H., Zhang, L., Xu, Z. C., Jin, Z. Q., Luo, L., Zhang, L., Zhao, S. Effect of electrolyte and temperature on interfacial tensions of alkylbenzene sulfonate solutions. Energy Fuels. 26, 2175–2181 (2012). https://doi.org/10.1021/ef201982s

158. Haftka, J. J. H., Scherpenisse, P., Oetter, G., Hodges, G., Eadsforth, C. V., Kotthoff, M., Hermens, J. L. M. Critical micelle concentration values for different surfactants measured with solid-phase microextraction fibers. Environmental Toxicology and Chemistry, 35, 2173–2181 (2016). https://doi.org/10.1002/etc.3397

159. Zeppieri, S., Rodríguez, J., López de Ramos, A. L. Interfacial tension of alkane + water systems. Journal of Chemical Engineering Data. 46, 1086–1088 (2001). https://doi.org/10.1021/je000245r

160. Aoudia, M., Al-Maamari, R. S., Nabipour, M., Al-Bemani, A. S., Ayatollahi, S. Laboratory study of alkyl ether sulfonates for improved oil recovery in high-salinity carbonate reservoirs: A case study. Energy Fuels. 24, 3655–3660 (2010). https://doi.org/10.1021/ef100266p

161. Kamal, M., Sultan, A. S., Hussein, I. A. Screening of amphoteric and anionic surfactants for cEOR applications using a novel approach. Colloids and Surfaces A: Physicochemical and Engineering Aspects. 476, 17–23 (2015). https://doi.org/10.1016/j.colsurfa.2015.03.023

162. Girifalso, L. A., Good, R. J. A theory for the estimation of surface and interfacial energies. I. Derivation and application to interfacial tension. Journal of Physical Chemistry, 61, 904–909 (1957). https://doi.org/10.1021/j150553a013

163. Rosen, M. J. Surfactants and interfacial phenomena (3rd ed.). Hoboken, NJ: John Wiley & Sons, Inc. (2004)

164. Abraham, H., Acree, W. E. The hydrogen bond properties of water from 273K to 573K; equations for the prediction of gas-water partition coefficients. Physical Chemistry Chemical Physics. 14, 7433–7440 (2012). https://doi.org/10.1039/C2CP40542C

165. Vashisth, C., Whitby, C. P., Fornasiero, D., Ralston, J. Interfacial displacement of nanoparticles by surfactant molecules in emulsions. Journal of Colloid and Interface Science, 349, 537–543 (2010). https://doi.org/10.1016/j.jcis.2010.05.089

166. Raghavan, S. R., Kaler, E. W. Highly viscoelastic wormlike micellar solutions formed by cationic surfactants with long unsaturated tails. Langmuir. 17, 300–306 (2001). https://doi.org/10.1021/la0007933

167. Moghadam, T., Azizian, S. Effect of ZnO nanoparticle and hexadecyltrimethylammonium bromide on the dynamic and equilibrium oil–water interfacial tension. Journal of Physical Chemistry B. 118, 1527–1534 (2014). https://doi.org/10.1021/jp4106986

168. Gaonkar, A. G. Effects of salt, temperature, and surfactants on the interfacial tension behavior of a vegetable oil/water system. Journal of Colloid and Interface Science, 149, 256–260 (1992). https://doi.org/10.1016/0021-9797(92)90412-F

169. Ling, N. N. A., Haber, A., Graham, F., Aman, Z. M., May, E. F., Fridjonsson, E. O., Johns, M. L. Quantifying the effect of salinity on oilfield water-in-oil emulsion stability. Energy Fuels, 32, 10042–10049 (2018). https://doi.org/10.1021/acs.energyfuels.8b02143

170. Korson, L., Drost-Hansen, W., Millero, F. J. Viscosity of water at various temperatures. Journal of Physical Chemistry. 73, 34–39 (1969). https://doi.org/10.1021/j100721a006

171. B. Hess, C. Kutzner, D. van der Spoel, E. Lindahl, GROMACS 4: Algorithms for highly efficient, load-balanced, and scalable molecular simulation, J. Chem. Theory Comput. 4. 435-447 (2008). 10.1021/ct700301q

172. W. R. P. Scott, P.H. Hunenberger, I.G. Tironi, A.E. Mark, S.R. Billeter, J. Fennen, A.E. Torda, T. Huber, P. Kruger, W. F. van Gunsteren, The GROMOS biomolecular simulation program package, J. Phys. Chem. A 103, 3596-3607 (1999). 10.1021/jp984217f.

173. J. Hermans, H.J.C. Berendsen, W.F. van Gunsteren, J.P.M.Postma, A consistent empirical potential for water–protein interactions, Biopolymers. 23, 1513-1518 (1984). 10.1002/bip.360230807.

174. H.J.C. Berendsen, J.R. Grigera, T.P. Straatsma, The missing term in effective pair potentials, J. Phys. Chem. 91, 6269-6271 (1987).

175. A.W. Schuttelkopf, D.M.F. van Aalten, PRODRG: a tool for high-throughput crystallography of protein-ligand complexes, Acta Cryst. 60, 1355-1363 (2004). 10.1107/S0907444904011679.

176. P.D.T. Huibers, Quantum-chemical calculations of the charge distribution in ionic surfactants, Langmuir. 15, 7546-7550 (1999). 10.1021/la990367l.

177. W. Humphrey, A. Dalke, K. Schulten, VMD: Visual molecular dynamics, J. Mol. Graphics 14, 33-38 (1996). 10.1016/0263-7855(96)00018-5

178. Md.S. Alam, A.M. Siddiq, V. Mythili, M.Priyadharshini, N. Kamely, A.B. Mandal, Effect of organic additives and temperature on the micellization of cationic surfactant cetyltrimethylammonium chloride: Evaluation of thermodynamics, J. Mol. Liq. 199, 511-517 (2014). 10.1016/j.molliq.2014.09.026

179. C.M. Phan, T.N. Le, C.V. Nguyen, S. Yusa, Modeling adsorption of cationic surfactants at air/water interface without using the Gibbs equation, Langmuir. 29, 4743-4749 (2013). 10.1021/la3046302

180. H. Matsubara, A. Onohara, Y. Imai, K. Shimamoto, T. Takiue, M. Aratono, Effect of temperature and counterion on adsorption of imidazolium ionic liquids at air–water interface, Colloids Surfaces A Physicochem. Eng. Asp. 370, 113–119 (2010). https://doi.org/10.1016/j.colsurfa.2010.08.057

181. B.P. Binks, A. Espert, P.D.I. Fletcher, L. Soubiran, Phase behaviour of microemulsions stabilised by double chain cationic surfactants and alcohol co-surfactants, Colloids Surfaces A Physicochem. Eng. Asp. 212 135–145 (2003). https://doi.org/10.1016/ S0927-7757(02)00300-X

182. W.K. Kegel, H.N.W. Lekkerkerker, Phase behaviour of an ionic microemulsion systemas a function of the cosurfactant chain length, Colloids Surfaces A Physicochem. Eng. Asp. 76, 241–248 (1993). https://doi.org/10.1016/0927-7757(93)80084-R

183. S. Iglauer, Y. Wu, P. Shuler, Y. Tang, W.A. Goddard, Alkyl polyglycoside surfactant– alcohol cosolvent formulations for improved oil recovery, Colloids Surfaces A Physicochem. Eng. Asp. 339, 48–59 (2009). https://doi.org/10.1016/j.colsurfa.2009.01.015

184. J.L. Salager, I. Loaiza-Maldonado, M.Minana-Perez, F. Silva, Surfactant-oil-water systems near the affinity inversion part i: relationship between equilibrium phase behavior and emulsion type and stability, J. Disper. Sci. Technol. 3 279–292 (1982). https://doi.org/10.1080/01932698208943642.

185. H.A. Mayson, D.G. Hayes, V.S. Urban, Characterization of microemulsion systems formed by a mixed 1,3-dioxolane ethoxylate/octyl glucoside surfactant system, J. Surfactant Deterg. 12, 277–283 (2009). https://doi.org/10.1007/s11743-009-1122-x.

186. P. Izquierdo, J. Esquena, Th.F. Tadros, C. Dederen, M.J. Garcia, N. Azemar, C. Solans, Formation and stability of nano-emulsions prepared using the phase inversion temperature method, Langmuir. 18, 26–30 (2002). https://doi.org/10.1021/la010808c

187. W.M. Haynes (Ed.), CRC Handbook of Chemistry and Physics, CRC Press, Florida, (2014).

188. I. Benjamin. Molecular structure and dynamics at liquid-liquid interfaces, Annu. Rev. Phys. Chem. 48, 407–451 (1997). https://doi.org/10.1146/annurev.physchem.48.1.407

189. A.Z. Hezave, S. Dorostkar, S. Ayatollahi, M. Nabipour, B. Hemmateenejad, Investigating the effect of ionic liquid (1-dodecyl-3-methylimidazolium chloride ([C12mim] [Cl])) on the water/oil interfacial tension as a novel surfactant, Colloids Surfaces A Physicochem. Eng. Asp. 421, 63–71 (2013). https://doi.org/10.1016/j.colsurfa.2012.12.008

190. G. Qu, C. Xue,M. Zhang, S. Liang, Y. Han, W. Ding, Molecular dynamics simulation of sulfobetaine-type zwitterionic surfactants at the decane/water interface: structure, interfacial properties, J. Disper. Sci. Technol. 37, 1710–1717 (2016). https://doi.org/10.1080/01932691.2015.1135400

191. B. Bagchi,Water dynamics in the hydration layer of biomolecules and self-assembly, Chem. Rev. 105, 3197–3219 (2005). https://doi.org/10.1021/cr020661+

192. H. Chen, E. Ruckenstein, Hydrated ions: from individual ions to ion pairs to ion clusters, J. Phys. Chem. B 119, 12671–12676 (2015). https://doi.org/10.1021/acs.jpcb.5b06837

193. A.M. Tikhonov, H. Patel, S. Garde, M.L. Schlossman, Tail ordering due to headgroup hydrogen bonding interactions in surfactantmonolayers at the water−oil interface, J. Phys. Chem. B 110, 19093–19096 (2006). https://doi.org/10.1021/jp064120q

194. M.R. Watry, G.L. Richmond, Comparison of the adsorption of linear alkanesulfonate and linear alkylbenzenesulfonate surfactants at liquid interfaces, J. Am. Chem. Soc. 112, 875–883 (2000). https://doi.org/10.1021/ja9917666

195. T. Zhao, G. Xu, S. Yuan, Y. Chen, H. Yan, Molecular dynamics study of alkyl benzene sulfonate at air/water interface: effect of inorganic salts, J. Phys. Chem. B. 114, 5025-5033 (2010). doi: 10.1021/jp907438x

196. A.A. Ivanova, A.N. Cheremisin, A. Barifcani, S. Iglauer, C. Phan, Molecular insights in the temperature effect on adsorption of cationic surfactants at liquid/liquid interfaces, J. Mol. Liq. doi:10.1016/j.molliq.2019.112104

197. S.S. Jang, S.T. Lin, P. K. Maiti, M. Blanco, W. A. Goddard III, Molecular dynamics study of a surfactant-mediated decane-water interface: effect of molecular architecture of alkyl benzene sulfonate, J. Phys. Chem. B. 108, 12130-12140 (2004). doi:10.1021/jp048773n

198. M.H. Badizad, M.M. Koleini, R. Hartkamp, S. Ayatollahi, M.H. Ghazanfari, How do ions contribute to brine-hydrophobic hydrocarbon Interfaces? An in silico study, J. Colloid Interface Sci. 575, 337-346 (2020). doi:10.1016/j.jcis.2020.04.060

199. D.W. Green, G. P. Willhite. Enhanced Oil Recovery. SPE Textbook Series. (1998)

200. H. Y. Cai, Y. Zhang, Z.Y. Liu, J.G. Li, Q.T. Gong, Q. Liao, L. Zhang, S. Zhao, Molecular dynamics simulation of binary betaine and anionic surfactant mixtures at decane - Water interface, J. Mol. Liq. 266, 82-89 (2019).10.1016/j.molliq.2018.06.047

201. N.G. Tsierkezos, I. E. Molinou, Thermodynamic properties of water + ethylene glycol at 283.15, 293.15, 303.15, and 313.15 K, J. Chem. Eng. Data. 43, 989-993 (1998). doi:10.1021/je9800914

202. N. Anton, P. Saulnier, A. Béduneau, J.P. Benoit, Salting-out effect induced by temperature cycling on a water/nonionic surfactant/oil system, J. Phys. Chem. B 111, 3651-3657 (2007). 10.1021/jp0664768

203. J. Zhang, L. Li, J. Wang, H. Sun, J. Xu, D. Sun, Double inversion of emulsions induced by salt concentration, Langmuir. 28, 6769-6775 (2012) .10.1021/la300695v

204. R. Aveyard, S. M. Saleem, Interfacial tensions at alkane-aqueous electrolyte interfaces, J. Chem. Soc., Faraday Trans. 1 72, 1609-1617 (1976). 10.1039/F19767201609

205. M. Puerto, G.J. Hirasaki, C.A. Miller, J.R. Barnes, Surfactant systems for EOR in high-temperature, high-salinity environments. SPE J. 17, 11–19 (2010). 10.2118/129675-PA

206. H.I. Okur, Y. Chen, D.M. Wilkins, S. Roke, The Jones-Ray effect reinterpreted: Surface tension minima of low ionic strength electrolyte solutions are caused by electric field induced water/water correlations, Chem. Phys. Lett. 684, 433-442 (2017). 10.1016/j.cplett.2017.06.018

207. C. M. Phan, C. V. Nguyen, T. T. T. Pham, Molecular arrangement and surface tension of alcohol solutions. J. Phys. Chem. B 120, 3914-3919 (2016). 10.1021/acs.jpcb.6b01209

208. C.V. Nguyen, C. M. Phan, H. M. Ang, H. Nakahara, O. Shibata, Y. Moroi, Molecular dynamics investigation on adsorption layer of alcohols at the air/brine interface. Langmuir. 31, 50-56 (2015). 10.1021/la504471

209. P.K. Yuet, D. Blankschtein, Molecular dynamics simulation study of water surfaces: comparison of flexible water models, J. Phys. Chem. B 114, 13786-13795 (2010). 10.1021/jp1067022

210. N. Ikeda, M. Aratono, K. Motomura, Thermodynamic study on the adsorption of sodium chloride at the water/hexane interface, J. Colloid Interface Sci. 149, 208-215 (1992). 10.1016/0021-9797(92)90405-B

211. P. Warszynski, K. Lunkenheimer, G. Czichocki, Effect of counterions on the adsorption of ionic surfactants at fluid-fluid interfaces, Langmuir. 18, 2506-2514 (2002). 10.1021/la010381+

212. D.M. Mitrinović, A.M. Tikhonov, M. Li, Z. Huang, M.L. Schlossman, Noncapillary-wave structure at the water-alkane interface, Phys. Rev. Lett. 85, 582-585 (2000). 10.1103/PhysRevLett.85.582

213. Z. Adamczyk, G. Para, P. Warszynski, Influence of ionic strength on surface tension of cetyltrimethylammonium bromide, Langmuir 15, 8383-8387 (1999). 10.1021/la990241o

214. M.A. Brown, A. Goel, Z. Abbas, Effect of electrolyte concentration on the stern layer thickness at a charged interface, Angew. Chem. Int. Ed. 55, 3790-3794 (2016). 10.1002/anie.201512025

215. J. L. Rivera, C. McCabe, P. T. Cummings, Molecular simulations of liquid-liquid interfacial properties: water–n-alkane and water-methanol–n-alkane systems, Phys. Rev. E. 67 (2002). doi: 10.1103/PhysRevE.67.011603

216. Litton, D.A., Garofalini, S. H. Modeling of hydrophilic wafer bonding by molecular dynamics simulations. Journal of Applied Physics. 89 (2001). http://dx.doi.org/10.1063/1.1351538

217. Cruz-Chu, E. R., Aksimentiev, A., Schulten, K. Water-silica force field for simulating nanodevices. J. Phys. Chem. B. 110, 21497-21508 (2006). https://doi.org/10.1021/jp063896o

218. Cygan, R. T., Liang, J.J., Kalinicjev, A.G. Molecular models of hydroxide, oxyhydroxide, and clay phases and the development of a general force field. J. Phys. Chem. B. 108, 1255-1266 (2004). 10.1021/jp0363287

219. Allen, M. P. Tildesley, D. J. Computer Simulation of Liquids. Oxford University Press: Oxford, UK, (2004).

220. Luo, M., Song, Y., Dai, L. Heterogeneous or competitive self-assembly of surfactants and nanoparticles at liquid–liquid interfaces. J Mol. Simul. 35, 773-784 (2008). https://doi.org/10.1080/08927020902769851

221. A.A. Ivanova, C. Phan A. Barifcani, S. Iglauer, A.N. Cheremisin, Effect of nanoparticles on viscosity and interfacial tension of aqueous surfactant solutions at high salinity and high temperature, J. Surfactants Deterg. (2019). doi:10.1002/jsde.12371